Nitroxide Polymer Mediated Oxidation of Cellulose: Preparation and Applications

by

TINGTING SUN

submitted in accordance with the requirements
for the degree of

DOCTOR OF PHILOSOPHY

at the

UNIVERSITY OF SOUTH AFRICA

SUPERVISOR: PROF X LIU

CO-SUPERVISORS: PROF D HILDEBRANDT
PROF E TANG

MARCH 2022

DECLARATION

Name: Tingting Sun

Student number: 67630243

Degree: Doctor of Philosophy

Exact wording of the title of the thesis as it appears on the electronic copy submitted for examination:

Nitroxide polymer mediated oxidation of cellulose: Preparation and applications

I declare that the above thesis is my own work and that all the sources that I have used or quoted have been indicated and acknowledged by means of complete references.
I further declare that I submitted the thesis to originality checking software and that it falls within the accepted requirements for originality.
I further declare that I have not previously submitted this work, or part of it, for examination at Unisa for another qualification or at any other higher education institution.

Tingting Sun

SIGNATURE

13 March 2022

DATE

ABSTRACT

2, 2, 6, 6-Tetramethylpiperidine-N-oxyl radical (TEMPO) is a stable nitroxyl radical, as well as a highly efficient selective oxidation catalyst. It can efficiently catalyze the selective oxidation of C6 primary hydroxyl groups of cellulose to carboxyl groups in water for the production of oxidized cellulose, which is widely used in a variety of high-tech fields. However, the TEMPO-mediated oxidation system has two major disadvantages: difficulty in separating the catalyst from the aqueous reaction mixture; serious depolymerizaiton of cellulose. In this thesis, TEMPO was loaded onto a polymer carrier with a defined molecular structure to enable TEMPO recycling and reduce the degradation of cellulose.

Firstly, an acrylamide-vinylamine copolymer PVAm-supported TEMPO catalyst (PVAm-T) was designed and developed for selective catalytic oxidation of cellulose. PVAm was prepared by using the Hoffmann degradation of polyacrylamide (PAM) method. The amine groups in the copolymer reacted with the carbonyl groups in 4-oxo-TEMPO to form the catalyst PVAm-T. It was used as a catalyst, instead of free TEMPO, for selective catalytic oxidation of the C6 primary hydroxyl groups of cellulose in water.

The study found that the catalyst has good catalytic performance and a low degree of degradation of cellulose. The carboxyl content of oxidized cellulose was equivalent to 76% of the level of free TEMPO. Furthermore, the catalyst PVAm-T was easy to

recycle by dialysis and the recycling performance was excellent. Interestingly, it was found that PVAm-T could effectively reduce the degradation of oxidized cellulose.

Secondly, G1.0 polyamidoamine (PAMAM) dendrimers was synthesized by repeated Michael addition method and ester aminolysis of ethylenediamine and methyl acrylate. Through reductive amination reaction of the primary amines in PAMAM and the carbonyl groups in 4-oxo-TEMPO, the water-soluble PAMAM immobilized TEMPO (G1.0 PAMAM-TEMPO) was successfully prepared. A polyethylene glycol monomemethyl ether (mPEG) modified PAMAM-TEMPO catalyst, called mPEG-G1.0 PAMAM-Tx, was prepared by means of reaction of the aldehyde group in mPEG-CHO and the amino group in PAMAM-TEMPO. mPEG-G1.0 PAMAM-Tx was used as a catalyst instead of free TEMPO for the selective catalytic oxidation of primary hydroxyl groups in cellulose to carboxyl groups with water as the reaction medium.

The results showed that the cellulose catalytic performance of mPEG-G1.0 PAMAM-T30 was equivalent to 84% of the level of free TEMPO and that the depolymerization of cellulose was also greatly reduced. Interestingly, the positive charge and suitable size of mPEG-G1.0 PAMAM-Tx effectively reduced the formation of C6 aldehydes and C2/C3 ketones. After extracting the supernatant of the oxidation mixture with dichloromethane, mPEG-G1.0 PAMAM-Tx was recovered and re-used for further oxidation cycles. No significant reduction in catalytic performance was found after four oxidation cycles.

Following this process, the applications of TEMPO oxidized cellulose (TOC) were studied. TOC has abundant carboxyl groups and so adsorbs heavy metal ions extremely well. However, TOC has a small particle size and abundant carboxyl groups and is easily dispersed in water, making separation difficult. To address this issue, PAMAM-modified magnetic nanoparticle supported TEMPO catalysts, called Gn PAMAM-Tx-MNP, were prepared and used to prepare the TOC. Gn PAMAM-Tx-MNP and TOC were crosslinked by glutaraldehyde to give a magnetic oxidized cellulose/nano-Fe_3O_4 composite (TOC-Gn PAMAM-Tx-MNP). TOC-Gn PAMAM-Tx-MNP was applied as an adsorption material to adsorb Pb^{2+} in water. The adsorption capacity of TOC-Gn PAMAM-Tx-MNP was up to 109 mg/g, i.e. equivalent to that of TOC with the same carboxy content. Furthermore, it was easily recovered by magnetic separation and the cycling performance was good.

4-nitrophenol (4-NP) is a highly toxic compound. Ag nanoparticles prepared with PAMAM as a template (PAMAM-Ag) can achieve the effect of uniform dispersion of Ag nanoparticles and can be used as a catalyst to rapidly transform 4-NP into 4-aminophenol (4-AP). However, re-use is difficult. To address this issue, PAMAM-Ag was covalently attached to TOC by an aldehyde-amine reaction between TOC-containing aldehyde groups and PAMAM-Ag containing amino groups. The TOC immobilized PAMAM-Ag (TOC-PAMAM-Ag) was used to catalyze the reaction of reducing 4-NP to 4-AP. It was found that the imine bonds contained in TOC-PAMAM-

Ag were transformed into stable amine bonds in the catalytic reduction process, making TOC-PAMAM-Ag stable. The effect of the catalyst loading amount and carboxyl content was investigated and it was found that increasing the carboxyl content is beneficial in improving catalytic activity. The cyclic catalytic performance was stable, and the catalytic activity remained at a good level after several cycles.

ACKNOWLEDGEMENTS

This research project would not have been possible without the support of many people. I wish to express my deepest gratitude to the following people:

1. My supervisor, Prof. Xinying Liu, who helped me a lot throughout my graduate studies, e.g. helping me develop the research plan, revise the paper and deal with school affairs.
2. My co-supervisor, Prof. Erjun Tang, who gave me assistance, support and guidance with the study and writing the paper.
3. Special thanks also go to Prof. Shaojie Liu for his kind help, guidance and advice regarding the study.
4. Graduate friends, Mr Yusheng Zhang (IDEAS UNISA), Mr Jianqi Shen (IDEAS UNISA) and Mr Jianli Chang (IDEAS UNISA), for helping me with school affairs. Ms Xiaomeng Chu (HEBUST) and Mr Xuteng Xing (HEBUST) for helping me with the scientific research.
5. UNISA and Hebei University of Science & Technology, for funding my studies.

I also wish to express my love and gratitude to my entire family, for their encouragement and understanding throughout the duration of my studies.

LIST OF PUBLICATIONS

1. **Sun T**, Wang H, Liu J, Chu X, Xing X, Liu S, Tang E, Liu X, Hildebrandt D. Recoverable acrylamide-vinylamine copolymer immobilized TEMPO mediated oxidation of cellulose with good catalytic performance and low cellulose degradation. Cellulose, 2021, 28(7): 4151-4164.

2. **Sun T**, Liang H, Liu S, Tang E, Fu C. Magnetic nanoparticles modified by polyamidoamine-immobilized TEMPO for catalytic oxidation of monomethoxy poly (ethylene glycol). Journal of Nanoparticle Research, 2020, 22(6): 163.

3. Wang H, Wang X, **Sun T**, Li P, Chu X, Xing X, Liu S, Tang E. Recoverable, water-soluble polyethylene glycol-immobilized N-hydroxyphthalimide, as mediator for cellulose oxidation in the presence of NaBr and NaClO. Cellulose, 2021, 28(18): 11315-11328.

4. **Sun T**, Liu S, Tang E, Liu X. Preparation of oxidized cellulose/nano-Fe_3O_4 composite using Gn PAMAM-T modified nano-Fe_3O_4 as oxidation catalyst and cellulose cross-linker for efficient adsorption of Pb^{2+}. Submitted for review 2022.

5. **Sun T**, Liu S, Tang E, Liu X. A recoverable polyethylene glycol modified polyamidoamine immobilized TEMPO catalyst for efficient catalytic oxidation of cellulose. Submitted for review 2022.

TABLE OF CONTENTS

LIST OF FIGURES

LIST OF TABLES

LIST OF ABBREVIATIONS AND SYMBOLS

Abbreviation	Full name
3D	Three-dimensional
4-oxo-TEMPO	4-oxo-2, 2, 6, 6-tetramethylpiperidine-1-oxyl
AC_2O	Acetic anhydrate
AIBN	Azodiisobutyronitrile
AM	Acrylamide
APTS	3-aminopropyltriethoxysilane
ARGET ATRP	Activators regenerated by electron transfer atom transfer radical polymerization
ATRP	Atom transfer free radical polymerization
CAN	Ammonium cerium nitrate
CMC	Carboxymethyl cellulose
DCM	Dichloromethane
DMAc	N-dimethylacetamide
DMSO	Dimethyl sulfoxide
DP	Degree of polymerization
EDTA	Ethylene diamine tetraacetic acid
ESR	Electron spin resonance
FT-IR	Fourier transform infrared spectroscopy
GLA	Glutaricdialdehyde
GPC	Gel permeation chromatography
HBT	N-hydroxybenzotriazole
HEC	Hydroxyethyl cellulose
HPC	Hydroxypropyl cellulose
HPMC	Hydroxypropyl methylcellulose
IPN	Interpenetrating polymer networks
MA	Methyl acrylate
mCPBA	3-Chloroperoxybenzoic acid
MNP	Magnetic Fe_3O_4 nanoparticles
MS	Mass spectroscopy
NHPI	N-hydroxyphthalimide
NHTPPI	N-hydroxy-3, 4, 5, 6-tetraphenylphthalimide

Abbreviation	Full name
NMMO	N-methylmorpholine-N-oxide
NMR	Nuclear magnetic resonance spectroscopy
PVAm	Acrylamide-vinylamine copolymer
PAA	Polyacrylic acid
PAM	Polyacrylamide
PAMAM	Polyamidoamine
PEG	Polyethylene glycol
PVAm	Polyvinylamine
SEM	Scanning electron microscope
TBAF	Tetra butyl ammonium fluoride
TEM	Transmission electron microscope
TEMP	4-amino-2, 2, 6, 6-tetramethylpiperidine
TEMPO	2, 2, 6, 6-tetramerylpiperidine-1-oxyl
TGA	Thermal gravimetric analyzer
TOC	TEMPO oxidized cellulose
UV-vis	Ultraviolet-visible spectrophotometer
VA	Violuric acid
VSM	Vibrating sample magnetometer
XPS	X-ray photoelectron spectrometer
XRD	X-ray diffractometer

Symbol	Full name	Unit
CrI	Crystallinity Index	---
q	Adsorption capacity of Pb^{2+}	mg/g
$[\eta]$	Limiting viscosity number	---
h	Mean terminal distance	nm
R	Mean radius	nm
ρ	Density	g/cm^3
R^2	Regression correlation coefficient	---

CHAPTER 1 INTRODUCTION

1.1 Background

Biomass materials that come from plants or animals are renewable and can reduce environmental deterioration. Therefore, using biomass resources has received increasing attention since fossil fuels, oil and coal are found to be non-renewable [1-5].

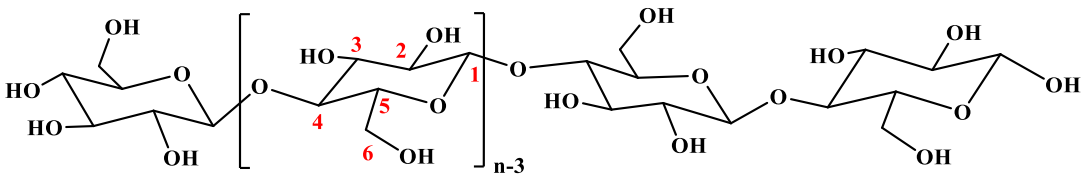

Fig. 1.1 Molecular structure of cellulose

Cellulose is an abundant biomass material that has been widely used in various fields, such as clothing, packaging, building materials, food, medicine, paper and cosmetics. Each monosaccharide unit in cellulose has one primary hydroxy group (C6-OH) and two secondary hydroxy groups (C2-OH and C3-OH), as shown in Fig. 1.1. These hydroxyl groups contribute to the high hydrophilicity of the cellulosic material. In addition, natural cellulose with a dense crystal structure tends to have a large number of intramolecular and intermolecular hydrogen bonds and hydrophobic interactions, which can form both the hydrophobic layer and the hydrophilic layer in cellulose molecules [6-11]. (See Fig. 1.2.) These structural features make cellulose insoluble in water and in common organic solvents. Therefore, unmodified cellulose can only meet a very few application requirements, which means that modifying the cellulose for

industrial applications is of great research significance.

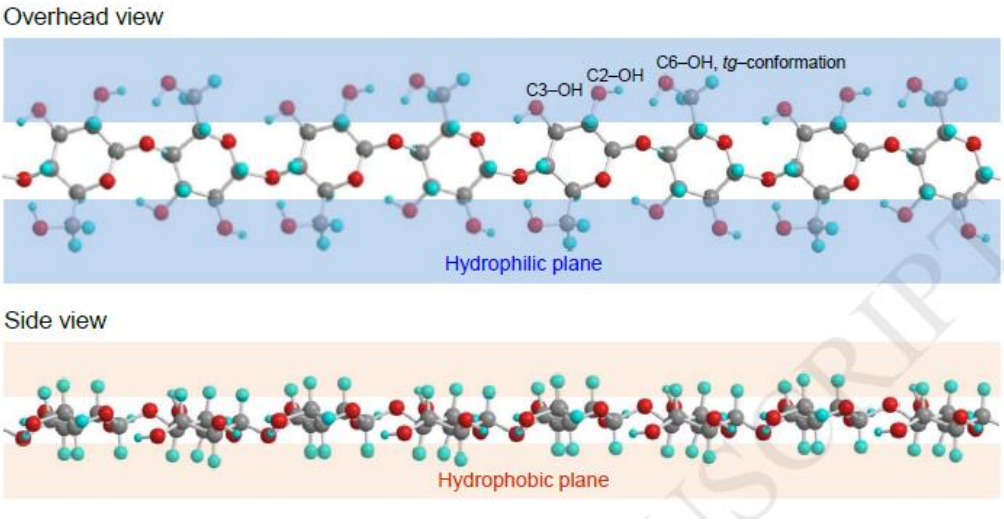

Fig. 1.2 Hydrophilic and hydrophobic planes of cellulose molecules marked with the primary C6-OH, and secondary C2-OH and C3-OH groups in a monosaccharide unit

Direct oxidation of the hydroxyl groups provides an interesting route to introduce carbonyl and carboxyl groups into cellulose, and it has emerged as a promising method for cellulose modification. Oxidation of secondary hydroxyl groups (C2 and C3) can be achieved using various common oxidants, such as periodate [12, 13] and hypochlorite [14]. The oxidation of C6 primary hydroxyl groups is usually performed by 2, 2, 6, 6-tetramerylpiperidine-1-oxyl (TEMPO) [15].

TEMPO mediated oxidation of polysaccharides was first reported in 1994 [16-19]. Since then, the selective oxidation of cellulose using TEMPO as the mediator has become a popular area of research. The C6 primary hydroxyl groups of cellulose are effectively converted into carboxyl groups by the TEMPO/NaBr/NaClO system to

produce the TEMPO oxidized cellulose (TOC) [16-21]. TOC has many advantages, including strong oxygen-barrier properties, high optical transparency and high dimensional thermal stability, and has been widely used in high-tech fields. As a key step in the preparation of TOC, TEMPO-mediated oxidation has the advantages of mild reaction conditions, a fast reaction rate and high oxidation selectivity [22-29].

1.2 Problem Statement

The TEMPO-mediated oxidation system still has two major drawbacks. Firstly, TEMPO is an expensive and toxic reagent for aquatic life, and it can pollute water if it is discarded into the environment. Secondly, it leads to severe depolymerization of the cellulose backbone after oxidation, resulting in poor mechanical properties of oxidized cellulose [30-33].

1.3 Research Aims

To overcome the drawbacks of TEMPO mediated oxidation of cellulose, as described in this thesis, the TEMPO is loaded onto a polymer carrier with a defined molecular structure, in order to produce a catalyst containing TEMPO, which can be recycled to reduce the degradation of cellulose using the process described below.

(1) Prepare nitroxide polymers with high degree of TEMPO loading as recoverable catalysts for cellulose oxidation.

(2) Use the defined molecular structure of nitroxide polymers and a post-treatment process to alleviate cellulose degradation.

(3) Apply the prepared oxidized cellulose as the adsorption material for adsorbing the heavy metal ions in the water.

(4) Prepare oxidized cellulose-loaded nano-silver particles for efficient reduction of 4-nitrophenol.

1.4 Dissertation Overview

The dissertation consists of eight chapters. Most of the chapters are written in the form of scientific journal articles, as they have been prepared for publication or have been published as part of the academic results of this research.

An overview of this thesis is provided below.

Chapter 1 provides the background to the research, the problem statement, the research aims and the dissertation outline.

Chapter 2 is the literature review, which reviews the modifications and applications of cellulose.

Chapter 3 introduces the reagents, equipment and characterization methods used in this dissertation.

Chapter 4 describes the development of a recoverable acrylamide-vinylamine

copolymer supported TEMPO catalyst called PVAm-T used for selective oxidation of cellulose. First, the copolymer of PVAm was obtained by Hofmann degradation of polyacrylamide. The carbonyl group of 4-oxo-TEMPO was reacted with the amine group of PVAm in a condensation reduction reaction to produce PVAm-T. The C6 primary hydroxyl group of cellulose was selectively oxidized with PVAm-T. The carboxyl content of oxidized cellulose reached 76% of the carboxyl level of the TEMPO. This macromolecular catalyst was recovered by dialysis and had good recycling performance. In the oxidizing process, it can inhibit the formation of C6 aldehyde and C2/C3 ketone, and can alleviate the degradation of cellulose.

Chapter 5 presents a water-soluble polyethylene glycol modified polyamidoamine (PAMAM) immobilized TEMPO catalyst (mPEG-Gn PAMAM-Tx) with different PAMAM generations and different degrees of TEMPO loading for use in oxidizing cellulose. PAMAM dendrimers of G1.0-G3.0 were synthesized by the repeated Michael addition and ester aminolysis of ethylenediamine and methyl acrylate. Using the reductive amination reaction of primary amines in the PAMAM and carbonyl groups in 4-oxo-TEMPO, the water-soluble PAMAM immobilized TEMPO (PAMAM-TEMPO) was successfully prepared. mPEG-Gn PAMAM-Tx was prepared by means of the reaction of the aldehyde group in PEG-CHO and the amino group in PAMAM-TEMPO. It was applied as the catalyst for oxidizing the C6 hydroxyl groups in cellulose to carboxyl groups. The results showed that its catalytic performance was equivalent to 84% of that of the free TEMPO. After extracting the supernatant of the oxidation

mixture with dichloromethane (DCM), mPEG-Gn PAMAM-Tx was recovered and re-used for further oxidation cycles. No significant reduction in catalytic performance was found after four oxidation cycles. Furthermore, the degradation of cellulose was largely alleviated.

Chapter 6 describes the use of PAMAM modified magnetic nanoparticle supported TEMPO, called Gn PAMAM-Tx-MNP, for preparing oxidized cellulose. After oxidation, Gn PAMAM-Tx-MNP and oxidized cellulose were crosslinked by glutaraldehyde (GLA) to give the magnetic oxidized cellulose/nano-Fe_3O_4 composite (TOC-Gn PAMAM-Tx-MNP). TOC-Gn PAMAM-Tx-MNP is a recoverable adsorption material and this was applied to adsorb Pb^{2+} in water. Its adsorption capacity was up to 109 mg/g, equivalent to that of TOC with the same carboxy content. Furthermore, it was easily recovered by magnetic separation, and the cycling performance was good.

Chapter 7 describes the preparation of the composite of TOC loaded nano-Ag for catalytic reduction of 4-nitrophenol (4-NP) to 4-aminophenol (4-AP). Ag nanoparticles were prepared using PAMAM as a template, and PAMAM-Ag was then covalently attached to TOC by aldehyde-amine reaction between the TOC containing aldehyde groups and PAMAM-Ag containing amino groups. In the catalytic reduction of 4-NP to 4-AP, the unstable imine bond contained in TOC loaded nano-Ag was transformed into a more stable amine bond. It was found that TOC loaded nano-Ag had good

catalytic performance and can be re-used.

Chapter 8 summarizes all the research contents provided in this dissertation.

References

[1] Zhang H, Wei X. Research on energy substitution and the path of endogenous economic growth [J]. Journal of Beijing Institute of Technology (Social Sciences Edition), 2014, (4): 42-49.

[2] Cao W. Research on the assessment and selection of renewable energy industrial technology [D]. Beijing Jiaotong University, 2012.

[3] Klemm D, Heublein B, Fink H, et al. Cellulose: Fascinating biopolymer and sustainable raw material [J]. Angewandte Chemie International Edition, 2005, 44(22): 3358-3393.

[4] Narayan R. Polymeric materials from agricultural feedstocks [M]. Polymers from Agricultural Coproducts, 1994, 1: 2-28

[5] Kaplan D. Introduction to biopolymers from renewable resources [M]. Biopolymers from Renewable Resources. Springer, Berlin, Heidelberg, 1998: 1-29.

[6] Hufendiek A, Trouillet V, Meier M, et al. Temperature responsive cellulose-graft-copolymers via cellulose functionalization in an ionic liquid and RAFT polymerization [J]. Biomacromolecules, 2014, 15(7): 2563-2572.

[7] Lindman B, Karlström G, Stigsson L. On the mechanism of dissolution of cellulose [J]. Journal of Molecular Liquids, 2010, 156(1): 76-81.

[8] Bragd P, Van Bekkum H, Besemer A. TEMPO-mediated oxidation of polysaccharides: Survey of methods and applications [J]. Topics in Catalysis, 2004, 27(1): 49-66.

[9] Medronho B, Romano A, Miguel M, et al. Rationalizing cellulose (in) solubility: Reviewing basic physicochemical aspects and role of hydrophobic interactions [J]. Cellulose, 2012, 19(3): 581-587.

[10] Isogai A, Hänninen T, Fujisawa S, et al. Catalytic oxidation of cellulose with nitroxyl radicals under aqueous conditions [J]. Progress in Polymer Science, 2018, 86: 122-148.

[11] Zugenmaier P. Conformation and packing of various crystalline cellulose fibers [J]. Progress in Polymer Science, 2001, 26(9): 1341-1417.

[12] Kim U, Kuga S, Wada M, et al. Periodate oxidation of crystalline cellulose [J]. Biomacromolecules, 2000, 1(3): 488-492.

[13] Llàcer Navarro S, Nakayama K, Idström A, et al. The effect of sulfate half-ester groups on cellulose nanocrystal periodate oxidation [J]. Cellulose, 2021, 28(15): 9633-9644.

[14] Matsuki S, Kayano H, Takada J, et al. Nanocellulose production via one-pot formation of C2 and C3 carboxylate groups using highly concentrated NaClO aqueous solution [J]. ACS Sustainable Chemistry & Engineering, 2020, 8(48): 17800-17806.

[15] Bragd P, Van Bekkum H, Besemer A. TEMPO-mediated oxidation of polysaccharides: Survey of methods and applications [J]. Topics in Catalysis, 2004, 27(1): 49-66.

[16] De Nooy A, Besemer A, Van Bekkum H. Highly selective TEMPO mediated oxidation of primary alcohol groups in polysaccharides [J]. Recueil des Travaux Chimiques des Pays-Bas, 1994, 113(3): 165-166.

[17] De Nooy A, Besemer A, van Bekkum H. Highly selective nitroxyl radical-mediated oxidation of primary alcohol groups in water-soluble glucans [J]. Carbohydrate Research, 1995, 269(1): 89-98.

[18] De Nooy A, Besemer A, Van Bekkum H. On the use of stable organic nitroxyl radicals for the oxidation of primary and secondary alcohols [J]. Synthesis, 1996, 1996(10): 1153-1176.

[19] Adam W, Saha-Möller C, Ganeshpure P. Synthetic applications of nonmetal catalysts for homogeneous oxidations [J]. Chemical Reviews, 2001, 101(11): 3499-3548.

[20] Saito T, Isogai A. TEMPO-mediated oxidation of native cellulose. The effect of oxidation conditions on chemical and crystal structures of the water-insoluble fractions [J]. Biomacromolecules, 2004, 5(5): 1983-1989.

[21] Fukuzumi H, Saito T, Iwata T, et al. Transparent and high gas barrier films of cellulose nanofibers prepared by TEMPO-mediated oxidation [J]. Biomacromolecules, 2009, 10(1): 162-165.

[22] Hong S, Yoo S, Lee J, et al. Sonochemically activated synthesis of gradationally complexed Ag/TEMPO-oxidized cellulose for multifunctional textiles with high electrical conductivity, super-hydrophobicity, and efficient EMI shielding [J]. Journal of Materials Chemistry C, 2020, 8(40): 13990-13998.

[23] Xie W, Liu W, Dang Y, et al. Unveiling the effect of homogenization degree on electrochemical performance of TEMPO-mediated oxidized cellulose separators for lithium-ion batteries [J]. European Polymer Journal, 2020, 127: 109587.

[24] Yeasmin S, Yeum J, Yang S. Fabrication and characterization of pullulan-based nanocomposites reinforced with montmorillonite and tempo cellulose nanofibril [J]. Carbohydrate Polymers, 2020, 240: 116307.

[25] Kuramae R, Saito T, Isogai A. TEMPO-oxidized cellulose nanofibrils prepared from various plant holocelluloses [J]. Reactive and Functional Polymers, 2014, 85: 126-133.

[26] Shimizu M, Saito T, Fukuzumi H, et al. Hydrophobic, ductile, and transparent nanocellulose films with quaternary alkylammonium carboxylates on nanofibril surfaces [J]. Biomacromolecules, 2014, 15(11): 4320-4325.

[37] Sone A, Saito T, Isogai A. Preparation of aqueous dispersions of TEMPO-oxidized cellulose nanofibrils with various metal counterions and their super deodorant performances [J]. ACS Macro Letters, 2016, 5(12): 1402-1405.

[28] Isogai A, Bergström L. Preparation of cellulose nanofibers using green and sustainable chemistry [J]. Current Opinion in Green and Sustainable Chemistry, 2018, 12: 15-21.

[29] Sone A, Saito T, Isogai A. Preparation of aqueous dispersions of TEMPO-oxidized cellulose nanofibrils with various metal counterions and their super deodorant performances [J]. ACS Macro Letters, 2016, 5(12): 1402-1405.

[30] Zhang S, Feng J, Feng J, et al. Carbon aerogels by pyrolysis of TEMPO-oxidized cellulose [J]. Applied Surface Science, 2018, 440: 873-879.

[31] Shibata I, Isogai A. Depolymerization of cellouronic acid during TEMPO-mediated oxidation [J]. Cellulose, 2003, 10(2): 151-158.

[32] Saito T, Hirota M, Tamura N, et al. Individualization of nano-sized plant cellulose fibrils by direct surface carboxylation using TEMPO catalyst under neutral conditions [J]. Biomacromolecules, 2009, 10(7): 1992-1996.

[33] Jun S, Park S, Kang N. One-pot method of synthesizing TEMPO-oxidized bacterial cellulose nanofibers using immobilized TEMPO for skincare applications [J]. Polymers, 2019, 11(6): 1044.

CHAPTER 2 LITERATURE REVIEW

2.1 Cellulose

Cellulose is the most abundant natural polysaccharide on earth, and one of the most promising substitutes for petroleum-derived synthetic polymers. It has the advantages of biocompatibility, biodegradability, renewability and good mechanical strength. It comes mainly from wood, plants, algae and bacteria. Cellulose consists of linear β-1,4-linked D-glucose units, and has abundant hydroxyl active groups that can form intermolecular and intramolecular bonds in polymer chains, making it difficult to dissolve in common solvents. Hence, cellulose is relatively stable and has high axial stiffness [1-3]. There are four main crystalline variants of cellulose: cellulose I, II, III and IV. The difference between cellulose I, II, III and IV is with the hydrogen bonding pattern in its crystal structure. The macromolecular chain of cellulose I has a parallel orientation, while other cellulose macromolecular chains have an anti-parallel orientation. Cellulose I have an excellent elastic modulus and mechanical properties [4-7].

Cellulose is known to be almost insoluble in water and most organic solvents. To expand the scope of application of cellulose, it is necessary to treat cellulose, in terms of the following aspects: 1) Finding a suitable solvent to dissolve the cellulose evenly without damaging the cellulose structure. 2) Using cellulose derivatives instead of cellulose. 3) Introducing new active groups by oxidation of the hydroxyl groups on

cellulose or grafting monomer onto the cellulose.

2.1.1 Cellulose dissolution

Several solvents have been used for dissolving cellulose, including N-methylmorpholine-N-oxide (NMMO) [8-10], LiCl/N-dimethylacetamide (LiCl/DMAc) [11, 12], metal-complex solutions [13, 14], ionic liquids (ILs) [15-18], tetra butyl ammonium fluoride/dimethyl sulfoxide (TBAF/DMSO) [19-22], inorganic molten inorganic salt hydrates [23-28], organic-base solutions [29] and alkali/urea solutions [30-32].

Table 2.1 Solvents commonly used for dissolving cellulose

Solvent	Solubility wt.%	Dissolving process	Characteristics
NMMO	4-17	The active N-O dipoles and the oxygen groups of NMMO can form hydrogen bonds with cellulose, leading to disruption of the cellulose's intermolecular hydrogen bonds, and eventually establishing a strong complex by forming new hydrogen bonds.	Thermal instability; Side reactions; High temperature; Uncontrolled fibrillation of NMMO.
LiCl/DMAc	3-16	The protonated -OH of cellulose forms strong hydrogen bonds with Cl^- and Li^+. The intermolecular hydrogen-bonding networks of cellulose can be broken when the Li^+-Cl^- ion pairs split.	Thermal stability; High cost; Difficult to recycle.
Metal-complex	4-12	Copper (II) hydroxide is precipitated from a copper sulfate solution by using either ammonia or sodium hydroxide. Cu^{2+} and	Side reactions; Difficult to recycle.

Solvent	Solubility wt.%	Dissolving process	Characteristics
		$(C_6H_8O_5)_n^{2-}$ ions can form a complex to dissolve cellulose.	
ILs	4-25	The positively-charged or negatively-charged groups on the cellulose chains interact with the oxygen or hydrogen atoms on the hydroxyl group of cellulose to break the hydrogen bonds. The negative ions of ILs attach to the hydroxyl group of cellulose to form a negatively-charged complex. A cation is inserted between the molecular bundles to separate the cellulose molecules.	High thermal stability; Chemical stability; High solubility; Corrodes the machine; Solvent-recycling efficiency is low.
TBAF/DMSO	10-20	There is a strong ion-dipole interaction between fluoride ions from TBAF and the hydroxyl groups of cellulose. The highly electronegative fluoride ions form hydrogen bonds with the cellulose hydroxyl groups to deconstruct the hydrogen bond network of cellulose.	Mild conditions; Dissolves quickly.
Inorganic molten salt hydrates	2-11	Dissolution of cellulose depends on direct interaction of the cellulose hydroxyl groups with the metal ions. The intermolecular and intramolecular hydrogen bonds of cellulose are broken due to the addition of the inorganic salt. Coordination bonds are formed between the metal ion and the oxygen of the hydroxyl groups of cellulose.	Inexpensive; Easier to prepare; Environmentally friendly.
Organic base	9-13.5	The preferable wrapping interaction between cations and the cellulose glucose ring prevents aggregation among the cellulose chains. The anion forms new hydrogen bonds with the hydroxyl groups of cellulose. The hydrophobic cation of the	Easily recycled and re-used; Synthesis is relatively complicated and high-cost.

Solvent	Solubility wt.%	Dissolving process	Characteristics
		organic base accumulates at the cellulose interface and decreases the surface tension, leading to the dissolution of the cellulose.	
Alkali/urea solutions	4-11	NaOH forms new hydrogen bonds with the cellulose at low temperatures. Urea hydrate is encapsulated by hydrogen bond between NaOH and cellulose, forming inclusion complexs with tubular structure. Weak interactions between the urea and the cellulose can weaken the effect of the hydrophobic interactions among the cellulose molecules, resulting in the dissolution of cellulose.	Non-toxicity; Low cost; Low energy consumption.

2.1.2 Cellulose derivatives

The commonly used cellulose derivatives are hydroxypropyl methylcellulose (HPMC), hydroxyethyl cellulose (HEC), carboxymethyl cellulose (CMC) and hydroxypropyl cellulose (HPC) (See Table 2.2).

2.1.2.1 Hydroxypropyl methylcellulose

HPMC is a cellulose derivative widely used in controlled release applications because of its thickening, gelling and swelling properties. In addition, it has the advantages of non-toxic properties, easy compression, swelling properties and can accommodate high drug levels [42, 43]. HPMC is mainly used to make hydrogels for medical use, such as stents, film and membranes. Larsson et al. studied the addition of HPMC as a pore-forming agent in micro fibrillated cellulose film and the adjustment of film permeability

[44]. Zeeshan et al. applied HPMC to scaffold engineering by crosslinking chitosan [36]. Seyedlar et al. also used HPMC as a composite hydrogel for scaffold engineering [37].

2.1.2.2 Hydroxyethyl cellulose

HEC with good hydrophilicity, good biocompatibility and good degradability, is a water-soluble cellulose ether. The abundance of active OH groups in the HEC chain makes it easy to modify so as to obtain new materials with improved properties [38, 40, 41]. Because of its biocompatibility and non-immunogenicity, HEC is often used as a stabilizer or thickener in pharmaceutical and cosmetic products [39].

2.1.2.3 Carboxymethyl cellulose

CMC is a water-soluble cellulose derivative that has been widely used in the biopolymer industry. It is produced in a non-aqueous monochloroacetic acid/soda solvent medium by carboxymethyl partial substitution of 2, 3 and 6 hydroxyl groups on the main chain of cellulose [42]. It has biocompatibility, biodegradability, excellent absorption/adsorption, high swelling capacity and good optical properties. The hydrogel prepared when using it can be used for enzyme fixation, wound healing and as an adsorption material [43-45].

2.1.2.4 Hydroxypropyl cellulose

HPC is derived through the reaction of alkali cellulose with propylene oxide. Propylene

oxide acts as a substitute through ether bonds of three reactive hydroxyl groups on the cellulose monomer [46]. Due to its viscosity, HPC is commonly used as a thickener, emulsion and adhesive in solid medicine [47]. It can also be used to prepare hydrogels for medical and pharmaceutical applications.

Table 2.2 Comparison of cellulose and its derivatives

Compound	Monomer	Synthesis	Structure
Cellulose	---	Obtained from plants	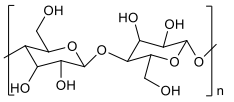
HPMC		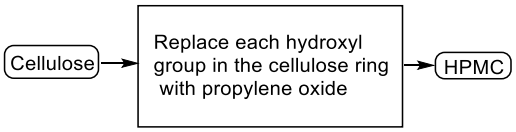	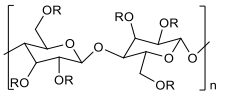
HEC		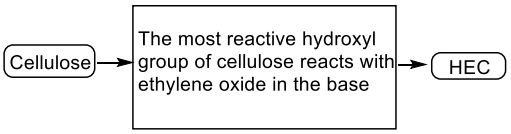	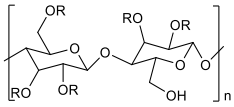 R=H or CH_2CH_2OH
CMC		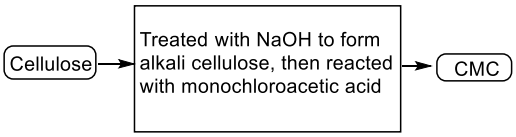	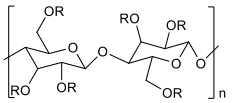 R=H or CH_2COONa
HPC	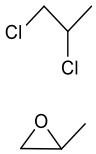	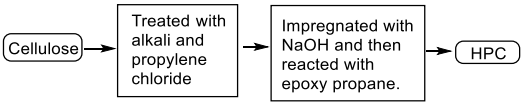	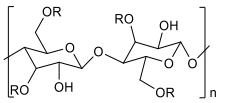 R=O-CH_2CH_3-OH

2.1.3 Direct chemical modification

Direct chemical modification means that functional groups are attached to the hydroxyl groups of the cellulose backbone by a variety of chemical methods, such as alkaline treatment, silynation, etherification, halogenation, esterification and oxidation [48, 49]. Chemical modification of cellulose can introduce new active groups to solve the problem of unstable cellulose [50].

2.1.3.1 Alkaline treatment

Cellulose is difficult to modify and apply without any chemical treatment due to its strong rigidity and hydrogen bond structure. Alkaline treatment results in changes in cellulose surface area, average pore volume and pore size. Sodium hydroxide is a reagent commonly used for saponification. It converts ester groups to carboxylate salts and alcohols. Chemical treatments with alkaline solutions at different concentrations were used to isolate cellulose from soybean [51-53], potato tuber cells [54] and hemp fiber [55]. These treatments led to partial separation of the cellulose from the cell wall.

2.1.3.2 Silynation

The interaction between silane coupling agents and cellulose is well known [56], and silane surface modification is a popular cellulose modification method. The silane coupling agent that goes through the hydrolysis, condensation and bonding stages can improve the degree of cross-linking in the interface area. The silane reacts with the hydroxyl group of cellulose to form a polysiloxane structure, which is hydrolyzed to silanol, and then reacts with the hydroxyl group of the cellulose to form a stable covalent bond. Functionalized silanes have been widely investigated and used. Studies have found that cellulose materials crosslinked with silane are effective adsorbents for removing metals in aqueous solution due to the presence of amino groups on amino silane and hydroxyl on cellulose. Hokkanen et al. found that the aminopropyl triethoxysilane modified cellulose adsorbent is very effective in removing Ni(II), Cu(II)

and Cd(II) from water [57].

2.1.3.3 Etherification

The C2, C3 and C6-OH groups of monosaccharide units of cellulose can be partly replaced by other groups through etherification, in order to synthesize cellulose ether. Cellulose reacts with ethylene oxide or other epoxy compounds to form cellulose ethers [58]. A typical hydroxypropyl reaction takes place: cellulose reacts with epichlorohydrin to produce reactive epoxides, and is further functionalized with polyethylene imine as a chelating agent [59]. A cyano group can be introduced to the cellulose structure by etherification of acrylonitrile and cellulose [60]. The cyano group of cellulose can be further amidoximated by reacting with hydroxylamine to produce an adsorption material [61].

2.1.3.4 Halogenation

Several chemical reagents are used as precursors for transferring halogen elements to the cellulose polymer chain [62]. Zhou et al. studied a method to fix glucose and trimethylammonium chloride on the surface of cellulose [63].

2.1.3.5 Esterification

Cellulose ester is a derivative of cellulose, which is formed by replacing a free hydroxyl group of cellulose with one or more acids. HCl, Na_2CO_3 and Na_2HPO_4 are all used to treat cellulose [64]. Cellulose acetate is a semi-synthetic polymer synthesized by

esterification of cellulose with acetic acid. This material is widely used in commercial applications, including film, fibers, plastic and coatings [65]. The treatment of cellulose by cyclic anhydride is a widely studied method for adding carboxyl groups to the surface of cellulose. Citrate and maleic anhydrides are also used in esterification reactions [66].

2.1.3.6 Oxidation

Cellulose is very sensitive to various oxidants because of its polyol structure. The extensive changes that occur in the oxidation process means that the physical and chemical properties of the product depend largely on a variety of factors, such as the oxidant used, the pH of the oxidizing medium and so on. The chemical structure of cellulose is changed by oxidation of the hydroxyl group to the corresponding carbonyl or carboxyl. A wide range of potential cellulose oxidants can be classified as non-selective oxidants and selective oxidants, such as periodates and nitroxyl radicals.

(1) Periodates

Periodate is a special oxidant capable of oxidizing the hydroxyl groups on adjacent carbon atoms (C2 and C3) in the glucose unit of cellulose to form two aldehyde groups. At the same time, the C-C bond between C2 and C3 is broken. The efficiency of iodate oxidation can be improved by using metal chloride which can break the intermolecular hydrogen bonds in the cellulose molecules [67]. The reaction time plays a crucial role in reaction efficiency. Increasing the reaction time can increase the number of aldehyde

groups formed. [68].

(2) Non-persistent nitroxyl radicals

Some non-persistent free radicals, such as N-hydroxyphthalimide (NHPI), N-hydroxybenzotriazole (HBT), violuric acid (VA), and N-hydroxy-3, 4, 5, 6-tetraphenylphthalimide (NHTPPI), have shown high oxidation efficiency of cellulose in the presence of dilute solutions of NaClO and NaBr at pH 10 at room temperature [69-72]. The reaction mechanism is the parent hydroxyl precursor being activated and transformed into the corresponding radical compound. In the presence of NaClO and NaBr, these nitroxyl radicals are oxidized to N-oxammonium ions, at which point the primary hydroxyl group of cellulose is converted to the carboxyl group in the aldehyde stage. This process appears to be selective, and the morphology of the oxidized cellulose does not appear to change.

(3) Stable nitroxyl radicals

Nooy et al. first applied TEMPO-mediated oxidation to water-soluble polysaccharides (such as potato starch, starch dextrin and pullulan), in which NaClO was the main oxidant, with co-catalyst NaBr and catalyst TEMPO at pH 10-11. The C6 primary hydroxyl groups of polysaccharides were selectively oxidized to carboxyl groups, and the corresponding polysaccharide aldehyde acid was quantitatively obtained [73, 74]. Chang and Robyt applied TEMPO-mediated oxidation to water-soluble natural polysaccharides, water-soluble polysaccharide derivatives and water-insoluble natural

polysaccharides such as cellulose and chitin [75]. Isogai's group has published a series of papers that systematically explore the many details of TEMPO-oxidized cellulose. The effects of TEMPO dosage, oxidation time and temperature on carboxyl content and the degree of polymerization of cellulose were investigated. The comparison of TEMPO/NaBr/NaOCl and TEMPO/NaOCl/NaO_2Cl on cellulose oxidation at different pH value was also explored [76-80].

TEMPO-oxidation can efficiently transform cellulose with high reaction speed, high yield, good selectivity and mild reaction conditions. This method is highly selective, and the primary hydroxyl group is completely oxidized, while the secondary hydroxyl group is unaffected. TEMPO reacts in situ with the oxidant, resulting in the formation of the nitrosonium ion, which is then converted to N-hydroxy-2, 2, 6, 6-tetramethylpiperidine. In this process, the primary hydroxyl of cellulose is oxidized to a carboxyl group. The formation of 1 mole of carboxylic acid requires the consumption of 2 moles of nitrosonium ion. The optimal pH value of the reaction mixture (about 10.5) was maintained by adding an alkali to neutralize the carboxylic acid. Therefore, the consumption of sodium hydroxide can be used as a measure of the degree of transformation from OH groups to carboxyl groups [81].

When the pH was 10, the C6 hydroxyl group of cellulose was effectively converted to a sodium carboxylate group, thus preserving its original fiber morphology, crystallinity and crystal size. TEMPO, reaction time and temperature were found to be the key

factors that control cellulose depolymerization. In TEMPO-mediated oxidation, the depolymerization of cellulose is attributed to the presence of sodium hypochlorite in the system, which leads to a rupture of glucose unit C2-C3 and the formation of dialdehyde and dicarboxylic groups. In order to solve the depolymerization issue, some research has been done on the TEMPO/NaBr/NaOCl system. The results show that the TEMPO/NaOCl/$NaClO_2$ system under weakly acidic (pH=3.5-6.8) catalytic oxidation [82-85], electro-TEMPO-mediated oxidation of cellulose [86, 87], TEMPO/laccase/O_2 in water under neutral conditions [88, 89] and TEMPO/Na_2SO_4/NaClO at pH 10 [90] can obtain oxidized cellulose with a high degree of polymerization (DP).

Both stable and non-persistent nitroxyl radicals used as mediators require large amounts of sodium bromide (10-30%) to restart the catalytic cycle. However, from both an industrial and an environmental perspective, a process that does not include the use of sodium bromide would be a better option than the current process.

2.1.4 Grafting modification

Grafting of polymer to cellulose is an important means of modification of cellulose. Various specific groups can be connected to the main chain of cellulose by grafting the polymerization of different monomers, so that the grafted cellulose has targeted properties to meet the requirements of special applications. The active site of the reaction can be free radicals or chemical groups, and suitable polymers are grafted onto cellulose to form the grafted cellulose. The commonly used grafting methods are

chemical-initiation grafting, photografting, and high energy radiation grafting.

2.1.4.1 Chemical initiation grafting

Chemically-initiated grafting can be accomplished by radical or ionic polymerization. The initiator is very important because it determines the path of grafting in the chemical process [91]. Ammonium cerium nitrate (CAN), persulfates and azodiisobutyronitrile (AIBN) are mainly used as initiators in radical polymerization [92-94]. In ionic polymerization, a Lewis base liquid such as alkyl aluminum is usually used as the reactant. Grafting in melting and atom transfer free radical polymerization (ATRP) are promising grafting technologies.

2.1.4.2 Photografting

Photografting initiation is an effective method to introduce various vinyl monomers into cellulose materials. The energy of UV-light is absorbed by sensitizer, monomer, polymer or the electron band structure of excited cellulose molecule. The chromophore absorption of macromolecules is weak, and the excited molecular intermediates can be cleaved into active radicals to initiate the grafting reaction. If the absorption of light does not lead to free radical site formation through bond breaking, this process can be facilitated by the addition of photosensitizers [95].

Photografting cellulose materials has been widely studied due to the advantages of easy availability of UV-light sources, selective reaction and low light energy requirements.

Acrylonitrile was grafted onto the surface of cellulose by light grafting. Subsequently, the cyanide group reacted with hydroxylamine by the reaction amidoxime. Acrylonitrile photografted cellulose has been used for the removal of Cu(II) ions from an aqueous solution [96].

2.1.4.3 High energy radiation grafting

Radiation-induced grafting provides a unique advantage for the preparation of functional copolymers due to the simplicity and flexibility of reactions initiated by commercial ionizing radiation sources. Unlike photo priming and plasma priming, this technique can modify the surface of the main chain in stages [97]. There are two main methods of radiation-induced grafting: (1) simultaneous irradiation (direct or mutual irradiation) and (2) pre-irradiation. With the first method, the cellulose is immersed in pure monomer or a monomer solution and irradiated. The homopolymerization that may be initiated can be suppressed by applying a low radiation dose or adding inhibitors to grafting solutions [98]. With the pre-irradiation method, the cellulose is irradiated in a vacuum or inert medium to produce free radicals, and then brought into contact with the monomer under controlled conditions so as to initiate the grafting reaction. Cellulose modified by radiation-induced grafting can improve its flame retardant properties and its water resistance, wear resistance and corrosion resistance.

2.2 Immobilized TEMPO catalysts for cellulose oxidation

TEMPO mediated oxidation of cellulose is one of the effective ways to functionalize

cellulose by selective oxidation of C6 primary hydroxyl to aldehyde or carboxyl groups. In addition, this method has attracted extensive attention in the field of nano-cellulose preparation [99]. However, TEMPO is a toxic chemical to aquatic life and it cannot be released into waste effluent after oxidation, as it can accumulate in the environment. This issue creates a need to recycle TEMPO, and requires that the process is a sustainable technology. So, the re-use of TEMPO is critical to develop a green and cost-effective process for the preparation of oxidized cellulose.

The immobilization of free TEMPO onto organic and inorganic supports provides a potential method for easily recycling the catalyst. The immobilized TEMPO catalysts have been applied to selective oxidation of various low-molecular weight substances, such as benzyl alcohol and monosaccharides, and have shown excellent catalytic properties and good recycling performance. So far, only a few successful cases have been reported for cellulose oxidation using immobilized TEMPO as the catalyst.

By grafting 4-carboxyl-TEMPO to polyvinylamine (PVAm), Pelton et al. prepared a water-soluble PVAm-supported TEMPO (PVAm-TEMPO) to oxidize the C6 hydroxyl of cellulose to aldehyde groups. After oxidation, PVAm-TEMPO was grafted to the cellulose surface as a primer layer to promote wet cellulose-to-cellulose adhesion [100]. They also immobilized TEMPO on polyacrylic acid (PAA) by acylation between amino groups of 4-NH_2-TEMPO and carboxyl groups of PAA to produce another water-soluble nitroxide polymer of PAA-TEMPO. Unlike with PVAm-TEMPO, it was

necessary to adsorb a layer of PVAm on the surface of cellulose to make the PAA-TEMPO play a catalytic oxidation role. They aimed to graft PVAm onto the cellulose surface, and TEMPO recovery was not considered. However, these studies serve as useful references for future research on selective oxidation of cellulose with water-soluble polymers immobilized TEMPO as a catalyst.

Araki J. and Iida M. rafted 4-OH-TEMPO to polyethylene glycol 2000 (mPEG2000) to prepare a water-soluble catalyst of mPEG2000-TEMPO for selective catalytic oxidation of the C6 primary hydroxyl group of the cellulose [101]. mPEG2000-TEMPO was recovered by extraction using DCM and re-used for further oxidation cycles. The degree of oxidation of cellulose using mPEG2000-TEMPO as the catalyst was much lower than that of free TEMPO, especially when it was re-used [101].

Patankar S. and Renneckar S. prepared a magnetically separable TEMPO nano catalyst to oxidize cellulose pulp in water [102]. The catalyst was easily separated from the reaction mixture for re-use using an external magnet. The reaction rate with this heterogeneous solid catalyst was equivalent to about 50% of that of free TEMPO at 65 ℃. By increasing the reaction temperature and prolonging the reaction time, the degree of oxidation could meet the requirements for producing nanocellulose [102].

Recently, we synthesized a nitroxide block copolymer of poly (ethylene glycol)-b-poly(2, 2, 6, 6-tetramethylpiperidinyloxy-4-yl-methacrylate) (PEG-PTMA) using

activators regenerated by electron transfer atom transfer radical polymerization (ARGET ATRP) [103]. The catalytic oxidation performance of cellulose using this block copolymer in the water/acetonitrile medium were studied. The carboxyl content of oxidized cellulose obtained in the PEG-PTMA mediated oxidation reached 1.07 mmol/g - equivalent to 73.2% of the value for the oxidized cellulose with free TEMPO oxidation (1.46 mmol/g). Furthermore, the block copolymer was easy to recycle, and the activity did not decrease after four cycles. However, the catalytic activity decreased noticeably when water was used as the reaction medium. The reason may be that both the nitroxide radical copolymers and cellulose were water-insoluble polymers, and the contact between them was greatly restrained due to a high level of steric hindrance.

2.3 Applications of TOC

The TEMPO mediated oxidation of cellulose in a mild aqueous environment is a more environmentally friendly method for producing TOC. The resulting TOC demonstrates good crystallinity, a high aspect ratio, high zeta potential in an aqueous solution, high elastic modulus and high tensile strength. These characteristics result in TOC widely used in adsorbents, water purification membranes, energy storage and conversion materials, intelligent materials and other products (Table 2.3).

Table 2.3 The list of possible applications of modified cellulose reported in the literature

Applications fields		Schematic diagram	References
Adsorption	Organic pollutants	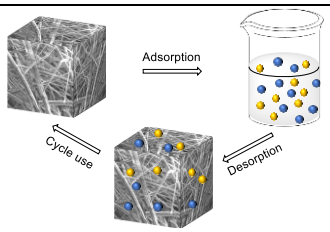	[107-110]
	Heavy metals		[111-114]
Energy and electronic devices	Lithium-ion batteries	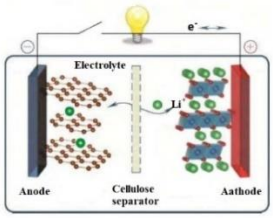	[115-121]
	Proton exchange membranes	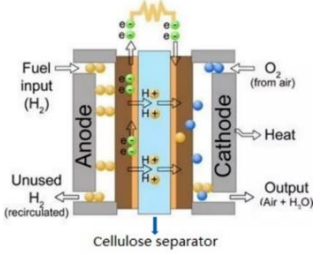	[122-125]
	Supercapacitors	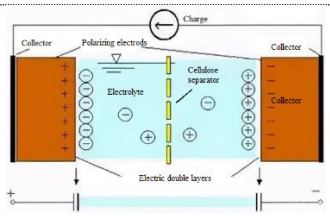	[126-128]
Water purification membranes	Microfiltration (MF)	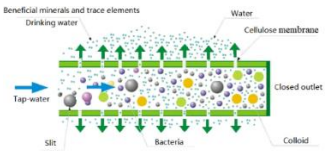	[129-135]
	Ultrafiltration (UF)		
	Nanofiltration (NF)		
	Reverse osmosis (RO)		
	Forward osmosis (FO)		
Smart materials	Thermal response membranes	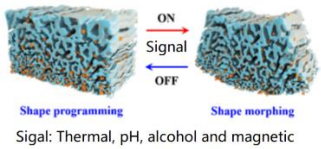 Sigal: Thermal, pH, alcohol and magnetic	[136-140]
	pH response membranes		
	Alcohol sensing devices		
	Magnetic hydrogels		
Other applications	Insulation materials		[141-146]
	Vapor resistance membranes		

Applications fields		Schematic diagram	References
	Catalytic membranes		
	Conductive membranes		
	Electronics		
	Food packaging		

2.3.1 Adsorption and removal of organic pollutants and heavy metals

Removing toxic and non-biodegradable heavy metals from wastewater is a challenging. In this regard, adsorption removal is one of the most effective and efficient processes. Common adsorbents such as activated carbon and molecular sieve, adsorption performance is good, but the price is expensive; Therefore, the use of environmentally friendly materials from natural resources has attracted attention. Cellulose is a promising resource because of its renewability.

In recent years, the application of TOC in the removal of organic compounds and heavy metals from water by electrostatic action has been widely studied. The Abundant carboxyl functional groups in TOC can adsorb cationic substances from aqueous solution. TOC has been reported to adsorb effectively diverse organic pollutants and heavy-metal cations, such as Ni(II), Cr(VI), Ag(I), Pb(II), Cu(II), Cd(II) and Co(II) [104-106].

2.3.1.1 Adsorption of organic pollutants

Several persistent organic pollutants are found in waterways, including oil, dye,

pharmaceutical products and pesticides. How to remove it has attracted extensive attention.

Recently, TOC-based adsorbents have been synthesized, and their capacity for adsorbing dye investigated. Batmaz R. et al. studied the capacity of TOC for adsorbing methylene blue (positively charged dye) [107]. The TOC adsorption capacity for methylene blue was improved to 769 mg/g approximately 6.5 times. Chen et al. synthesized high-intensity ultrasonicated TOC aerogel [108]. The aerogel demonstrated good adsorption of methylene blue and toluidine blue, due to their good ductility, flexibility and outstanding water uptake properties.

Hussain et al. prepared a graphene oxide (GO)/TOC monolith for adsorption of methylene blue. The adsorption capacity of the methylene blue was much higher than that of the reported GO-based adsorbents [109]. Melone et al. prepared adsorbent sponges for water remediation using TOC as a 3D scaffold and branched PEI as the crosslinking agent [110]. The p-nitrophenol adsorption capacity of the bPEI-TOC sponge was higher than that of microporous activated carbon, hyper-crosslinked magnetic polymer and nano-GO.

Organic pollutants are toxic water pollutant, which can be effectively removed by adsorption. TOC-based adsorbents have good adsorption capacity for organic pollutants and can be recycled by simple acid washing.

2.3.1.2 Adsorption of heavy metals

Copper is the most common metal ion pollutant in industrial wastewater. Liu et al. reported that TOC had a good adsorption effect on Cu(II) due to the presence of carboxylic acid groups on the surface, and the adsorption capacity was 75 mg/g, much higher than many other types of adsorption materials [111].

TOC was also used to remove various other metal ions from aqueous solutions. Isobe et al. prepared TEMPO-oxidized cellulose hydrogel. It has good adsorption capacity for Cu(II), and the maximum adsorption capacity is 268.2 mg/g. In addition, TOC gel also has high adsorption capacity for other harmful metal ions [112].

Yang et al. prepared TOC and polyacrylonitrile (PAN) nanofiber membranes [113]. The membrane showed good adsorption capacity for Cr(VI) and Pb(II) due to the large specific surface areas and high concentration of sulfhydryl group. Isogai et al. used TOC to remove multiple metal ions [114].

In conclusion, the removal of metal ions in aqueous solution by adsorbent materials is mainly driven by electrostatic interaction and the complexation between TOC and metal ions. TOC-based adsorbents have good adsorption capacity for organic pollutants and metal ions.

2.3.2 Energy and electronic devices

2.3.2.1 Lithium-ion batteries

Owing to the excellent energy density, rapid charging, high operating voltage, low self-discharge rate and high service life, lithium-ion batteries (LIBs) have become an important element in energy-storage systems. Polyethylene (PE) and polypropylene (PP) based membranes have been widely used as separators in LIBs. However, low porosity and poor electrolyte wettability affect electrolyte storage capacity and limit ionic conductivity and LIB performance. Additionally, PP and PE membranes have low thermal stability, resulting in rapid thermal shrinkage and safety problems. Therefore, it is necessary to develop new separators with excellent electrolyte wettability and high heat resistance for LIBs [115-117]. Cellulose has been widely studied as a separation material in LIBs due to its excellent good thermal stability electrolyte wettability, and good mechanical properties. Several reports have reported the use of TOC for electrochemical devices such as Li/Na-ion batteries.

TOC has good mechanical properties as a binder for flexible LIBs. Lu et al. prepared flexible LIBs electrode with TOC as a binder [118]. Huang et al. successfully prepared bacterial TOC membranes with rich porosity and good affinity for lithium electrode and liquid electrolyte, and used them as separation membranes for LIBs batteries [119].

LIBs already dominate the market of power supplies for portable electronic devices. However, lithium is expensive and environmentally unfriendly to extract, which limits

the further development of energy-storage devices. Sodium-ion batteries (NIBs) have attracted much attention due to the abundance and cheap of sodium salts recently [120]. Shen et al. prepared NIB anodes using TOC. The anode showed good cycling stability, which indicates the potential of TOC in the development of cheap NIBs [121].

2.3.2.2 Proton exchange membranes (PEM)

PEM fuel cells are widely used in fuel generation. An important component of a PEM fuel cell is two electrodes separated by a PEM. Nafion is a sulfonated tetrafluoroethylene fluoropolymer widely used in PEM fuel cells as a membrane material with excellent chemical and mechanical stability. However, Nafion is expensive and exhibits low proton conductivity, high gas permeability and low thermal stability due to high temperature dehydration [122, 123].

Jankowska et al. studied different types of cellulose used in PEM. TOC has the best conductivity compared to other materials. This may be related to carboxyl groups on TOC surface, which are effective proton receptors and donors [124]. Guccini et al. used TOC membrane as the power source of fuel cell, showing high proton conductivity [125].

In conclusion, TOC membranes have shown great potential for the construction of a new generation of PEM fuel cells due to their excellent environmental performance.

2.3.2.3 Supercapacitors

Flexible supercapacitors are very competitive energy-storage devices and have been widely used in wearable electronic products. However, the development of flexible supercapacitors with low cost and high performance using sustainable materials remains a challenge. Thin and high-performance flexible electrodes can be obtained by selecting TOC aerogel with high porosity and electrolyte absorption [126, 127].

Zhou et al. prepared conductive MOF (c-MOF) nanolayers on TOC by interface synthesis of TOC as supports for the growth of c-MOF nanolayers. The TOC/c-MOF hybrid nanofibers can be assembled into suspended nanoparticles easily, showing excellent electrical conductivity, layered micro-meso-porosity and excellent mechanical properties [128].

2.3.3 Water purification

Membrane separation technology includes microfiltration (MF), ultrafiltration (UF), nanofiltration (NF), reverse osmosis (RO) and forward osmosis (FO) based on membrane aperture. It is an important commercial water treatment option because of its efficiency, low cost and ease of operation [129]. Polymer membrane is widely used because of its low cost and good processing performance. TOC has also been shown to an excellent raw material because of its special chemical and mechanical properties and the ability to form different structures that exhibit good filtration propertiese [130-132].

Ma et al. prepared a TOC MF membrane with high negative charge on the membrane surface that exhibited good rejection of bacteria, and thus showed good adsorption ability for a positively charged dye (crystal violet), which was 16 times higher than the commercial MF film [133].

Ma et al. used TOC to fix the top barrier layer of the novel UF membrane on a PAN/PET substrate with a maximum aperture of about 55 nm. Transmittance of the TOC-based UF membrane was five times greater than the control membrane. In the oil-water emulsion UF test, the water permeance of the TOC-based UF membrane was about eight times greater than the control membrane [134].

Thin-film composite (TFC) membranes are commonly used in NF, RO and FO. The TFC membranes show high salt rejection and good water flux that far exceeds that of first-generation RO membranes. They are composed of a dense polyamide surface and substrate layer. TFC membranes have been widely used in seawater desalination due to their excellent filtration performance and wide pH range of applications (pH=2-11) [135].

In summary, compared with traditional membranes, using TOC as a membrane material can significantly improve membrane flux. TOC is very hydrophilic and can form water channels in the matrix when used as a dielectric layer for composite membranes. Due to its excellent performance, TOC has broad application prospects in terms of water

treatment as a high-flux membrane.

2.3.4 Smart materials

Smart responsive materials can reversibly self-adjust their form or chemical structure in response to chemical or physical signals or stimuli, resulting in reversible changes in many properties, such as permeability, wettability, ductility and surface activity. Smart responsive materials that use TOC with non-toxic, stable, functional surfaces are attracting increasing interest in smart materials applications. In recent years, TOC has been applied to smart materials due to its low cost, reproducibility and biocompatibility, including thermal response membranes, pH response membranes, alcohol sensing devices and magnetic hydrogels [136].

Hakalahti et al. used PNIPAM to modify TOC membranes and developed a novel thermal response membrane [137]. The water permeability of the membrane varies with temperature. In aqueous solution, PNIPAM changed from a hydrophilic state to a hydrophobic state above the LCST (32 ℃) [137].

TOC with pH-responsive properties exhibits interesting properties for biomedical and food safety applications. Way et al. prepared a pH-responsive material, which exhibited good pH-responsive wettability with a rapid wettability change from hydrophilic to hydrophobic when the pH changed from acidic to alkaline conditions [138].

Sensor devices convert changes in the physical environment into readable signals. Xu et al. assembled an alcohol sensing device containing a membrane sensor composed of bacterial TOC, which showed high ethanol selectivity by intelligently distinguishing ethanol from water [139].

Due to the weak mechanical strength of traditional magnetic hydrogels, their applications are severely limited. Wang et al. prepared self-recovery magnetic hydrogels with outstanding mechanical properties and good magnetic properties, by dispersing Fe_3O_4 nanoparticles uniformly in polyacrylamide (PAM) hydrogel with the help of TOC. Due to the network structure and chemical reactions between hydrogels, the tensile strength is increased from 150 kPa to 780 kPa [140].

2.3.5 Other applications

In addition to the water purification membranes, energy applications and smart materials discussed above, materials based on TOC have been explored in many other areas, such as insulation materials, vapor resistance membranes, catalytic membranes and conductive membranes and in the field of electronics and food packaging [141-146].

2.4 Conclusion

Cellulose material has become a promising green material because of its unique structure, good mechanical properties, sustainability and richness. Cellulose can be

functionalized with carboxyl groups. Free TEMPO was supported on organic and inorganic carriers to realize the recycling of catalyst.

Recent advances with TOC in environmental remediation, energy, smart materials and other fields were discussed. Although functionalized TOC often displays good performance that is comparable or even superior to traditional materials, further research is required to explore the use of TOC-based materials or membranes for various applications, with recyclability and reusability in the long term.

References

[1] Zhang X, Ma X, Hou T, et al. Inorganic salts induce thermally reversible and anti-freezing cellulose hydrogels [J]. Angewandte Chemie International Edition, 2019, 58(22): 7366-7370.

[2] Moon R, Martini A, Nairn J, et al. Cellulose nanomaterials review: Structure, properties and nanocomposites [J]. Chemical Society Reviews, 2011, 40(7): 3941-3994.

[3] Ling S, Chen W, Fan Y, et al. Biopolymer nanofibrils: Structure, modeling, preparation, and applications [J]. Progress in Polymer Science, 2018, 85: 1-56.

[4] Luo X, Zhang L. New solvents and functional materials prepared from cellulose solutions in alkali/urea aqueous system [J]. Food Research International, 2013, 52(1): 387-400.

[5] Klemm D, Heublein B, Fink H, et al. Cellulose: Fascinating biopolymer and sustainable raw material [J]. Angewandte Chemie International Edition, 2005, 44(22): 3358-3393.

[6] Liu H, Cheng G, Kent M, et al. Simulations reveal conformational changes of methylhydroxyl groups during dissolution of cellulose Iβ in ionic liquid 1-ethyl-3-methylimidazolium acetate [J]. The Journal of Physical Chemistry B, 2012, 116(28): 8131-8138.

[7] Nishiyama Y. Structure and properties of the cellulose microfibril [J]. Journal of Wood Science, 2009, 55(4): 241-249.

[8] Liebert T. Cellulose solvents-remarkable history, bright future [M]. Cellulose

Solvents: For Analysis, Shaping and Chemical Modification. American Chemical Society, 2010: 3-54.

[9] Perez S, Samain D. Structure and engineering of celluloses [J]. Advances in Carbohydrate Chemistry and Biochemistry, 2010, 64: 25-116.

[10] Zhao H, Kwak J, Wang Y, et al. Interactions between cellulose and N-methylmorpholine-N-oxide [J]. Carbohydrate Polymers, 2007, 67(1): 97-103.

[11] McCormick C, Callais P, Hutchinson Jr B. Solution studies of cellulose in lithium chloride and N, N-dimethylacetamide [J]. Macromolecules, 1985, 18(12): 2394-2401.

[12] Waghorne W, Ward A, Clune T, et al. Effect of different cations on the N-CO rotational barrier of N, N-dimethylacetamide. Variable temperature proton magnetic resonance study [J]. Journal of the Chemical Society, Faraday Transactions 1: Physical Chemistry in Condensed Phases, 1980, 76: 1131-1137.

[13] Seger B, Burchard W. Structure of cellulose in cuoxam [C]. Macromolecular Symposia. Basel: Hüthig & Wepf Verlag, 1994, 83(1): 291-310.

[14] Saalwächter K, Burchard W, Klüfers P, et al. Cellulose solutions in water containing metal complexes [J]. Macromolecules, 2000, 33(11): 4094-4107.

[15] Pinkert A, Marsh K, Pang S, et al. Ionic liquids and their interaction with cellulose [J]. Chemical Reviews, 2009, 109(12): 6712-6728.

[16] Liu J, Lam J, Tang B. Acetylenic polymers: Syntheses, structures, and functions [J]. Chemical Reviews, 2009, 109(11): 5799-5867.

[17] Wang H, Gurau G, Rogers R. Ionic liquid processing of cellulose [J]. Chemical Society Reviews, 2012, 41(4): 1519-1537.

[18] Zhang J, Zhang H, Wu J, et al. NMR spectroscopic studies of cellobiose solvation in EmimAc aimed to understand the dissolution mechanism of cellulose in ionic liquids [J]. Physical Chemistry Chemical Physics, 2010, 12(8): 1941-1947.

[19] Sen S, Martin J, Argyropoulos D S. Review of cellulose non-derivatizing solvent interactions with emphasis on activity in inorganic molten salt hydrates [J]. ACS Sustainable Chemistry & Engineering, 2013, 1(8): 858-870.

[20] Heinze T, Dicke R, Koschella A, et al. Effective preparation of cellulose derivatives in a new simple cellulose solvent [J]. Macromolecular Chemistry and Physics, 2000, 201(6): 627-631.

[21] Köhler S, Heinze T. New solvents for cellulose: Dimethyl sulfoxide/ammonium fluorides [J]. Macromolecular Bioscience, 2007, 7(3): 307-314.

[22] Xu D, Edgar K. TBAF and cellulose esters: Unexpected deacylation with unexpected regioselectivity [J]. Biomacromolecules, 2012, 13(2): 299-303.

[23] Fischer S, Thümmler K, Pfeiffer K, et al. Evaluation of molten inorganic salt hydrates as reaction medium for the derivatization of cellulose [J]. Cellulose, 2002, 9(3): 293-300.

[24] Fischer S, Voigt W, Fischer K. The behaviour of cellulose in hydrated melts of the composition $LiX \cdot n\ H_2O$ ($X= I^-, NO_3^-, CH_3COO^-, ClO_4^-$) [J]. Cellulose, 1999, 6(3): 213-219.

[25] Lu X, Shen X. Solubility of bacteria cellulose in zinc chloride aqueous solutions [J]. Carbohydrate Polymers, 2011, 86(1): 239-244.

[26] Fischer S, Thümmler K. Molten inorganic salts as reaction medium for cellulose

[M]. Cellulose Solvents: For Analysis, Shaping and Chemical Modification. American Chemical Society, 2010: 91-101.

[27] Fischer S, Leipner H, Thümmler K, et al. Inorganic molten salts as solvents for cellulose [J]. Cellulose, 2003, 10(3): 227-236.

[28] Isogai A, Atalla R. Dissolution of cellulose in aqueous NaOH solutions [J]. Cellulose, 1998, 5(4): 309-319.

[29] Wang Y, Liu L, Chen P, et al. Cationic hydrophobicity promotes dissolution of cellulose in aqueous basic solution by freezing-thawing [J]. Physical Chemistry Chemical Physics, 2018, 20(20): 14223-14233.

[30] Cai J, Zhang L. Rapid dissolution of cellulose in LiOH/urea and NaOH/urea aqueous solutions [J]. Macromolecular Bioscience, 2005, 5(6): 539-548.

[31] Wang S, Lu A, Zhang L. Recent advances in regenerated cellulose materials [J]. Progress in Polymer Science, 2016, 53: 169-206.

[32] Duan B, Tu H, Zhang L. Material research progress of the sustainable polymer-cellulose [J]. Acta Polymerica Sinica, 2020, 51(1): 66-86.

[33] Zhao D, Shi X, Liu T, et al. Synthesis of surfactant-free hydroxypropyl methylcellulose nanogels for controlled release of insulin [J]. Carbohydrate Polymers, 2016, 151: 1006-1011.

[34] Ghorpade V, Yadav A, Dias R. Citric acid crosslinked cyclodextrin/hydroxypropylmethylcellulose hydrogel films for hydrophobic drug delivery [J]. International Journal of Biological Macromolecules, 2016, 93: 75-86.

[35] Larsson M, Hjärtstam J, Larsson A. Novel nanostructured microfibrillated

cellulose–hydroxypropyl methylcellulose films with large one-dimensional swelling and tunable permeability [J]. Carbohydrate Polymers, 2012, 88(2): 763-771.

[36] Zeeshan R, Mutahir Z, Iqbal H, et al. Hydroxypropylmethyl cellulose (HPMC) crosslinked chitosan (CH) based scaffolds containing bioactive glass (BG) and zinc oxide (ZnO) for alveolar bone repair [J]. Carbohydrate Polymers, 2018, 193: 9-18.

[37] Seyedlar R, Nodehi A, Atai M, et al. Gelation behavior of in situ forming gels based on HPMC and biphasic calcium phosphate nanoparticles [J]. Carbohydrate Polymers, 2014, 99: 257-263.

[38] Sun N, Wang T, Yan X. Self-assembled supermolecular hydrogel based on hydroxyethyl cellulose: Formation, in vitro release and bacteriostasis application [J]. Carbohydrate Polymers, 2017, 172: 49-59.

[39] Kong B, Kim A, Park S. Properties and in vitro drug release of hyaluronic acid-hydroxyethyl cellulose hydrogels for transdermal delivery of isoliquiritigenin [J]. Carbohydrate Polymers, 2016, 147: 473-481.

[40] Zhao Y, He M, Jin H, et al. Construction of highly biocompatible hydroxyethyl cellulose/soy protein isolate composite sponges for tissue engineering [J]. Chemical Engineering Journal, 2018, 341: 402-413.

[41] El Fawal G, Abu-Serie M, Hassan M, et al. Hydroxyethyl cellulose hydrogel for wound dressing: Fabrication, characterization and in vitro evaluation [J]. International Journal of Biological Macromolecules, 2018, 111: 649-659.

[42] Basta A, El-Saied H, Hasanin M, et al. Green carboxymethyl cellulose-silver complex versus cellulose origins in biological activity applications [J]. International

Journal of Biological Macromolecules, 2018, 107: 1364-1372.

[43] Rasoulzadeh M, Namazi H. Carboxymethyl cellulose/graphene oxide bio-nanocomposite hydrogel beads as anticancer drug carrier agent [J]. Carbohydrate Polymers, 2017, 168: 320-326.

[44] Benhalima T, Ferfera-Harrar H, Lerari D. Optimization of carboxymethyl cellulose hydrogels beads generated by an anionic surfactant micelle templating for cationic dye uptake: Swelling, sorption and reusability studies [J]. International Journal of Biological Macromolecules, 2017, 105: 1025-1042.

[45] Salama A, Etri S, Mohamed S, et al. Carboxymethyl cellulose prepared from mesquite tree: New source for promising nanocomposite materials [J]. Carbohydrate polymers, 2018, 189: 138-144.

[46] Ogawa A, Nakayama S, Uehara M, et al. Pharmaceutical properties of a low-substituted hydroxypropyl cellulose (L-HPC) hydrogel as a novel external dressing [J]. International Journal of Pharmaceutics, 2014, 477(1-2): 546-552.

[47] Miao L, Hu J, Lu M, et al. Alkynyl-functionalization of hydroxypropyl cellulose and thermoresponsive hydrogel thereof prepared with P(NIPAAm-co-HEMAPCL) [J]. Carbohydrate Polymers, 2016, 137: 433-440.

[48] Ngah W, Hanafiah M. Removal of heavy metal ions from wastewater by chemically modified plant wastes as adsorbents: A review [J]. Bioresource Technology, 2008, 99(10): 3935-3948.

[49] O'Connell D, Birkinshaw C, O'Dwyer T. Heavy metal adsorbents prepared from the modification of cellulose: A review [J]. Bioresource Technology, 2008, 99(15):

6709-6724.

[50] Güçlü G, Gürdağ G, Özgümüş S. Competitive removal of heavy metal ions by cellulose graft copolymers [J]. Journal of Applied Polymer Science, 2003, 90(8): 2034-2039.

[51] Banvillet G, Depres G, Belgacem N, et al. Alkaline treatment combined with enzymatic hydrolysis for efficient cellulose nanofibrils production [J]. Carbohydrate Polymers, 2021, 255: 117383.

[52] Melikoğlu A, Bilek S, Cesur S. Optimum alkaline treatment parameters for the extraction of cellulose and production of cellulose nanocrystals from apple pomace [J]. Carbohydrate Polymers, 2019, 215: 330-337.

[53] Wang B, Sain M. Isolation of nanofibers from soybean source and their reinforcing capability on synthetic polymers [J]. Composites Science and Technology, 2007, 67(11-12): 2521-2527.

[54] Dufresne A, Dupeyre D, Vignon M. Cellulose microfibrils from potato tuber cells: Processing and characterization of starch-cellulose microfibril composites [J]. Journal of Applied Polymer Science, 2000, 76(14): 2080-2092.

[55] Wang B, Sain M, Oksman K. Study of structural morphology of hemp fiber from the micro to the nanoscale [J]. Applied Composite Materials, 2007, 14(2): 89-103.

[56] Xie Y, Hill C, Xiao Z, et al. Silane coupling agents used for natural fiber/polymer composites: A review [J]. Composites Part A: Applied Science and Manufacturing, 2010, 41(7): 806-819.

[57] Hokkanen S, Repo E, Suopajärvi T, et al. Adsorption of Ni(II), Cu(II) and Cd(II)

from aqueous solutions by amino modified nanostructured microfibrillated cellulose [J]. Cellulose, 2014, 21(3): 1471-1487.

[58] Fox S, Li B, Xu D, et al. Regioselective esterification and etherification of cellulose: A review [J]. Biomacromolecules, 2011, 12(6): 1956-1972.

[59] Navarro R, Sumi K, Matsumura M. Improved metal affinity of chelating adsorbents through graft polymerization [J]. Water Research, 1999, 33(9): 2037-2044.

[60] Zheng L, Dang Z, Yi X, et al. Equilibrium and kinetic studies of adsorption of Cd (II) from aqueous solution using modified corn stalk [J]. Journal of Hazardous Materials, 2010, 176(1-3): 650-656.

[61] Saliba R, Gauthier H, Gauthier R, et al. Adsorption of copper (II) and chromium (III) ions onto amidoximated cellulose [J]. Journal of Applied Polymer Science, 2000, 75(13): 1624-1631.

[62] Donia A, Yousif A, Atia A, et al. Preparation and characterization of modified cellulose adsorbents with high surface area and high adsorption affinity for Hg (II) [J]. Journal of Dispersion Science and Technology, 2014, 35(3): 380-389.

[63] Zhou Y, Jin Q, Zhu T, et al. Separation of chromium (VI) from aqueous solutions by cellulose modified with D-glucose and quaternary ammonium groups [J]. Cellulose Chemistry and Technology, 2012, 46(5): 319.

[64] Velazquez-Jimenez L, Pavlick A, Rangel-Mendez J. Chemical characterization of raw and treated agave bagasse and its potential as adsorbent of metal cations from water [J]. Industrial Crops and Products, 2013, 43: 200-206.

[65] Yang J, Kubota F, Baba Y, et al. Application of cellulose acetate to the selective

adsorption and recovery of Au (III) [J]. Carbohydrate Polymers, 2014, 111: 768-774.

[66] Chand P, Shil A K, Sharma M, et al. Improved adsorption of cadmium ions from aqueous solution using chemically modified apple pomace: Mechanism, kinetics, and thermodynamics [J]. International Biodeterioration & Biodegradation, 2014, 90: 8-16.

[67] Magnin D, Dumitriu S. Interactions between polysaccharides and polypeptides [J]. Polysaccharides: Structural Diversity and Functional Versatility, 2005: 305-306.

[68] Sirvio J, Hyvakko U, Liimatainen H, et al. Periodate oxidation of cellulose at elevated temperatures using metal salts as cellulose activators [J]. Carbohydrate Polymers, 2011, 83(3): 1293-1297.

[69] Saito T, Nishiyama Y, Putaux J, et al. Homogeneous suspensions of individualized microfibrils from TEMPO-catalyzed oxidation of native cellulose [J]. Biomacromolecules, 2006, 7(6): 1687-1691.

[70] Biliuta G, Fras L, Drobota M, et al. Comparison study of TEMPO and phthalimide-N-oxyl (PINO) radicals on oxidation efficiency toward cellulose [J]. Carbohydrate Polymers, 2013, 91(2): 502-507.

[71] Isogai A, Hänninen T, Fujisawa S, et al. Catalytic oxidation of cellulose with nitroxyl radicals under aqueous conditions [J]. Progress in Polymer Science, 2018, 86: 122-148.

[72] Coseri S, Nistor G, Fras L, et al. Mild and selective oxidation of cellulose fibers in the presence of N-hydroxyphthalimide [J]. Biomacromolecules, 2009, 10(8): 2294-2299.

[73] De Nooy A, Besemer A, Van Bekkum H. Highly selective nitroxyl radical-

mediated oxidation of primary alcohol groups in water-soluble glucans [J]. Carbohydrate Research, 1995, 269(1): 89-98.

[74] De Nooy A, Besemer A, Van Bekkum H. Selective oxidation of primary alcohols mediated by nitroxyl radical in aqueous solution. Kinetics and mechanism [J]. Tetrahedron, 1995, 51(29): 8023-8032.

[75] Chang P, Robyt J. Oxidation of primary alcohol groups of naturally occurring polysaccharides with 2, 2, 6, 6-tetramethyl-1-piperidine oxoammonium ion [J]. Journal of Carbohydrate Chemistry, 1996, 15(7): 819-830.

[76] Saito T, Isogai A. A novel method to improve wet strength of paper [J]. Tappi Journal (2002), 2005, 4(3): 3-8.

[77] Saito T, Hirota M, Tamura N, et al. Individualization of nano-sized plant cellulose fibrils by direct surface carboxylation using TEMPO catalyst under neutral conditions [J]. Biomacromolecules, 2009, 10(7): 1992-1996.

[78] Isogai A, Kato Y. Preparation of polyuronic acid from cellulose by TEMPO-mediated oxidation [J]. Cellulose, 1998, 5(3): 153-164.

[79] Bragd P, Van Bekkum H, Besemer A. TEMPO-mediated oxidation of polysaccharides: Survey of methods and applications [J]. Topics in Catalysis, 2004, 27(1): 49-66.

[80] Kuramae R, Saito T, Isogai A. TEMPO-oxidized cellulose nanofibrils prepared from various plant holocelluloses [J]. Reactive and Functional Polymers, 2014, 85: 126-133.

[81] Bordenave N, Grelier S, Coma V. Advances in selective C-6 oxidation of chitosan

by TEMPO [J]. Biomacromolecules, 2008, 9(9): 2377-2382.

[82] Saito T, Hirota M, Tamura N, et al. Oxidation of bleached wood pulp by TEMPO/NaClO/$NaClO_2$ system: Effect of the oxidation conditions on carboxylate content and degree of polymerization [J]. Journal of Wood Science, 2010, 56(3): 227-232.

[83] Saito T, Hirota M, Tamura N, et al. Individualization of nano-sized plant cellulose fibrils by direct surface carboxylation using TEMPO catalyst under neutral conditions [J]. Biomacromolecules, 2009, 10(7): 1992-1996.

[84] Isogai A, Saito T, Fukuzumi H. TEMPO-oxidized cellulose nanofibers [J]. Nanoscale, 2011, 3(1): 71-85.

[85] Li J, Kong M, Cheng X, et al. Preparation of biocompatible chitosan grafted poly (lactic acid) nanoparticles [J]. International Journal of Biological Macromolecules, 2012, 51(3): 221-227.

[86] Isogai T, Saito T, Isogai A. Wood cellulose nanofibrils prepared by TEMPO electro-mediated oxidation [J]. Cellulose, 2011, 18(2): 421-431.

[87] Jin Y, Edler K, Marken F, et al. Voltammetric optimisation of TEMPO-mediated oxidations at cellulose fabric [J]. Green Chemistry, 2014, 16(6): 3322-3327.

[88] Jiang J, Ye W, Liu L, et al. Cellulose nanofibers prepared using the TEMPO/laccase/O_2 system [J]. Biomacromolecules, 2017, 18(1): 288-294.

[89] Quintana E, Roncero M, Vidal T, et al. Cellulose oxidation by Laccase-TEMPO treatments [J]. Carbohydrate Polymers, 2017, 157: 1488-1495.

[90] Yui Y, Tanaka C, Isogai A. Functionalization of cotton fabrics by TEMPO-

mediated oxidation [J]. Sen'i Gakkaishi, 2013, 69: 222-228.

[91] Bhattacharya A, Misra B. Grafting: A versatile means to modify polymers: Techniques, factors and applications [J]. Progress in Polymer Science, 2004, 29(8): 767-814.

[92] Okieimen F, Sogbaike C, Ebhoaye J. Removal of cadmium and copper ions from aqueous solution with cellulose graft copolymers [J]. Separation and Purification Technology, 2005, 44(1): 85-89.

[93] Wojnárovits L, Földváry C, Takács E. Radiation-induced grafting of cellulose for adsorption of hazardous water pollutants: A review [J]. Radiation Physics and Chemistry, 2010, 79(8): 848-862.

[94] Navarro R, Sumi K, Matsumura M. Improved metal affinity of chelating adsorbents through graft polymerization [J]. Water Research, 1999, 33(9): 2037-2044.

[95] Yamada K, Saitoh Y, Haga Y, et al. Adsorption and desorption properties of grafted polyethylene films modified with polyethylenimine chains [J]. Journal of Applied Polymer Science, 2006, 102(6): 5965-5976.

[96] Kubota H, Shigehisa Y. Introduction of amidoxime groups into cellulose and its ability to adsorb metal ions [J]. Journal of Applied Polymer Science, 1995, 56(2): 147-151.

[97] Hemvichian K, Chanthawong A, Suwanmala P. Synthesis and characterization of superabsorbent polymer prepared by radiation-induced graft copolymerization of acrylamide onto carboxymethyl cellulose for controlled release of agrochemicals [J]. Radiation Physics and Chemistry, 2014, 103: 167-171.

[98] Desmet G, Takács E, Wojnárovits L, et al. Cellulose functionalization via high-energy irradiation-initiated grafting of glycidyl methacrylate and cyclodextrin immobilization [J]. Radiation Physics and Chemistry, 2011, 80(12): 1358-1362.

[99] Saito T, Isogai A. TEMPO-mediated oxidation of native cellulose. The effect of oxidation conditions on chemical and crystal structures of the water-insoluble fractions [J]. Biomacromolecules, 2004, 5(5): 1983-1989.

[100] Pelton R, Ren P, Liu J, et al. Polyvinylamine-graft-TEMPO adsorbs onto, oxidizes, and covalently bonds to wet cellulose [J]. Biomacromolecules, 2011, 12(4): 942-948.

[101] Araki J, Iida M. Surface carboxylation of cellulose nanowhiskers using mPEG-TEMPO: Its recovery and recycling [J]. Polymer Journal, 2016, 48(10): 1029-1033.

[102] Patankar S, Renneckar S. Greener synthesis of nanofibrillated cellulose using magnetically separable TEMPO nanocatalyst [J]. Green Chemistry, 2017, 19(20): 4792-4797.

[103] Liu S, Xing Y, Han J, et al. Catalytic oxidation of cellulose with a novel amphiphilic nitroxide block copolymer as a recoverable catalyst [J]. Cellulose, 2017, 24(9): 3635-3644.

[104] Karn B, Kuiken T, Otto M. Nanotechnology and in situ remediation: A review of the benefits and potential risks [J]. Environmental Health Perspectives, 2009, 117(12): 1813-1831.

[105] Fiol N, Vásquez M, Pereira M, et al. TEMPO-oxidized cellulose nanofibers as potential Cu (II) adsorbent for wastewater treatment [J]. Cellulose, 2019, 26(2): 903-

916.

[106] Zhu C, Liu P, Mathew A. Self-assembled TEMPO cellulose nanofibers: Graphene oxide-based biohybrids for water purification [J]. ACS Applied Materials & Interfaces, 2017, 9(24): 21048-21058.

[107] Batmaz R, Mohammed N, Zaman M, et al. Cellulose nanocrystals as promising adsorbents for the removal of cationic dyes [J]. Cellulose, 2014, 21(3): 1655-1665.

[108] Chen W, Li Q, Wang Y, et al. Comparative study of aerogels obtained from differently prepared nanocellulose fibers [J]. ChemSusChem, 2014, 7(1): 154-161.

[109] Hussain A, Li J, Wang J, et al. Hybrid monolith of graphene/TEMPO-oxidized cellulose nanofiber as mechanically robust, highly functional, and recyclable adsorbent of methylene blue dye [J]. Journal of Nanomaterials, 2018, 2018.

[110] Melone L, Rossi B, Pastori N, et al. TEMPO-oxidized cellulose cross-linked with branched polyethyleneimine: Nanostructured adsorbent sponges for water remediation [J]. ChemPlusChem, 2015, 80(9): 1408-1415.

[111] Liu P, Oksman K, Mathew A. Surface adsorption and self-assembly of Cu(II) ions on TEMPO-oxidized cellulose nanofibers in aqueous media [J]. Journal of Colloid and Interface Science, 2016, 464: 175-182.

[112] Isobe N, Chen X, Kim U, et al. TEMPO-oxidized cellulose hydrogel as a high-capacity and reusable heavy metal ion adsorbent [J]. Journal of Hazardous Materials, 2013, 260: 195-201.

[113] Yang R, Aubrecht K, Ma H, et al. Thiol-modified cellulose nanofibrous composite membranes for chromium(VI) and lead(II) adsorption [J]. Polymer, 2014,

55(5): 1167-1176.

[114] Saito T, Isogai A. Ion-exchange behavior of carboxylate groups in fibrous cellulose oxidized by the TEMPO-mediated system [J]. Carbohydrate Polymers, 2005, 61(2): 183-190.

[115] Huang X. Separator technologies for lithium-ion batteries [J]. Journal of Solid State Electrochemistry, 2011, 15(4): 649-662.

[116] Lee K T, Jeong S, Cho J. Roles of surface chemistry on safety and electrochemistry in lithium ion batteries [J]. Accounts of Chemical Research, 2013, 46(5): 1161-1170.

[117] Huang C, Ji H, Yang Y, et al. TEMPO-oxidized bacterial cellulose nanofiber membranes as high-performance separators for lithium-ion batteries [J]. Carbohydrate Polymers, 2020, 230: 115570.

[118] Lu H, Behm M, Leijonmarck S, et al. Flexible paper electrodes for li-ion batteries using low amount of TEMPO-oxidized cellulose nanofibrils as binder [J]. ACS Applied Materials & Interfaces, 2016, 8(28): 18097-18106.

[119] Huang C, Ji H, Yang Y, et al. TEMPO-oxidized bacterial cellulose nanofiber membranes as high-performance separators for lithium-ion batteries [J]. Carbohydrate Polymers, 2020, 230: 115570.

[120] Slater M, Kim D, Lee E, et al. Sodium-ion batteries [J]. Advanced Functional Materials, 2013, 23(8): 947-958.

[121] Shen F, Zhu H, Luo W, et al. Chemically crushed wood cellulose fiber towards high-performance sodium-ion batteries [J]. ACS Applied Materials & Interfaces, 2015,

7(41): 23291-23296.

[122] Wang Y, Chen K, Mishler J, et al. A review of polymer electrolyte membrane fuel cells: Technology, applications, and needs on fundamental research [J]. Applied Energy, 2011, 88(4): 981-1007.

[123] Bae B, Yoda T, Miyatake K, et al. Proton-conductive aromatic ionomers containing highly sulfonated blocks for high-temperature-operable fuel cells [J]. Angewandte Chemie International Edition, 2010, 49(2): 317-320.

[124] Jankowska I, Pankiewicz R, Pogorzelec-Glaser K, et al. Comparison of structural, thermal and proton conductivity properties of micro- and nanocelluloses [J]. Carbohydrate Polymers, 2018, 200: 536-542.

[125] Guccini V, Carlson A, Yu S, et al. Highly proton conductive membranes based on carboxylated cellulose nanofibres and their performance in proton exchange membrane fuel cells [J]. Journal of Materials Chemistry A, 2019, 7(43): 25032-25039.

[126] Zhang T, Lang J, Liu L, et al. Effect of carboxylic acid groups on the supercapacitive performance of functional carbon frameworks derived from bacterial cellulose [J]. Chinese Chemical Letters, 2017, 28(12): 2212-2218.

[127] Li S, Huang D, Zhang B, et al. Flexible supercapacitors based on bacterial cellulose paper electrodes [J]. Advanced Energy Materials, 2014, 4(10): 1301655.

[128] Zhou S, Kong X, Zheng B, et al. Cellulose nanofiber@ conductive metal-organic frameworks for high-performance flexible supercapacitors [J]. Acs Nano, 2019, 13(8): 9578-9586.

[129] Wang J, Zhuang S. Covalent organic frameworks (COFs) for environmental

applications [J]. Coordination Chemistry Reviews, 2019, 400: 213046.

[130] Baghbanzadeh M, Rana D, Lan C, et al. Effects of hydrophilic silica nanoparticles and backing material in improving the structure and performance of VMD PVDF membranes [J]. Separation and Purification Technology, 2016, 157: 60-71.

[131] Ling S, Chen W, Fan Y, et al. Biopolymer nanofibrils: Structure, modeling, preparation, and applications [J]. Progress in Polymer Science, 2018, 85: 1-56.

[132] Yano H, Sugiyama J, Nakagaito A, et al. Optically transparent composites reinforced with networks of bacterial nanofibers [J]. Advanced Materials, 2005, 17(2): 153-155.

[133] Ma H, Burger C, Hsiao B, et al. Nanofibrous microfiltration membrane based on cellulose nanowhiskers [J]. Biomacromolecules, 2012, 13(1): 180-186.

[134] Ma H, Burger C, Hsiao B, et al. Fabrication and characterization of cellulose nanofiber based thin-film nanofibrous composite membranes [J]. Journal of Membrane Science, 2014, 454: 272-282.

[135] Elimelech M, Phillip W. The future of seawater desalination: Energy, technology, and the environment [J]. Science, 2011, 333(6043): 712-717.

[136] He H, Cheng M, Liang Y, et al. Intelligent cellulose nanofibers with excellent biocompatibility enable sustained antibacterial and drug release via a pH-responsive mechanism [J]. Journal of Agricultural and Food Chemistry, 2020, 68(11): 3518-3527.

[137] Hakalahti M, Mautner A, Johansson L, et al. Direct interfacial modification of nanocellulose films for thermoresponsive membrane templates [J]. ACS Applied Materials & Interfaces, 2016, 8(5): 2923-2927.

[138] Way A, Hsu L, Shanmuganathan K, et al. pH-responsive cellulose nanocrystal gels and nanocomposites [J]. ACS Macro Letters, 2012, 1(8): 1001-1006.

[139] Xu X, Zhou J, Xin Y, et al. Alcohol recognition by flexible, transparent and highly sensitive graphene-based thin-film sensors [J]. Scientific Reports, 2017, 7(1): 1-10.

[140] Wang Y, Zhang J, Qiu C, et al. Self-recovery magnetic hydrogel with high strength and toughness using nanofibrillated cellulose as a dispersing agent and filler [J]. Carbohydrate Polymers, 2018, 196: 82-91.

[141] Zhou J, Hsieh Y. Nanocellulose aerogel-based porous coaxial fibers for thermal insulation [J]. Nano Energy, 2020, 68: 104305.

[142] Fukuzumi H, Saito T, Iwata T, et al. Transparent and high gas barrier films of cellulose nanofibers prepared by TEMPO-mediated oxidation [J]. Biomacromolecules, 2009, 10(1): 162-165.

[143] Ngo Y, Li D, Simon G, et al. Paper surfaces functionalized by nanoparticles [J]. Advances in Colloid and Interface Science, 2011, 163(1): 23-38.

[144] Shen Z, Feng J. Highly thermally conductive composite films based on nanofibrillated cellulose in situ coated with a small amount of silver nanoparticles [J]. ACS Applied Materials & Interfaces, 2018, 10(28): 24193-24200.

[145] Kuang Y, Chen G, Ming S, et al. Solvent resistance of 2, 2, 6, 6-tetramethylpiperidine-1-oxyl (TEMPO) treated cellulose nanofiber film for flexible electronics [J]. Cellulose, 2016, 23(3): 1979-1987.

[146] Roy S, Kim H, Kim J, et al. Incorporation of melanin nanoparticles improves

UV-shielding, mechanical and antioxidant properties of cellulose nanofiber based nanocomposite films [J]. Materials Today Communications, 2020, 24: 100984.

CHAPTER 3 EXPERIMENTAL: CHEMICAL REAGENTS, EQUIPMENT AND CHARACTERIZATION METHODS

3.1 Introduction

The TEMPO/NaBr/NaClO system was used for selective catalytic oxidation of cellulose. Aiming at TEMPO recovery and cellulose degradation mitigation in this system, TEMPO-containing polymers were designed, and the application of the oxidized cellulose obtained was studied. This chapter describes the chemicals and equipment used to analyze the resulting products.

3.2 Reagents and Equipment

Table 3.1 Chemical reagents

Name	Molecular formula	Purity (%)	Supplier	Function
Acrylamide	C_3H_5NO	99	Aladdin	Monomer
2,2'-Azobis (2-methylpropionitrile)	$C_8H_{12}N_4$	99	Aladdin	Initiator
Sodium tungstate dihydrate	Na_2WO_4	99.5	Aladdin	Complexing agent
Hydrogen peroxide	H_2O_2	30	Aladdin	Oxidizing agent
Ethylene diamine tetraacetic acid	$C_{10}H_{16}N_2O_8$	99.5	Aladdin	Complexing agent
Sodium cyanoborohydride	$NaBH_3CN$	95	Macklin	Reducing agent
Sodium bromide	NaBr	99	Aladdin	Cocatalyst

Name	Molecular formula	Purity (%)	Supplier	Function
Cellulose	$(C_6H_{10}O_5)_n$	99.3	Aladdin	Raw material
Sodium hypochlorite	NaClO	5.0	Aladdin	Oxidizing agent
mPEG	$HO(CH_2CH_2O)_nH$	99.5	Macklin	Carrier
Acetic anhydrate	$C_4H_6O_3$	98.5	Aladdin	Oxidizing agent
TEMPO	$C_9H_{18}NO$	99	Aladdin	Catalyst
Methyl acrylate	$C_4H_6O_2$	99	Aladdin	Monomer
Ethylenediamine	$C_2H_8N_2$	99	Aladdin	Monomer
3-Aminopropyltriethoxysilane	$C_9H_{23}NO_3Si$	98	Macklin	Cross-linking agent
Glutaraldehyde	$C_5H_8O_2$	50	Macklin	Cross-linking agent
3-Chloroperoxybenzoic acid	$C_7H_5ClO_3$	75	TCI	Oxidizing agent
4-Amino-2, 2, 6, 6-tetramethylpiperidine	$C_9H_{20}N_2$	98	Aladdin	Monomer

Table 3.2 Experimental equipment

Name	Specification	Supplier	Function
Fourier Transform Infrared Spectrophotometer	Thermo Nicolet 6700	Thermo Nicolet, USA	Determine the compound structure
Scanning Electron Microscope	S4800I	Hitachi Co. Ltd	Observe the surface morphology
Transmission Electron Microscope	JEM-2100	Jeol Co., Ltd, Japan	Observe the microstructure of the sample
Thermal Gravimetric Analyzer	SDT Q600	TA Instruments, USA	Determine the thermal stability
X-ray Diffractometer	D/MAX2500PC	Rigaku, Japan	Collect the crystalline or amorphous state

Name	Specification	Supplier	Function
Nuclear Magnetic Resonance Spectroscopy	Avance500MHz	Bruker, Germany	Characterize the compound structure
X-ray Photoelectron Spectrometer	ESCALAB250XI +	Thermo Co., Ltd	Determine the elemental composition
Mass Spectrometer	DSQII	Thermo, USA	Determine the average molecular weight
Gel Permeation Chromatography	Waters 1515	Waters, USA	Measure the molecular weight and polydispersity index
Ultraviolet-visible Spectrophotometer	UV-2550	Shimadzu, Japan	Measure the TEMPO density and the concentration of Pb^{2+}
Freezing Dryer	SC21CL	BiocoolCo., Ltd, China	Freeze-dried cellulose samples

3.3 Material Preparation

Details on the preparation of materials is provided in each section.

3.4 Characterization of Materials

The characteristics of each of the prepared samples were identified to analyze their structures and properties by means of the following: Fourier transform infrared spectroscopy (FT-IR); Scanning electron microscope (SEM); Transmission electron microscope (TEM); Thermal gravimetric analyzer (TGA); X-ray diffractometer (XRD); Nuclear magnetic resonance spectroscopy (NMR); X-ray photoelectron spectrometer (XPS); Gel permeation chromatography (GPC); Ultraviolet-visible spectrophotometer (UV-vis); conductivity titration and capillary viscometer.

3.4.1 FT-IR

The structures of samples were characterized using Fourier transform infrared spectroscopy. FT-IR spectra were obtained by scanning four times in the range of 400-4250 cm^{-1} with potassium bromide as background.

3.4.2 SEM

The overall morphology of the samples was observed by means of SEM. All specimens were ground in a mortar, and then sprayed with gold. The test was carried out with the acceleration voltage of 3 kV, the electron current intensity of 20 keV and the magnification of 200-70.0 K.

3.4.3 TEM

The sample was ground in an agate mortar and dispersed evenly in anhydrous ethanol using ultrasound. The sample solution was added to copper mesh, dried under an infrared lamp and observed by TEM.

3.4.4 TGA

The thermal stability of the samples was determined using the TGA. The samples were recorded at a constant heating rate of 10 ℃/min under a N_2 atmosphere at a temperature range from 25 ℃ to 800 ℃.

3.4.5 XRD

XRD was used to identify the crystalline or amorphous state of the samples. The sample is thoroughly ground into a uniform powder by an agate mortar. The sample powder was filled into the microscope slide. After the sample plane was flatten, the measurement was carried out with a step size of 0.02 degree. A blank run was performed to subtract and remove the environment background from the experimental data [1].

$$Crystallinity\ Index\ (CrI) = \frac{I_{200} - I_{am}}{I_{200}} * 100\% \qquad \text{Equation 3-1}$$

Where:

I_{200} = The maximum value of the cellulose I crystal peak intensity at 2θ=22-23°;

Iam = The minimum value of the cellulose I crystal peak intensity at 2θ=18-19°.

The particle sizes of MNP and Gn PAMAM-Tx-MNP can be quantitatively evaluated from the XRD data using the Debye-Scherrer equation, which gives a relationship between peak broadening in XRD and particle size.

$$D = \frac{k\lambda}{\beta \cos\theta} \qquad \text{Equation 3-2}$$

Where:

D is the thickness of the crystal;

k is the Debye–Scherrer constant (0.89);

λ is the X-ray wavelength (0.15406 nm);

β is the line broadening in radian obtained from the full width at half maximum;

θ is the Bragg angle (2θ).

3.4.6 NMR

The structure of the samples was characterized using NMR. All samples were analyzed as solutions in a deuterium generation reagent (30 mg/mL) at 25 ℃ in a standard 5 mm o.d. pipe.

3.4.7 XPS

The element distribution and the surface elemental composition were measured by XPS. The sample was prepared using the pressing tablet method and ground with a pestle and mortar immediately before XPS analysis, in order to generate fresh surfaces [2, 3].

3.4.8 MS

The average molecular weight of mPEG-Gn PAMAM-Tx was determined by MS.

3.4.9 GPC

GPC curves were recorded using a Waters 1515 instrument with a refractive index detector, using a calibration curve from the PEG standards in water (containing 0.02% NaN_3) at 35 ℃.

3.4.10 UV-vis

The TEMPO density of the water-soluble samples was tested using the UV-vis spectrophotometer at a 461 nm wavelength. The absorption performance of aqueous TEMPO solutions with different concentrations at the maximum absorption wavelength was measured to obtain the standard curve for TEMPO concentration and absorbance. Under the same conditions, the absorbance of the TEMPO containing polymer was determined, and the TEMPO content was obtained by comparing this with the standard curve.

The concentration of Pb^{2+} was measured using the UV-vis light spectrophotometer [4]. The adsorption capacity of q (mg/g) was calculated using Equation 3-3:

$$q = \frac{(c_0 - c) * V}{w} \qquad \text{Equation 3-3}$$

Where:

c_0 is the initial concentration of Pb^{2+} solution, mg/L;

C is the concentration of the Pb^{2+} solution after adsorption, mg/L;

V is the volume of the Pb^{2+} solution, L;

W is the mass of the adsorbent, g.

Desorption capacity q'(mg/g) was calculated according to Equation 3-4:

$$q' = \frac{c' * V'}{w} \qquad \text{Equation 3-4}$$

Where:

c' is the concentration of the Pb^{2+} solution after desorption, mg/L;

V' is the volume of the Pb^{2+} solution after desorption, L;

w is the mass of the adsorbent, g.

3.4.11 Conductivity titration

The $-NH_2$ content of the PVAm was measured by conductometric titration. PVAm was dissolved to and HCl solution to obtain P(AM-co-VAmHCl). P(AM-co-VAmHCl) (80 mg) was then completely dissolved in water (100 mL). It was then titrated with 0.1 M $AgNO_3$ at room temperature until the inflection point appeared. The content of $-NH_2$ in PVAm was calculated using Equation 3-5:

$$\frac{cV}{1000} = \frac{mx}{79.5x+71(1-x)} \qquad \text{Equation 3-5}$$

Where:

79.5, 71 is the unit molar mass of PVAmHCl and PAM, g/mol;

c is concentration of $AgNO_3$ solution, mol/L;

x is the degree of amination of PVAm, %;

V is the volume of consumed 0.1 M $AgNO_3$, mL;

m is the mass of P(AM-co-VamHCl), g.

The carboxyl content of oxidized cellulose fibers was determined by conductometric titrations and corrected by considering the effect of dilution as described in the literature [5-8]. A dried sample (0.04 g) was added to 15 mL of a 0.01 M HCl solution. After the

mixture was sufficiently stirred, the suspension was titrated with 0.01 M NaOH. The carboxyl group content (mmol/g) was calculated using the following Equation 3-6:

$$COOH\ \left(\frac{mmol}{g}\right) = c(V_2 - V_1)/m \qquad \text{Equation 3-6}$$

Where:

c is the NaOH concentration, mol/L;

m is the weight of the oven-dried sample, g;

V_1, V_2 is the min and max amount of NaOH that corresponds to the equivalent conductivity, mL.

3.4.12 The degree of viscosity of polymerization

The viscosity and thus the degree of polymerization (DP) of the samples in a copper ethylenediamine solution was measured using a capillary viscometer at 25 ℃ [9]. The DP and degradation degree (DD) of cellulose were estimated using Equation 3-7 and Equation 3-8, respectively:

$$[\eta] = 0.891DP^{0.963} \qquad \text{Equation 3-7}$$

Where:

DP is the average degree of viscosity of polymerization;

[η] is the limiting viscosity number.

$$Degradation\ degree = \frac{(DP_0 - DP_1)}{DP_0} \qquad \text{Equation 3-8}$$

Where:

DP_0 is the DP of raw cellulose;

DP_1 is the DP of oxidized cellulose.

3.4.13 Water retention value

The water retention value can reflect the binding force of cellulose in different oxidized states, the degree of moisture swelling and the degree of fine fibrosis eroded on the surface. After being freeze-dried and ground, the sample was fully absorbed water for 2 h at room temperature and centrifuged in a high-speed centrifuge of 10 000 r/min for 20 minutes. The sample in the lower layer was separated and weighed as m_1. This was dried for 5 h in a blowing oven at 110 ℃ and weighed as m_2 [10, 11].

$$Water\ retention\ value = 100 * (m_1 - m_2)/m_2 \qquad \text{Equation 3-9}$$

Where:

m_1 is the weight of cellulose sample after soaking;

m_2 is the constant weight cellulose sample after drying.

References

[1] Montanari S, Roumani M, Heux L, et al. Topochemistry of carboxylated cellulose nanocrystals resulting from TEMPO-mediated oxidation [J]. Macromolecules, 2005, 38(5): 1665-1671.

[2] Roncero M, Torres A, Colom J, et al. The effect of xylanase on lignocellulosic components during the bleaching of wood pulps [J]. Bioresource Technology, 2005, 96(1): 21-30.

[3] Tserki V, Zafeiropoulos N, Simon F, et al. A study of the effect of acetylation and propionylation surface treatments on natural fibres [J]. Composites Part A: Applied Science and Manufacturing, 2005, 36(8): 1110-1118.

[4] Li C, Wang Y. Determination of trace lead by ultraviolet spectrophotometry [J]. Chemistry & Bioengineering, 2015, 32(10): 67-69.

[5] Da Silva Perez D, Montanari S, Vignon M. TEMPO-mediated oxidation of cellulose III [J]. Biomacromolecules, 2003, 4(5): 1417-1425.

[6] Ragab G, Amin A. Atomic absorption spectroscopic, conductometric and colorimetric methods for determination of fluoroquinolone antibiotics using ammonium reineckate ion-pair complex formation [J]. Spectrochimica Acta Part A: Molecular and Biomolecular Spectroscopy, 2004, 60(4): 973-978.

[7] Milanovic J, Schiehser S, Milanovic P, et al. Molecular weight distribution and functional group profiles of TEMPO-oxidized lyocell fibers [J]. Carbohydrate Polymers, 2013, 98(1): 444-450.

[8] Yao W, Xu Q, Jin L, et al. Effects of TEMPO/NaBr/NaClO-oxidation of nanocrystalline cellulose on its properties [J]. Chemistry and Industry of Forest Products, 2015, 35(2): 31-37.

[9] Sun T, Wang H, Liu J, et al. Recoverable acrylamide-vinylamine copolymer immobilized TEMPO mediated oxidation of cellulose with good catalytic performance and low cellulose degradation [J]. Cellulose, 2021, 28(7): 4151-4164.

[10] Mishra S, Thirree J, Manent A, et al. Ultrasound-catalyzed TEMPO-mediated oxidation of native cellulose for the production of nanocellulose: Effect of process variables [J]. BioResources, 2011, 6(1): 121-143.

[11] Saito T, Isogai A. TEMPO-mediated oxidation of native cellulose. The effect of oxidation conditions on chemical and crystal structures of the water-insoluble fractions [J]. Biomacromolecules, 2004, 5(5): 1983-1989.

CHAPTER 4 VINYLAMINE POLYMER SUPPORTED TEMPO FOR CATALYTIC OXIDATION OF CELLULOSE

(Note: This work was published in Cellulose. DOI: 10.1007/s10570-021-03832-8)

4.1 Introduction

Cellulose is a water-insoluble polymer. If the catalyst for the oxidation reaction is also a water-insoluble polymer, there will be high steric resistance between the catalyst and the cellulose, which greatly reduces the performance of catalytic oxidation. In order to improve the catalytic performance of the TEMPO-anchored catalytic system for cellulose oxidation in a water medium, a water-soluble supported catalytic system must be prepared [1-5].

Water-soluble polyvinylamine (PVAm) with abundant primary amines can create a cationic interface on its surface in water [6]. The cationic interface on the surface can reduce the steric hindrance between PVAm and cellulose when oxidizing cellulose. In addition, the high amine content can improve TEMPO loading amount. Pelton R. et al. supported TEMPO on PVAm by means of the acylation reaction between the carboxyl of 4-COOH-TEMPO and amino of PVAm, in order to prepare PVAm-TEMPO. PVAm-TEMPO was used instead of TEMPO in the TEMPO/NaBr/NaClO system to obtain cellulose with aldehyde groups. Covalent bonds were formed when cellulose-containing aldehyde groups reacted with the primary amine groups of PVAm. This

promoted wet adhesion of cellulose-to-cellulose [7-12]. In this scheme, PVAm-TEMPO is grafted to the cellulose surface. The TEMPO cannot be recycled and the problem of cellulose depolymerization is not considered. Strategies that can be used to recover TEMPO and reduce the degree of degradation of cellulose in the TEMPO/NaBr/NaClO system used to oxidize cellulose have not been reported.

This chapter describes a process in which a water-soluble polymer immobilized TEMPO (PVAm-T) for catalytic oxidation of cellulose was prepared. First, polyacrylamide (PAM) was obtained by radical polymerization of acrylamide (AM), and then degraded to prepare the vinylamine polymer of PVAm by the Hofmann reaction. The carbonyl groups in 4-oxo-TEMPO were reacted with the -NH_2 groups in PVAm to synthesize PVAm-T. This was used to selectively oxidize cellulose to produce oxidized cellulose products with low degrees of degradation and high carboxyl contents. The effect of the PVAm-T structure on the degree of oxidation and the degree of degradation of cellulose were studied. The catalytic oxidation mechanism and recycling performance were also discussed.

4.2 Experiment

4.2.1 Preparation of PVAm-T

4.2.1.1 Synthesis of PAM

Solution polymerization [13]: Under a N_2 environment, AM (10.0 g, 0.14 mol), $Na_2S_2O_8$ (0.l g, 0.4 mmol), isopropanol (l0 mL, 0.26 mol) and water (1 L) were placed

in a three-necked flask. After reaction at 65 ℃ for 1 h, the product was precipitated using methanol and dried at 40 ℃ under vacuum to get PAM with a high molecular weight (Mn=20000).

Precipitation polymerization [14, 15]: Under a N_2 atmosphere, AM (10.0 g, 0.14 mol), AIBN (0.2 g, 1.22 mmol) and ethanol (100 mL) were placed in a three-necked flask and subjected to magnetic stirring at 60 ℃ for 2.5 h. It was then cooled to room temperature. The resulting solids were filtrated, washed with ethanol and dried to prepare PAM with a low molecular weight (Mn=7000).

4.2.1.2 Preparation of PVAm

PVAm was obtained using the Hofmann reaction with PAM [16-18]: 5% NaClO (8.83 mL, 12.5 mmol) and 15 M NaOH (1 mL, 0.015 mol) were placed in a three-necked flask and then cooled to -10 ℃ under magnetic stirring. An aqueous solution of PAM (6.8 wt.%, 14.7 mL) was slowly added. After 1.5 h, 11 M NaOH (32 mL, 0.352 mmol) that was cooled to -10 ℃ was added dropwise. The reaction was performed at -10 ℃ for 0.5 h and then maintained at 0 ℃ for 17 h. PVAm was precipitated from methanol, and then washed and dried.

4.2.1.3 Preparation of 4-oxo-TEMPO

As shown in Fig. 4.1, 4-oxo-TEMPO was prepared by oxidizing 2, 2, 6, 6-tetramethyl-4-piperidone with Na_2WO_4/H_2O_2/EDTA [19, 20]. 2, 2, 6, 6-Tetramethylpiperidone

(10.0 g), Na_2WO_4 (160 mg), EDTA (160 mg) and methanol (20 mL) were placed in a 100 mL three-necked flask with a magnetic stirrer. An H_2O_2 solution (16 mL) was slowly added at 18-22 ℃ and the mixture was stirred for 13 h. The resulting solution was evaporated to remove methanol and water, and the residue was saturated with anhydrous potassium carbonate. The upper brown oil layer was separated and lyophilized. After recrystallization with n-hexane, the orange needle-like crystals of 4-oxo-TEMPO were obtained with a yield of 90%.

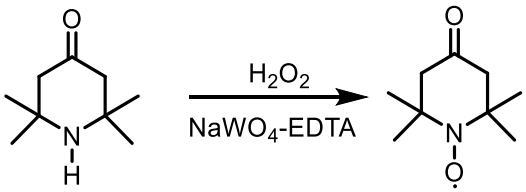

Fig. 4.1 The synthetic route of 4-oxo-TEMPO

4.2.1.4 Preparation of PVAm-T

The catalyst PVAm-T was obtained by the reaction between the carbonyl groups in 4-oxo-TEMPO and the primary amine groups in PVAm [21]. PVAm (containing 24 mmol $-NH_2$) and 4-oxo-TEMPO (2.043 g, 12 mmol) were dissolved in anhydrous methanol (20 mL). $NaBH_3CN$ (1.131 g, 18 mmol) was then added to the reaction mixture at 40 ℃. After reaction for 120 h, PVAm-T was obtained by filtration from methanol and dried under vacuum.

4.2.2 Selective oxidation of cellulose

The oxidation process was carried out based on a previously-published method [22-24].

PVAm-T (0.59 mmol TEMPO), NaBr (0.07 g, 0.68 mmol), cellulose (2.5 g) and water (188 mL) were placed in a 250 mL three-necked flask. A 5% NaClO solution (5 mmol/g cellulose) was then slowly added to the cellulose slurry at 25 ℃. The pH of the mixture was maintained at 10.5 by manual addition of 0.5 M NaOH. After 24 h, the reaction was quenched using ethanol (10 mL). The water-insoluble oxidized cellulose product was obtained by centrifugation and then freeze-dried. The concentrated supernatant was used for the next oxidation cycle. After several cycles, inorganic salts and degradation products were removed by dialysis of the concentrated supernatant. The dialyzate was then concentrated and precipitated into methanol to recover PVAm-T.

4.2.3 Post-reduction of oxidized cellulose

The oxidized cellulose (1.0 g) and 0.01 M $NaBH_4$ solution (50 mL) were placed in a three-necked flask while stirring. After reaction for 6 h at 25 ℃, the product was centrifuged and then immersed in 1 M CH_3COOH. Then it was centrifuged, washed and dried by lyophilization to obtain the reduced oxidized cellulose product [25, 26].

4.3 Results and Discussion

4.3.1 Preparation of PVAm-T

4.3.1.1 Schematic synthetic route of PVAm-T

PVAm was obtained by Hofmann degradation of PAM. PVAm-T was prepared by means of the reaction between carbonyl in 4-oxo-TEMPO and $-NH_2$ in PVAm (Fig. 4.2).

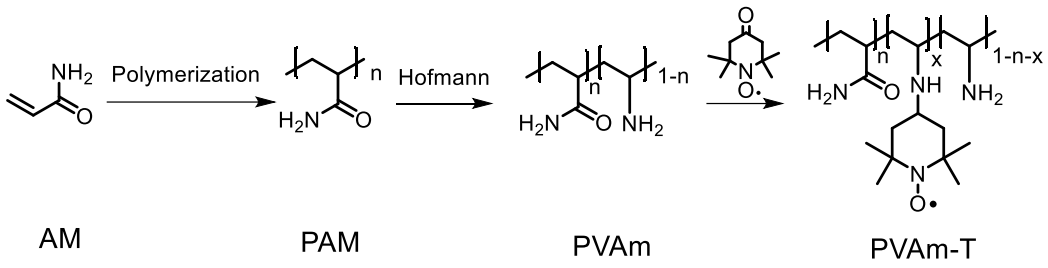

Fig. 4.2 The synthetic route of PVAm-T

4.3.1.2 FT-IR characterization

Successful synthesis of PVAm and PVAm-T was confirmed by FT-IR. The FT-IR spectra of PVAm with about 72.0% amination degree (Fig. 4.3) and PVAm-T with 55.1% TEMPO loading degree (4.19 mmol/g TEMPO loading amount) are shown in Fig. 4.4. In the spectrum of PAM, the absorption peaks of the stretching vibration of N-H and C=O of the acylamino groups were at 3431 cm^{-1} and 1607 cm^{-1}. In the spectrum of PVAm [27, 28], the absorption peak at 1509 cm^{-1} was the bending vibration of N-H. Furthermore, the intensity of the characteristic absorption peak of C=O at 1608 cm^{-1} was significantly reduced. In the spectrum of PVAm-T [20, 21], the characteristic absorption peaks at 2924 cm^{-1}, 1360 cm^{-1} and 1244 cm^{-1} were mainly caused by the N-O, C-N and -CH_3 of TEMPO.

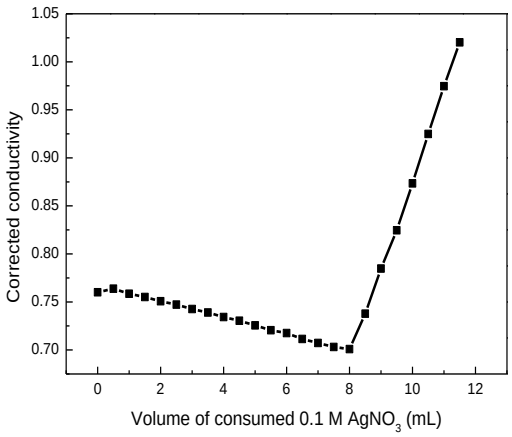

Fig. 4.3 Determination of amination degree of PVAm

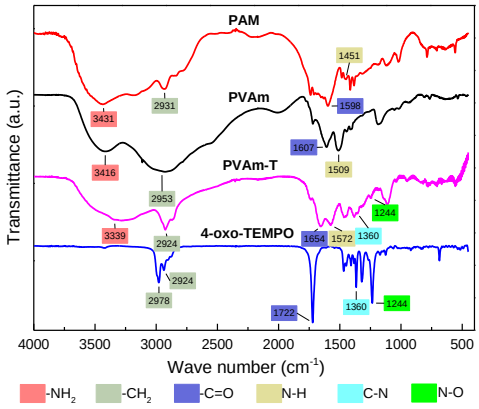

Fig. 4.4 FT-IR spectra of PAM, PVAm, 4-oxo-TEMPO and PVAm-T

4.3.1.3 UV-vis characterization

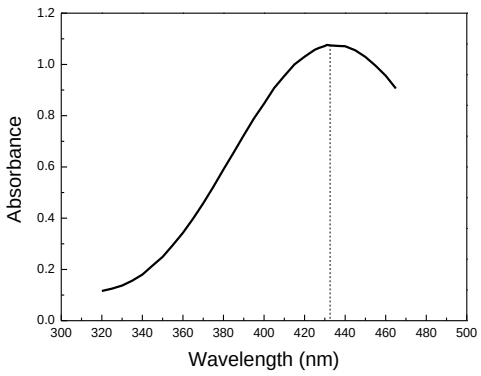

Fig. 4.5 UV-vis absorption spectrum of TEMPO

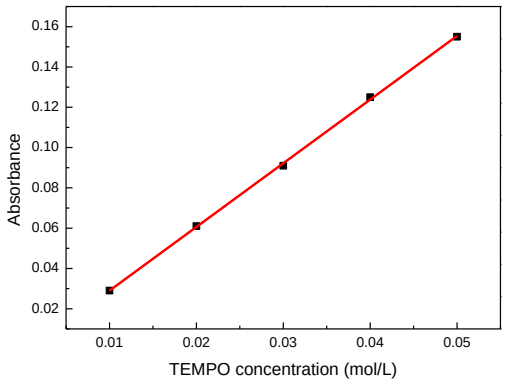

Fig. 4.6 UV-vis standard absorption curve of TEMPO

The TEMPO content of PVAm-T was determined by means of UV-vis spectrophotometry. The standard absorption curve was measured with TEMPO as the standard substance and water as the reference solution at 432 nm of the TEMPO maximum absorption wavelength (See Fig. 4.5). The TEMPO content of the sample was determined according to the standard absorption curve (Fig. 4.6) [29].

4.3.1.4 GPC characterization

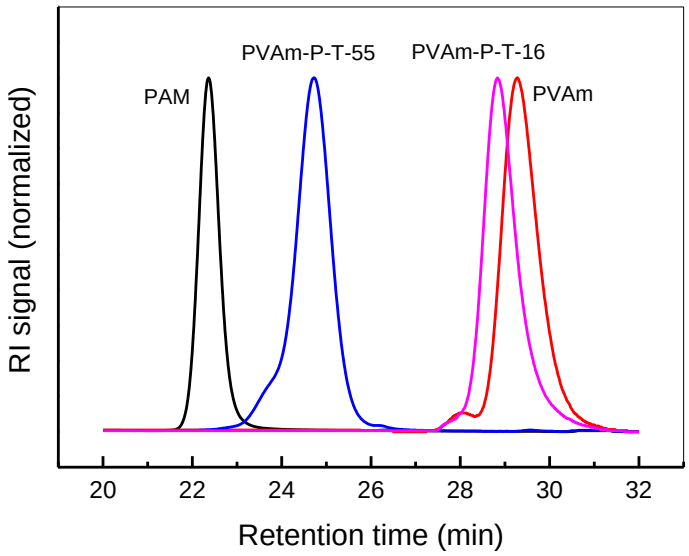

Fig. 4.7 GPC curves of the catalyst PVAm-T

Table 4.1 GPC results of PAM, PVAm and PVAm-T

	Mn	PDI
PAM	7000	1.02
PVAm	5200	1.05
PVAm-P-T-16	5600	1.07
PVAm-P-T-57	6300	1.04

The molecular weights of PAM, PVAm and PVAm-T were estimated by GPC [30-32]. The Mn values listed in Table 4.1 were the relative molecular weights of these polymers to the PEG standards; these were used to characterize the trends in Mn changes during the synthesis of PVAm-T. Fig. 4.7 clearly shows that the Mn of PVAm obtained by Hofmann degradation of PAM was significantly lower than that of the precursor, PAM.

Compared to PVAm, the Mn of PVAm-T with a 16% TEMPO loading degree (PVAm-P-T-16) increased correspondingly. As the TEMPO loading degree increased from 16% to 55%, the Mn of PVAm-P-T-55 increased accordingly. These results further confirmed successful preparation of PVAm-T.

PVAm-T catalysts with different molecular weights and TEMPO loading degrees were prepared to systematically analyse the structure of PVAm-T and the performance of selective oxidation of cellulose (Table 4.2). With the PAM obtained by solution polymerization (Mn=20000), an increase in the molar ratio of 4-oxo-TEMPO to -NH_2 in PVAm can improve the TEMPO loading degree of the catalyst. The catalyst has good water-solubility when the TEMPO loading degree is about 20% (2.52 mmol/g TEMPO loading amount). However, the catalyst was almost water-insoluble when the TEMPO loading degree was increased to about 40% (3.65 mmol/g TEMPO loading amount). In order to prepare a water-soluble catalyst with a high TEMPO loading degree, the precipitation polymerization was used to prepare PAM with low molecular weight (Mn=7000). With the PAM as a carrier, the prepared PVAm-T with 57% TEMPO loading degree still had good water solubility (4.25 mmol/g TEMPO loading amount).

Table 4.2 Prepared PVAm-T catalysts

PVAm-T catalysts	Water solubility	Carrier	Mn of PAM	Amination degree of carrier %	-NH_2 in PVAm/4-oxo-TEMPO	TEMPO loading amount mmol/g	TEMPO loading degree %
PVAm-S-T-19	Soluble			75.7	8:2	2.42	19.1
PVAm-S-T-20	Soluble			75.7	8:3	2.52	20.2
PVAm-S-T-21	Soluble	PVAm-S	20000	72.3	8:4	2.61	21.4
PVAm-S-T-40	Insoluble			77.4	8:6	3.65	39.8
PVAm-S-T-43	Insoluble			77.4	8:8	3.79	43.4
PVAm-P-T-16	Soluble			72.0	8:4	2.12	15.6
PVAm-P-T-29	Soluble			72.0	8:5	3.08	28.5
PVAm-P-T-31	Soluble			72.0	8:6	3.20	30.6
PVAm-P-T-37	Soluble	PVAm-P	7000	72.3	8:8	3.52	36.7
PVAm-P-T-41	Soluble			73.1	8:7	3.70	40.8
PVAm-P-T-55	Soluble			73.1	8:8	4.19	55.1
PVAm-P-T-57	Soluble			72.3	8:12	4.25	56.9

Note: Meaning of symbols in PVAm-T: S means PAM is prepared by solution polymerization. P means PAM is prepared by precipitation polymerization. The number is the TEMPO loading degree.

4.3.2 Selective oxidation of cellulose

Cellulose was selectively oxidized in water at pH=10.5 using PVAm-T as the catalyst, NaBr as the co-catalyst and NaClO as the oxidant (5 mmol/g cellulose).

4.3.2.1 Mechanism of selective catalytic oxidation of cellulose

The nitroxide radical is first oxidized into a positive ion using the oxidant NaBrO, followed by selective oxidation of cellulose [33-40]. The positive ion contacts the primary hydroxyl group on the cellulose surface through diffusion, oxidizes the primary

hydroxyl group into a carboxyl group, and is itself reduced into an intermediate hydroxylamine. This intermediate changes into a nitroxide radical through oxidation of NaBrO. At this time, the working cycle is completed and cyclic regeneration of the nitroxide radical is realized (Fig. 4.8).

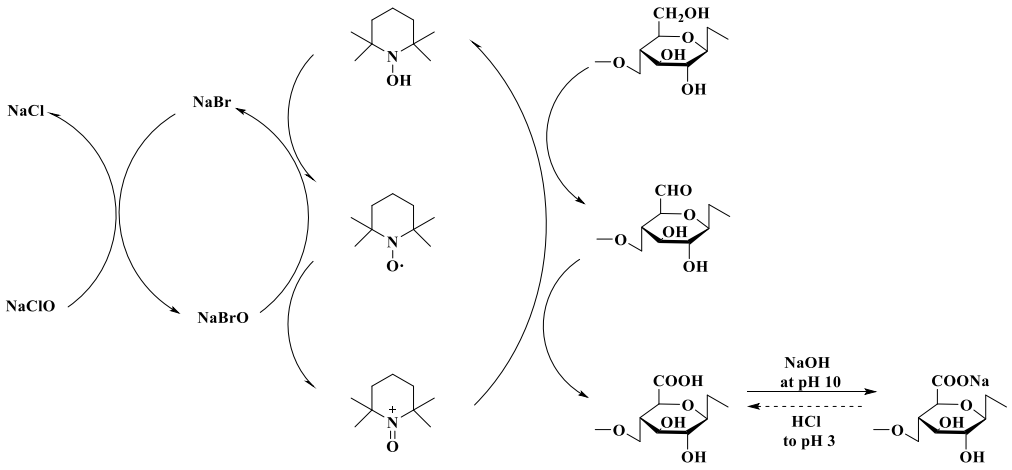

Fig. 4.8 Mechanism of selective catalytic oxidation of cellulose using the TEMPO/NaBr/NaClO system

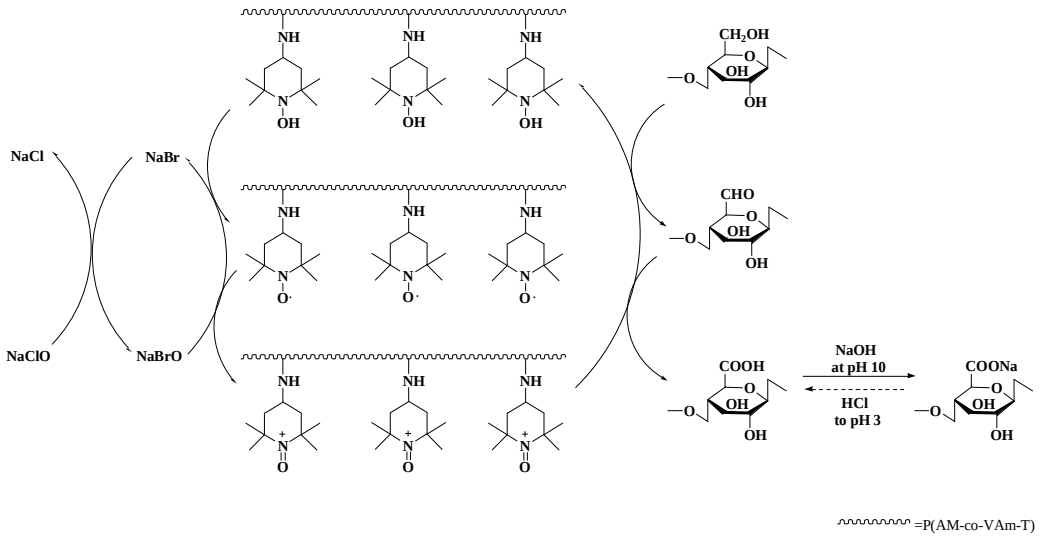

Fig. 4.9 Mechanism of cellulose oxidation catalyzed using the catalyst PVAm-T

The mechanism of PVAm-T mediated oxidation of cellulose is similar to the free TEMPO, as shown in Fig. 4.9. PVAm-T also undergoes the above state change process, and so achieves the purpose of selective catalytic oxidation of the C6 primary hydroxyl group of cellulose to a carboxyl group.

4.3.2.2 Oxidized cellulose characterization

(1) Structural characterization

Fig. 4.10 shows the FT-IR spectra of cellulose before and after oxidation. The intensity of the peak at 1615 cm^{-1} that corresponds to the -COONa group of PVAm-T was slightly weaker than that of TOC [41]. This shows that the catalyst of PVAm-T had a high degree of cellulose oxidation.

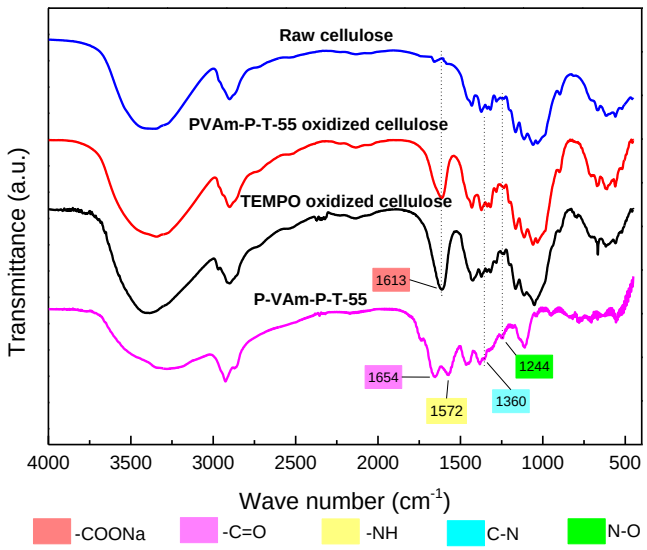

Fig. 4.10 The FT-IR spectra of raw cellulose, PVAm-T, TEMPO oxidized cellulose and PVAm-T oxidized cellulose

(2) Oxidation effect

The carboxyl content of oxidized cellulose was measured by conductometric titration [42, 43]. The carboxyl content in raw cellulose was 0.02 mmol/g. This would be due to the air oxidation [44]. The results show that the degree of cellulose oxidation using PVAm-T with a high molecular weight PAM (Mn=20000) as the carrier increased with the increase of TEMPO loading degree, as show in Fig. 4.11. However, the water solubility became poorer as the TEMPO loading amount increased, which complicated the process of catalyst separation from the oxidized product. With a low molecular weight and PAM (Mn=7000) as the carrier, the prepared catalyst showed increased water solubility, and the catalytic performance was improved (equivalent to 68%-76% of the free TEMPO level).

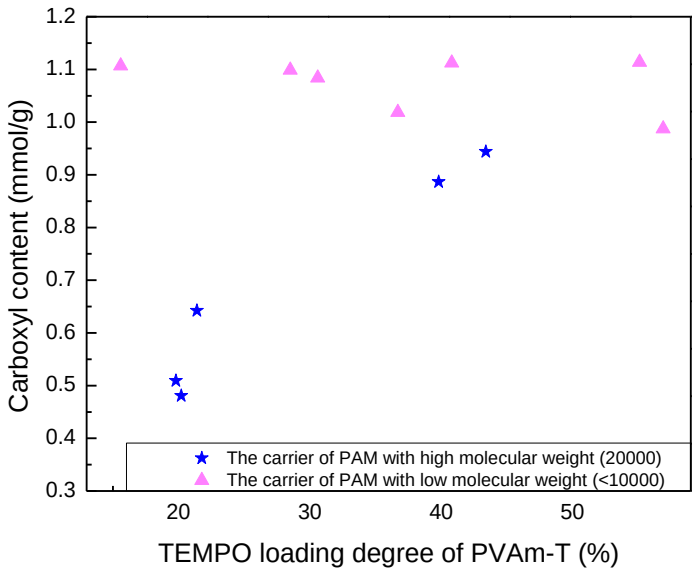

Fig. 4.11 Effects of TEMPO loading degree of PVAm-T on the carboxyl group content of oxidized cellulose

TEMPO loading degree seemed to have little effect on the catalytic performance of

PVAm-T with a low molecular weight PAM as the carrier. As the degree of TEMPO loading increased from 16% to 57%, the carboxyl group contents of the oxidized cellulose samples were close, about 1-1.1 mmol/g. This may be due to the excellent water solubility of the macromolecular catalyst with low molecular weight, producing a closer diffusion ability of the catalyst than that of free TEMPO. These results indicate that the molecular weight had a significant effect on the catalytic performance of the macromolecular catalyst.

(3) DP of cellulose

Significant depolymerization is inevitable during TEMPO catalytic oxidation of cellulose under alkaline conditions [45, 46]. As seen in Table 4.3, TEMPO mediated oxidation of cellulose was very efficient under the reaction conditions pH=10.5, TEMPO concentration of 3 mmol/L, NaClO concentration of 5 mmol/g cellulose. It only took four hours to obtain oxidized cellulose with 1.46 mmol/g carboxyl. However, this oxidation process led to significant degradation of the cellulose. The DP of TOC was significantly decreased to about 55-72 (Table 4.3), which is equivalent to 61%-66% degrees of degradation (the DP of raw cellulose was about 160).

The degradation of cellulose is mainly caused by β-alkoxy elimination or free radicals produced during the oxidation of the intermediate C6-aldehyde group formed under alkaline conditions in water [47-51]. The molecular structural features of the immobilized TEMPO can also affect cellulose degradation. The DP of PVAm-T

oxidized cellulose was largely higher (117-126, which corresponds to a 21%-27% degree of degradation) than that of TOC.

To reveal the mechanism of PVAm-T that affects the degradation of cellulose, a comparative experiment was carried out: 4-oxo-TEMPO was physically mixed with PVAm (according to the content in PVAm-T) to oxidize cellulose. The DD of oxidized cellulose was consistent with the TOC. Therefore, it can be concluded that PVAm-T, rather than PVAm, plays a key role in alleviating the degradation of cellulose in the oxidation process.

Table 4.3 TEMPO and PVAm-T oxidized cellulose

Oxidized cellulose	Carboxyl content (mmol/g)	DP	Mass yield (%)
TEMPO oxidized cellulose	0.489	72.4	90.2
	0.937	57.3	90.4
	1.331	55.3	90.6
PVAm-T oxidized cellulose	0.481	124.1	96.4
	0.642	125.7	96.0
	0.987	117.4	95.6
	1.019	117.7	95.4
	1.114	119.2	95.6

(4) Post-reduction

Shinoda et al. showed that TOC with small amounts of C6 aldehydes and C2/C3 ketones can cause depolymerization of cellulose when DP was measured in alkaline 0.5 M copper [52]. Post-reduction using $NaBH_4$ at pH=10 can remove the C6 aldehydes and

C2/C3 ketones that form hemiacetal bonds between fibers during the drying process [53, 54]. Therefore, the DP of oxidized cellulose was improved after post-reduction treatment. The experimental results shown in Table 4.4 confirm this. After post-reduction, the DP of TOC was largely increased, which suggests that this oxidized cellulose contained a large amount of C6 aldehydes and C2/C3 ketones.

Table 4.4 Catalytic performance of TEMPO and PVAm-P-T

Catalyst	Reaction conditions			Oxidized cellulose		
	Catalyst mmol/L	Time h	NaClO mmol/g cellulose	Carboxyl content mmol/g	DP	
					Before-reduction	Post-reduction
TEMPO	3	4	5	1.46	66	98
	6	4	5	1.55	62	88
	15	4	5	1.71	40	68
	30	4	5	1.74	40	69
	90	4	5	1.74	40	70
	3	4	10	1.66	35	65
	3	4	15	1.65	32	63
	3	2	5	0.75	68	99
	3	6	5	1.47	59	89
PVAm-P-T-37	3	24	5	1.02	118	118
	3	24	10	1.15	106	111
	3	24	15	1.16	95	99
	3	12	5	1.04	121	119
	3	44	5	1.05	94	101
PVAm-P-T-57	3	24	5	1.05	117	116
	3	24	10	1.16	104	109
	3	24	15	1.18	90	96
	3	12	5	1.05	124	125
	3	44	5	1.05	103	109

Spier et al. found that an increase in TEMPO concentration reduces depolymerization [55]. However, under our reaction conditions, the increase in TEMPO concentration seemed to have no effect on the degradation of cellulose. This was probably because cellulose is a water-insoluble highly crystalline polysaccharide. The PVAm-T oxidized cellulose had similar DP values before and after post-reduction, which shows that there was no side reaction in the process of PVAm-T mediated cellulose oxidation. It seems that PVAm-T can prevent the formation of C6 aldehydes and C2/C3 ketones by side reactions, which suggests that it has high oxidation selectivity. This may be another main reason why it can efficiently inhibit the degradation of cellulose.

The effect of reaction time on carboxyl content and the DP of oxidized cellulose were studied using the catalysts TEMPO and PVAm-T. The results showed that TEMPO-mediated cellulose oxidation was completed in 4 h, and PVAm-T mediated cellulose oxidation was completed in 12 h (Table 4.4). The DD of cellulose increased when the reaction time was prolonged. The DP of oxidized cellulose before and after post-reduction showed that the reaction time had no effect on the content of C6-aldehydes and C2/C3 ketones in PVAm-T oxidized cellulose. This indicates that it had high selectivity in the whole reaction process.

The effect of NaClO dosage on carboxyl content and DP was also studied. The carboxyl content of oxidized cellulose increased with an increase in the dosage of NaClO oxidant for TEMPO mediated oxidation of cellulose [56-59]. When using PVAm-T as the

catalyst, the trend in the change of carboxyl content of oxidized cellulose was the same as with TEMPO, and it also increased gradually with an increase in the amount of oxidant (5-15 mmol/g cellulose). (See Table 4.4.) Increasing the amount of NaClO increased the occurrence of side reactions and reduced the DP of the oxidized cellulose.

(5) Morphology

Compared with raw cellulose, it can be observed with naked eyes that the centrifuged oxidized cellulose is more transparent and the freeze-dried sample is more fluffy, as shown in Fig.4.12.

Raw cellulose | Oxidized freeze-dried cellulose | Raw cellulose after adding water | Centrifuged oxidized cellulose

Fig.4.12 Photos of cellulose before and after treatment

The SEM images of cellulose, TEMPO oxidized cellulose and PVAm-P-T oxidized cellulose were shown in Fig. 4.13. The TEMPO/NaBr/NaClO oxidation system oxidized cellulose into fibrillation [60]. With the progression of the oxidation process, some tiny microfibers are formed on the surface of cellulose. In this work, fibrillation of long fibers and the formation of fine particles was also observed in the SEM images of oxidized cellulose, which indicates that a large number of carboxylic acid groups were formed in the water-insoluble part after oxidation. Under the same oxidation conditions, it was found that the degree of surface erosion of TEMPO oxidized cellulose

and PVAm-P-T oxidized cellulose were similar, indicating that PVAm-P-T has a similar catalytic oxidation performance to that of TEMPO and that depolymerization occurred as a side reaction in the non-crystalline regions during the oxidation process [61-64].

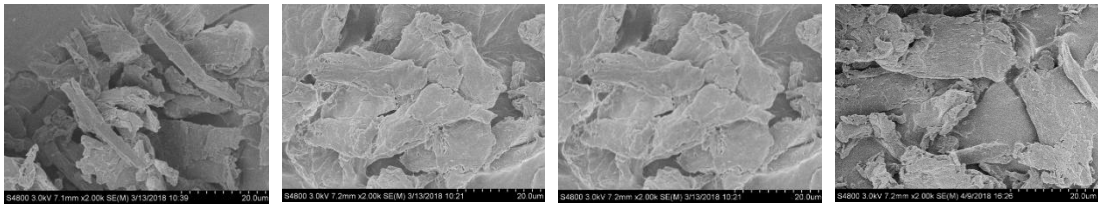

a) Raw cellulose b) TEMPO oxidized cellulose c) PVAm-P-T oxidized cellulose

Fig. 4.13 SEM images of cellulose and oxidized cellulose

(6) Water retention value

Table 4.5 Water retention values of raw cellulose and oxidized cellulose samples

Samples	Carboxyl content mmol/g	Water retention value %
Cellulose	0.02	241
PVAm-P-T oxidized cellulose	0.481	273
	0.642	285
	0.987	406
	1.019	437
	1.114	491
TEMPO oxidized cellulose	1.46	599

Table 4.5 shows that the water retention value of oxidized cellulose was significantly improved compared to that of raw cellulose. The water retention value of oxidized

cellulose was closely related to the degree of oxidation because the number of fine fibers increased [65, 66].

(7) XRD analysis

The oxidized cellulose samples were characterized by means of XRD (Fig. 4.14). Four diffraction peaks at 2θ=14.5°, 16.5°, 22.5° and 34.5° corresponded to the diffraction absorption peaks of the 110, $1\bar{1}0$, 200 and 004 crystal planes of cellulose I type crystal structure respectively [67-69]. This indicated that the crystal form of oxidized cellulose had not changed.

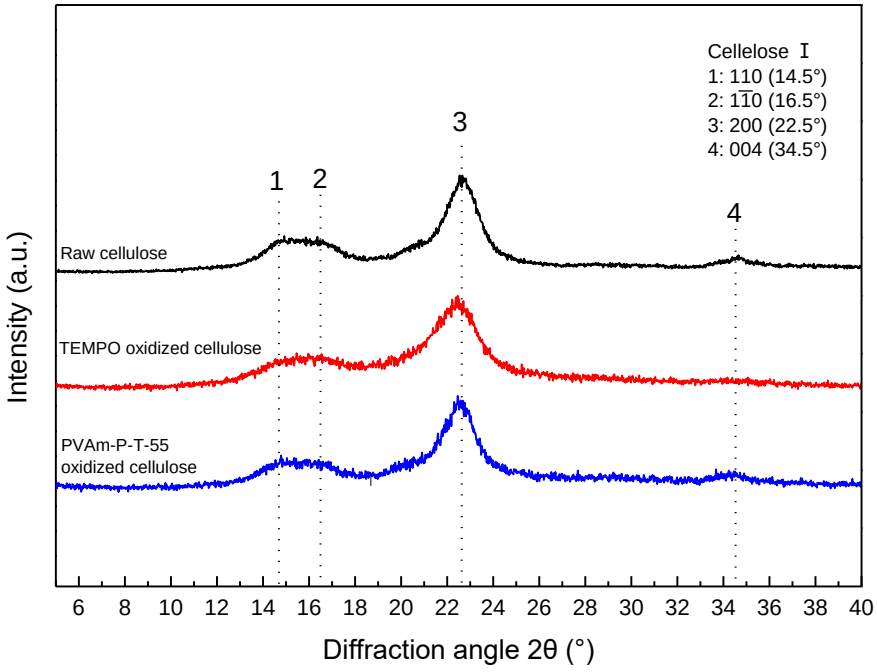

Fig. 4.14 X-ray diffraction patterns of raw cellulose and oxidized cellulose

Table 4.6 The CrI of raw cellulose and oxidized cellulose samples

Samples	Carboxyl content mmol/g	I_{am}	I_{200}	CrI %
Raw cellulose	0.02	0.327	1.000	67.3
PVAm-P-T	0.642	0.205	1.000	79.5
	0.987	0.191	1.000	80.9
	1.019	0.189	1.000	81.1
	1.114	0.166	1.000	83.4
TEMPO	1.46	0.147	1.000	85.3

Using the methods reported in the literature [70-73], the CrI values were estimated (Table 4.6). Compared to the raw cellulose (I_{am}=0.327, I_{200}=1.000, CrI=67.3%), the CrI of oxidized cellulose increased. The reason could be that part of the cellulose in the amorphous region was oxidized to soluble cellulose. It is then lost from the cellulose body in the subsequent washing process. Therefore, the CrI of oxidized cellulose obtained by centrifugation was increased. The CrI of TOC oxidized cellulose was higher than that of PVAm-P-T oxidized cellulose. This may be due to PVAm-P-T being bigger and less able to enter the interior of the cellulose; therefore, it can only oxidize the amorphous and crystalline areas on the surface of the cellulose [74, 75].

4.3.3 Recovery of PVAm-T by dialysis

As a water-soluble macromolecular TEMPO catalyst, PVAm-T should exist in the supernatant after the oxidation reaction [76]. The supernatant after oxidizing cellulose was concentrated by rotary evaporation and used for further catalytic oxidation. After multiple cycles, inorganic salts (NaClO) and degradation products (water-soluble

oxidized cellulose) were removed from the concentrated supernatant by dialysis. The resulting dialysate was concentrated and precipitated into methanol to recover PVAm-T for further oxidation cycles (Fig. 4.15). The recovered PVAm-T was consistent with the fresh catalyst in color, state, characteristic absorption peaks in FT-IR (Fig. 4.16) and TEMPO loading degree.

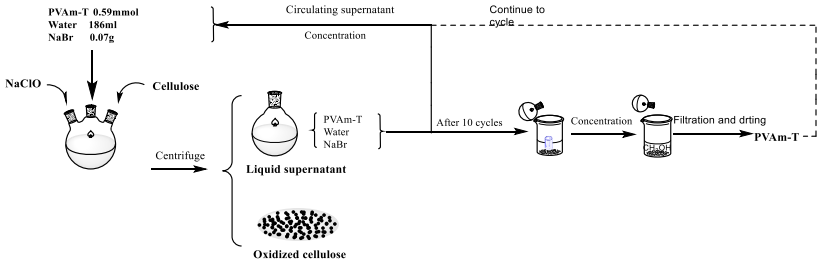

Fig. 4.15 Recovery process of PVAm-T

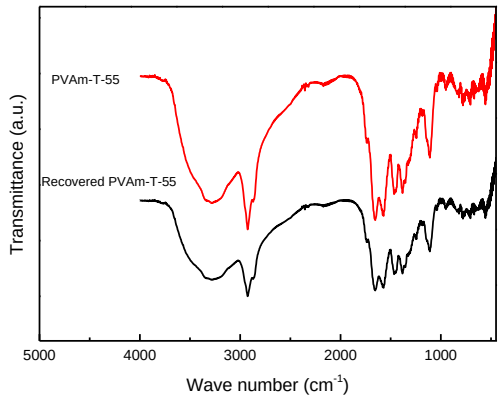

Fig. 4.16 FT-IR spectra of fresh and recovered PVAm-T-55

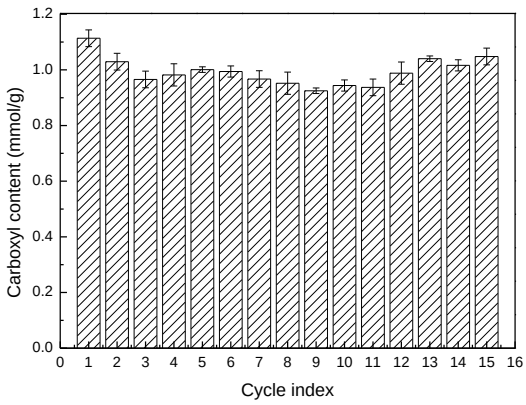

Fig. 4.17 The recyclability of PVAm-P-T-57

Fig. 4.17 shows that the recovered PVAm-T can still deliver oxidized cellulose with a high carboxyl content. Fig. 4.18 shows that the oxidized cellulose obtained using recycled PVAm-T as the catalyst still had good crystal morphology and high CrI.

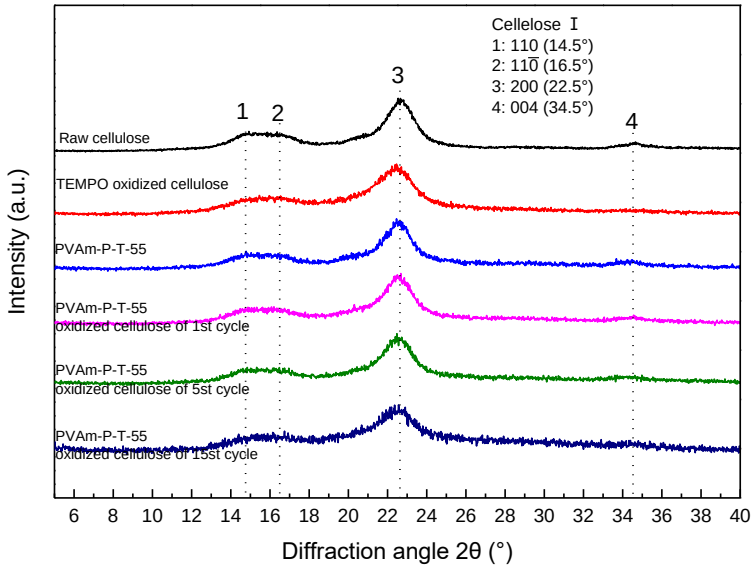

Fig. 4.18 X-ray diffraction patterns of oxidized cellulose obtained when using recycled PVAm-P-T-57 as the catalyst

4.4 Conclusion

A macromolecule water-soluble catalyst of PVAm-T was prepared and used for selective catalytic oxidation of cellulose. The catalytic performance of PVAm-T was up to 76% that of free TEMPO and did not change after recycling. The degree of degradation of PVAm-T oxidized cellulose (21%-27%) was clearly lower than that of TEMPO oxidized cellulose (61%-66%). PVAm-T with a positive charge and suitable size can effectively prevent the formation of C6 aldehydes and C2/C3 ketones due to side reactions. The oxidation is then mainly restricted to the exterior surface of porous cellulose, resulting in a significant reduction in the degradation of cellulose.

References

[1] John M, Thomas S. Biofibres and biocomposites [J]. Carbohydrate Polymers, 2008, 71(3): 343-364.

[2] Klemm D, Heublein B, Fink H, et al. Cellulose: Fascinating biopolymer and sustainable raw material [J]. Angewandte Chemie International Edition, 2005, 44(22): 3358-3393.

[3] Ye D, Montané D, Farriol X. Preparation and characterisation of methylcellulose from annual cardoon and juvenile eucalyptus [J]. Carbohydrate Polymers, 2005, 61(4): 446-454.

[4] Ye D, Farriol X. Preparation and characterization of methylcelluloses from some annual plant pulps [J]. Industrial Crops and Products, 2007, 26(1): 54-62.

[5] Yang J, Zhang L, Zuo S, et al. Production of cellulose nanofibers by TEMPO oxidation approach [J]. Journal of Northeast Forestry University, 2011, 39(3): 96-105.

[6] Pelton R. Polyvinylamine: A tool for engineering interfaces [J]. Langmuir, 2014, 30(51): 15373-15382.

[7] DiFlavio J, Pelton R, Leduc M, et al. The role of mild TEMPO-NaBr-NaClO oxidation on the wet adhesion of regenerated cellulose membranes with polyvinylamine [J]. Cellulose, 2007, 14(3): 257-268.

[8] Pelton R, Ren P, Liu J, et al. Polyvinylamine-graft-TEMPO adsorbs onto, oxidizes, and covalently bonds to wet cellulose [J]. Biomacromolecules, 2011, 12(4): 942-948.

[9] Liu J, Pelton R, Obermeyer J, et al. Laccase complex with polyvinylamine bearing

grafted TEMPO is a cellulose adhesion primer [J]. Biomacromolecules, 2013, 14(8): 2953-2960.

[10] Shi S, Pelton R, Fu Q, et al. Comparing polymer-supported TEMPO mediators for cellulose oxidation and subsequent polyvinylamine grafting [J]. Industrial & Engineering Chemistry Research, 2014, 53(12): 4748-4754.

[11] Fu Q, Sutherland A, Gustafsson E, et al. Relating redox properties of polyvinylamine-g-TEMPO/laccase hydrogel complexes to cellulose oxidation [J]. Langmuir, 2017, 33(32): 7854-7861.

[12] Yang D, Stimpson T, Soucy J, et al. Increasing wet adhesion between cellulose surfaces with polyvinylamine [J]. Cellulose, 2019, 26(1): 341-353.

[13] Elachari A, Coqueret X, Lablachecombier A, et al. Makromolekulare Chemie [J]. Macromol Chem Phys, 1993, 194: 1879.

[14] Guha S, Ray B, Mandal B. Anomalous solubility of polyacrylamide prepared by dispersion (precipitation) polymerization in aqueous tert-butyl alcohol [J]. Journal of Polymer Science Part A: Polymer Chemistry, 2001, 39(19): 3434-3442.

[15] Gaillard C, Strauss F. Ethanol precipitation of DNA with linear polyacrylamide as carrier [J]. Nucleic Acids Research, 1990, 18(2): 378.

[16] Elachari A, Coqueret X, Lablachecombier A, et al. Makromolekulare Chemie [J]. Macromol Chem Phys, 1993, 194: 1879.

[17] Tanaka H, Senju R. Preparation of polyvinylamine by the Hofmann Degradation of polyacrylamide [J]. Bulletin of the Chemical Society of Japan, 1976, 49(10): 2821-2823.

[18] Ye J, Geng Y, Xu H, et al. Preparation of polyvinylamine (PVAm) by modified Hofmann Degradation [J]. Fine Chemicals, 2012, 7.

[19] Bragd P, Van Bekkum H, Besemer A. TEMPO-mediated oxidation of polysaccharides: Survey of methods and applications [J]. Topics in Catalysis, 2004, 27(1): 49-66.

[20] Liu S, Liang H, Sun T, et al. A recoverable dendritic polyamidoamine immobilized TEMPO for efficient catalytic oxidation of cellulose [J]. Carbohydrate Polymers, 2018, 202: 563-570.

[21] Liu S, Liang H, Sun T, et al. A recoverable dendritic polyamidoamine immobilized TEMPO for efficient catalytic oxidation of cellulose [J]. Carbohydrate Polymers, 2018, 202: 563-570.

[22] Saito T, Isogai A. TEMPO-mediated oxidation of native cellulose: The effect of oxidation conditions on chemical and crystal structures of the water-insoluble fractions [J]. Biomacromolecules, 2004, 5(5): 1983-1989.

[23] Saito T, Kimura S, Nishiyama Y, et al. Cellulose nanofibers prepared by TEMPO-mediated oxidation of native cellulose [J]. Biomacromolecules, 2007, 8(8): 2485-2491.

[24] Shibata I, Isogai A. Depolymerization of cellouronic acid during TEMPO-mediated oxidation [J]. Cellulose, 2003, 10(2): 151-158.

[25] Nabar G, Shenai V. Studies in chemically modified celluloses. III. Estimation of free carboxylic acid groups in oxycellulose [J]. Journal of Applied Polymer Science, 1970, 14(5): 1215-1226.

[26] Shenai V, Sudan R. Studies in chemically modified celluloses. IV. Lactones in

chemically modified celluloses [J]. Journal of Applied Polymer Science, 1972, 16(3): 545-550.

[27] Zhao H, Li Q, Xu W, et al. Study on synthesis and thermal property of polyvinylamine [C]. Advanced Materials Research. Trans Tech Publications Ltd, 2011, 150: 1500-1503.

[28] Achari A, Coqueret X, Lablache-Combier A, et al. Preparation of polyvinylamine from polyacrylamide: a reinvestigation of the hofmann reaction [J]. Die Makromolekulare Chemie: Macromolecular Chemistry and Physics, 1993, 194(7): 1879-1891.

[29] Sun T. Preparation and application of water-soluble macromolecular catalyst containing TEMPO [D]. Hebei University of Science and Technology, 2019.

[30] Klein J, Westerkamp A. Peculiarities of polyacrylamide analysis by aqueous GPC [J]. Journal of Polymer Science: Polymer Chemistry Edition, 1981, 19(3): 707-718.

[31] Sanzari I, Humphrey E, Dinelli F, et al. Effect of patterned polyacrylamide hydrogel on morphology and orientation of cultured NRVMs [J]. Scientific Reports, 2018, 8(1): 1-12.

[32] Lira L, Martins K, De Torresi S. Structural parameters of polyacrylamide hydrogels obtained by the Equilibrium Swelling Theory [J]. European Polymer Journal, 2009, 45(4): 1232-1238.

[33] Coseri S, Biliuta G, Simionescu B, et al. Oxidized cellulose-survey of the most recent achievements [J]. Carbohydrate Polymers, 2013, 93(1): 207-215.

[34] Saito T, Isogai A. Introduction of aldehyde groups on surfaces of native cellulose

fibers by TEMPO-mediated oxidation [J]. Colloids and Surfaces A: Physicochemical and Engineering Aspects, 2006, 289(1-3): 219-225.

[35] De Nooy A, Besemer A, Van Bekkum H. Selective oxidation of primary alcohols mediated by nitroxyl radical in aqueous solution. Kinetics and Mechanism [J]. Tetrahedron, 1995, 51(29): 8023-8032.

[36] De Nooy A, Besemer A, Van Bekkum H. On the use of stable organic nitroxyl radicals for the oxidation of primary and secondary alcohols [J]. Synthesis, 1996, 1996(10): 1153-1176.

[37] De Nooy A, Besemer A, Van Bekkum H. Highly selective nitroxyl radical-mediated oxidation of primary alcohol groups in water-soluble glucans [J]. Carbohydrate Research, 1995, 269(1): 89-98.

[38] Bailey W, Bobbitt J, Wiberg K. Mechanism of the oxidation of alcohols by oxoammonium cations [J]. The Journal of Organic Chemistry, 2007, 72(12): 4504-4509.

[39] Isogai A, Saito T, Fukuzumi H. TEMPO-oxidized cellulose nanofibers [J]. Nanoscale, 2011, 3(1): 71-85.

[40] Goldstein S, Samuni A. Kinetics and mechanism of peroxyl radical reactions with nitroxides [J]. The Journal of Physical Chemistry A, 2007, 111(6): 1066-1072.

[41] Fukuzumi H. Studies on structures and properties of TEMPO-oxidized cellulose nanofibril films [J]. University of Tokyo, Japan, 2012.

[42] Fu Q, Gray Z, Van der Est A, et al. Phase behavior of aqueous poly (acrylic acid-g-TEMPO) [J]. Macromolecules, 2016, 49(13): 4935-4939.

[43] Ragab G, Amin A. Atomic absorption spectroscopic, conductometric and

colorimetric methods for determination of fluoroquinolone antibiotics using ammonium reineckate ion-pair complex formation [J]. Spectrochimica Acta Part A: Molecular and Biomolecular Spectroscopy, 2004, 60(4): 973-978.

[44] Yao W, Xu Q, Jin L, et al. Effects of TEMPO/NaBr/NaClO-oxidation of nanocrystalline cellulose on its properties [J]. Chemistry and Industry of Forest Products, 2015, 35(2): 31-37.

[45] Saito T, Isogai A. TEMPO-mediated oxidation of native cellulose. The effect of oxidation conditions on chemical and crystal structures of the water-insoluble fractions [J]. Biomacromolecules, 2004, 5(5): 1983-1989.

[46] Isogai T, Yanagisawa M, Isogai A. Degrees of polymerization (DP) and DP distribution of cellouronic acids prepared from alkali-treated celluloses and ball-milled native celluloses by TEMPO-mediated oxidation [J]. Cellulose, 2009, 16(1): 117-127.

[47] Shinoda R, Saito T, Okita Y, et al. Relationship between length and degree of polymerization of TEMPO-oxidized cellulose nanofibrils [J]. Biomacromolecules, 2012, 13(3): 842-849.

[48] Isogai A, Kato Y. Preparation of polyuronic acid from cellulose by TEMPO-mediated oxidation [J]. Cellulose, 1998, 5(3): 153-164.

[49] Ibert M, Marsais F, Merbouh N, et al. Determination of the side-products formed during the nitroxide-mediated bleach oxidation of glucose to glucaric acid [J]. Carbohydrate Research, 2002, 337(11): 1059-1063.

[50] Shibata I, Isogai A. Depolymerization of cellouronic acid during TEMPO-mediated oxidation [J]. Cellulose, 2003, 10(2): 151-158.

[51] Coseri S. Cellulose: To depolymerize… or not to? [J]. Biotechnology Advances, 2017, 35(2): 251-266.

[52] Shinoda R, Saito T, Okita Y, et al. Relationship between length and degree of polymerization of TEMPO-oxidized cellulose nanofibrils [J]. Biomacromolecules, 2012, 13(3): 842-849.

[53] Liang H, Cao M, Yang D, et al. Polyamidoamine immobilized TEMPO mediated oxidation of cellulose: Effect of macromolecular catalyst structure on the reaction rate, oxidation degree and degradation degree [J]. Fibers and Polymers, 2020, 21(6): 1251-1258.

[54] Isogai A. Cellulose nanofibers: Recent progress and future prospects [J]. Journal of Fiber Science and Technology, 2020, 76(10): 310-326.

[55] Spier V, Sierakowski M, Reed W, et al. Polysaccharide depolymerization from TEMPO-catalysis: Effect of TEMPO concentration [J]. Carbohydrate Polymers, 2017, 170: 140-147.

[56] Saito T, Shibata I, Isogai A, et al. Distribution of carboxylate groups introduced into cotton linters by the TEMPO-mediated oxidation [J]. Carbohydrate Polymers, 2005, 61(4): 414-419.

[57] Kuramae R, Saito T, Isogai A. TEMPO-oxidized cellulose nanofibrils prepared from various plant holocelluloses [J]. Reactive and Functional Polymers, 2014, 85: 126-133.

[58] Saito T, Isogai A. Introduction of aldehyde groups on surfaces of native cellulose fibers by TEMPO-mediated oxidation [J]. Colloids and Surfaces A: Physicochemical

and Engineering Aspects, 2006, 289(1-3): 219-225.

[59] Shinoda R, Saito T, Okita Y, et al. Relationship between length and degree of polymerization of TEMPO-oxidized cellulose nanofibrils [J]. Biomacromolecules, 2012, 13(3): 842-849.

[60] Montanari S, Roumani M, Heux L, et al. Topochemistry of carboxylated cellulose nanocrystals resulting from TEMPO-mediated oxidation [J]. Macromolecules, 2005, 38(5): 1665-1671.

[61] Puangsin B, Fujisawa S, Kuramae R, et al. TEMPO-mediated oxidation of hemp bast holocellulose to prepare cellulose nanofibrils dispersed in water [J]. Journal of Polymers and the Environment, 2013, 21(2): 555-563.

[62] Tahiri C, Vignon M. TEMPO-oxidation of cellulose: Synthesis and characterisation of polyglucuronans [J]. Cellulose, 2000, 7(2): 177-188.

[63] Milanovic J, Kostic M, Milanovic P, et al. Influence of TEMPO-mediated oxidation on properties of hemp fibers [J]. Industrial & Engineering Chemistry Research, 2012, 51(29): 9750-9759.

[64] Lin C, Zeng T, Wang Q, et al. Effects of the conditions of the TEMPO/NaBr/NaClO system on carboxyl groups, degree of polymerization, and yield of the oxidized cellulose [J]. BioResources, 2018, 13(3): 5965-5975.

[65] Mishra S, Thirree J, Manent A, et al. Ultrasound-catalyzed TEMPO-mediated oxidation of native cellulose for the production of nanocellulose: Effect of process variables [J]. BioResources, 2011, 6(1): 121-143.

[66] Saito T, Isogai A. TEMPO-mediated oxidation of native cellulose. The effect of

oxidation conditions on chemical and crystal structures of the water-insoluble fractions [J]. Biomacromolecules, 2004, 5(5): 1983-1989.

[67] Xing L, Hu C, Zhang W, et al. Transition of cellulose supramolecular structure during concentrated acid treatment and its implication for cellulose nanocrystal yield [J]. Carbohydrate Polymers, 2020, 229: 115539.

[68] Megashah L, Ariffin H, Zakaria M, et al. Modification of cellulose degree of polymerization by superheated steam treatment for versatile properties of cellulose nanofibril film [J]. Cellulose, 2020, 27(13): 7417-7429.

[69] Jiang S, Farooq A, Han F, et al. Investigation of a widely applicable process for extracting carboxyl-rich cellulose nanocrystal (CNC) [J]. Fibers and Polymers, 2021, 22(3): 647-657.

[70] Wang Z, Yao Z, Zhou J, et al. Isolation and characterization of cellulose nanocrystals from pueraria root residue [J]. International Journal of Biological Macromolecules, 2019, 129: 1081-1089.

[71] Agarwal U, Ralph S, Baez C, et al. Effect of sample moisture content on XRD-estimated cellulose crystallinity index and crystallite size [J]. Cellulose. 24 (5): 1971-1984., 2017, 24(5): 1971-1984.

[72] Wang H, Wang X, Sun T, et al. Recoverable, water-soluble polyethylene glycol-immobilized N-hydroxyphthalimide, as mediator for cellulose oxidation in the presence of NaBr and NaClO [J]. Cellulose, 2021, 28(18): 11315-11328.

[73] Sankhla S, Sardar H, Neogi S. Greener extraction of highly crystalline and thermally stable cellulose micro-fibers from sugarcane bagasse for cellulose nano-

fibrils preparation [J]. Carbohydrate Polymers, 2021, 251: 117030.

[74] Saito T, Isogai A. TEMPO-mediated oxidation of native cellulose. The effect of oxidation conditions on chemical and crystal structures of the water-insoluble fractions [J]. Biomacromolecules, 2004, 5(5): 1983-1989.

[75] Tahiri C, Vignon M. TEMPO-oxidation of cellulose: Synthesis and characterisation of polyglucuronans [J]. Cellulose, 2000, 7(2): 177-188.

[76] Liu S, Sun T, Yang D, et al. Polyacrylic acid supported TEMPO for selective catalytic oxidation of cellulose: recovered by its pH sensitivity [J]. Cellulose, 2018, 25(10): 5687-5696.

CHAPTER 5 POLYETHYLENE GLYCOL MODIFIED POLYAMIDOAMINE IMMOBILIZED TEMPO CATALYST FOR EFFICIENT CATALYTIC OXIDATION OF CELLULOSE

(Note: This research is expected to appear in the Journal of Cellulose.)

5.1 Introduction

Polyethylene glycol (PEG) has excellent solubility in polar and non-polar solvents (including DCM and water) and very narrow and defined polydispersity indices, making it a new carrier for TEMPO in a biphasic media (such as the oxidation of water insoluble alcohols in the presence of NaClO and NaBr in water/DCM) [1-6]. Polyethylene glycol monomethyl ether (mPEG) has a similar structure and properties to PEG. Wan et al. supported TEMPO on mPEG to prepare a water-soluble macromolecular TEMPO catalyst and found that it could catalyze the oxidation of different allyl alcohols and aromatic primary alcohols in an acetonitrile/water medium, showing excellent catalytic performance [7].

Araki and Iida immobilized TEMPO on mPEG2000 to prepare mPEG2000-TEMPO for oxidizing cellulose for purposes of preparing carboxylated nanocellulose [8]. The catalytic performance in the first oxidation cycle could reach 60% of that of free TEMPO. The catalyst was then recovered by extraction with DCM and re-used for

further oxidation cycles. However, because TEMPO itself has good water solubility, loading it on PEG with poorer water solubility than TEMPO cannot increase its water solubility further. The large size of PEG tends to reduce its catalytic activity when used to oxidize a water-insoluble macromolecular substrate such as cellulose in water.

In a previous work, we synthesized an amphiphilic nitroxide block copolymer of poly(ethylene glycol)-b-poly(2, 2, 6, 6-tetramethylpiperidinyloxy-4-yl-methacrylate) (PEG-PTMA) by means of activators regenerated by electron transfer atom transfer radical polymerization (ARGET ATRP) [9]. The catalytic oxidation performance of cellulose in the acetonitrile/water system was studied and the oxidation level was equivalent to 73.2% of free TEMPO. The block copolymer was easy to recycle by DCM extraction and the activity did not decrease after multiple cycles. However, the catalytic activity was very low when used in water, because the block copolymer was water-insoluble.

Dendrimer is a kind of synthetic macromolecule with a highly branched, regular three-dimensional structure [10-14]. Dendritic polyamidoamine (PAMAM) has excellent water-solubility, and was used to prepare an immobilized TEMPO called Gn PAMAM-Tx for efficient catalytic oxidation of cellulose in water. Its catalytic effect was similar to that of free TEMPO [15, 16]. However, its recycling process is complex, and the supernatant of the oxidation mixture must be salted out before the catalyst is extracted with N-dimethylformamide, because PAMAM has excellent water solubility and poor

solubility in conventional organic solvents.

PEG-modified PAMAM may combine the advantages of these two macromolecules [17-24] and it was hoped that a TEMPO immobilized catalyst with high catalytic oxidation performance and easy recycling feature might be achieved. Based on this, mPEG modified PAMAM macromolecules (mPEG-Gn PAMAM) with different PAMAM generations were prepared. With mPEG-Gn PAMAM as the carrier, the water-soluble mPEG-Gn PAMAM immobilized TEMPO catalysts (mPEG-Gn PAMAM-Tx) with different TEMPO loading amounts were obtained and used for selective oxidation of cellulose, in order to produce oxidized cellulose products. The effect of the structure of mPEG-Gn PAMAM-Tx on the catalytic oxidation of cellulose was investigated. After recovery by DCM extraction, mPEG-Gn PAMAM-Tx was re-used to evaluate its recycling performance.

5.2 Experiment

5.2.1 Preparation of PEG modified PAMAM immobilized TEMPO catalyst called mPEG-Gn PAMAM-Tx

5.2.1.1 Preparation of mPEG-CHO

mPEG-aldehyde was prepared by oxidation of mPEG with DMSO/acetic anhydrate [25, 26]. The mPEG (5 g, 5 mmol, Mn=1000 g/mol) was then completely dissolved in anhydrous DMSO/chloroform (30.0 mL, 9v/v) under a N_2 atmosphere. After adding acetic anhydride (5.0 mL, 50 mmol) to the solution, the mixture was stirred for 25 h at

25 ℃. The product was then precipitated with prechilled diethyl ether. The precipitate was filtered, and the crude product obtained was dissolved in chloroform and re-precipitated twice using diethyl ether for purification. After drying under vacuum, mPEG-CHO was obtained.

5.2.1.2 Preparation of Gn PAMAM

PAMAM dendrimers with different generations (Gn PAMAM, where n represents the generation of PAMAM) were prepared, following the method reported in previous reports, but with minor modifications [32, 33].

Methylacrylate (43.0 g, 0.5 mol) was placed in a three-necked flask containing 30 mL of methanol while stirring. The solution of ethylenediamine (5.0 g, 0.083 mol) in methanol (10 mL) was added dropwise at 0 ℃. After the solution was added the reaction was carried out at 25 ℃ for 24 h. The excess methanol and methyl acrylate were then removed using a rotatory evaporator to obtain G0.5 PAMAM.

In a N_2 environment, ethylenediamine (57.7 g, 0.96 mol) was placed in a three-necked flask containing 100 mL methanol while stirring. G0.5 PAMAM (16.2 g, 0.04 mol) in methanol (10 mL) was then slowly added at 0 ℃. After dripping, the reaction was carried out at 25 ℃ for 24 h. The excess ethylene diamine and methanol were then removed by rotary evaporation to obtain G1.0 PAMAM.

By repeating the above two steps, G2.0 and G3.0 PAMAM dendrimers were obtained.

5.2.1.3 Preparation of Gn PAMAM-Tx

Gn PAMAM-Tx was prepared by the reaction of reducing amination between the primary amines in PAMAM and carbonyls in 4-oxo-TEMPO, in which T and x represented TEMPO and the TEMPO loading degree on PAMAM, respectively.

The preparation of G1.0 PAMAM-T30 is given as an example: In a N_2 environment, G1.0 PAMAM (1.032 g, 2 mmol) and 4-oxo-TEMPO (the molar ratio of 4-oxo-TEMPO to primary amine in PAMAM was 1.5) were added to methanol (30 mL) while stirring. At 40 ℃, $NaBH_3CN$ (24 mmol) was added to the reaction mixture in three equal parts after 3 h, 24 h and 48 h respectively. After reaction, the excess $NaBH_3CN$ was quenched with a saturated aqueous $NaHCO_3$ solution. After filtering, the unreacted 4-oxo-TEMPO in the filtrate was extracted by ethyl acetate, and G1.0 PAMAM-T30 was obtained by evaporating the water phase.

5.2.1.4 Preparation of mPEG-Gn PAMAM-Tx

The preparation of mPEG-G1.0 PAMAM-T30 is given as an example: Under a N_2 atmosphere, G1.0 PAMAM-T30 (1.0 g, 4.94 mmol NH_2) and mPEG-CHO (4.94 g, 4.94 mmol) were fully dissolved in methanol (40 mL). Under magnetic agitation at 40 ℃, $NaCH_3CN$ (0.465 g 7.41 mmol) was added to the reaction system in three batches, i.e. at 3 h, 24 h and 48 h, respectively. After 96 h, the excess $NaBH_3CN$ was quenched by

adding a saturated aqueous $NaHCO_3$ solution. It was then filtrated to obtain the filtrate containing mPEG1000-G1.0 PAMAM-T30. The filtrate was evaporated to remove water and methanol, and then vacuum dried to obtain mPEG1000-G1.0 PAMAM-T30.

5.2.1.5 Preparation of mPEG-T

Under a N_2 environment, mPEG-CHO (1.0 g, 1 mmol), DCM (20 mL) and 4-amino-2, 2, 6, 6-tetramethylpiperidine (4-NH_2-TEMP, 0.68 g, 4 mmol) were placed in a three-necked flask. $NaBH_3CN$ (1.51 g, 24 mmol) was added in three equal parts under magnetic stirring at 40 ℃. After 96 h, a saturated aqueous $NaHCO_3$ solution was added to the reaction solution to quench the excess $NaBH_3CN$, and the concentrated DCM phase was poured into cold ether for precipitation. The precipitate was filtered and dried to obtain mPEG-TEMP.

mPEG-TEMP (0.578 g, 0.5 mmol) and DCM (20 mL) were placed in a three-necked flask at 0 ℃. The DCM of 3-chloroperoxybenzoic acid (20 mL, the molar ratio of 3-chloroperoxybenzoic acid to PEG-TEMP is 2:1) was slowly added. After stirring for 1 h, the reaction solution was poured into cold ether (300 mL) for precipitation. Through filtering and vacuum drying, the PEG immobilized TEMPO called mPEG-T was obtained.

5.2.2 mPEG-Gn PAMAM-Tx mediated oxidation of cellulose

The experimental method used was the same as that described in item 4.2.2.

5.2.3 Post-reduction of oxidized cellulose

The experimental method used was the same as that described in 4.2.3.

5.3 Results and Discussion

5.3.1 Synthetic route of mPEG-Gn PAMAM-Tx

In this section of the study, a water-soluble TEMPO-immobilized mediator for catalytic oxidation of cellulose, with mPEG modified PAMAM as the carrier, was designed to achieve both high catalytic oxidation performance and easy recovery characteristics. The preparation route is shown in Fig. 5.1. PAMAM dendrimers of G1.0-G3.0 were synthesized by means of the repeated Michael addition and ester aminolysis of ethylenediamine and methyl acrylate. Through the reductive amination reaction of -NH_2 in PAMAM and -C=O in 4-oxo-TEMPO, the PAMAM immobilized TEMPO called Gn PAMAM-Tx was prepared. The mPEG modified PAMAM immobilized TEMPO mediator called mPEG-Gn PAMAM-Tx was obtained by means of a condensation reduction reaction of the aldehyde group in PEG-CHO and the amino group in Gn PAMAM-Tx, with $NaBH_4$ used as the reducing agent.

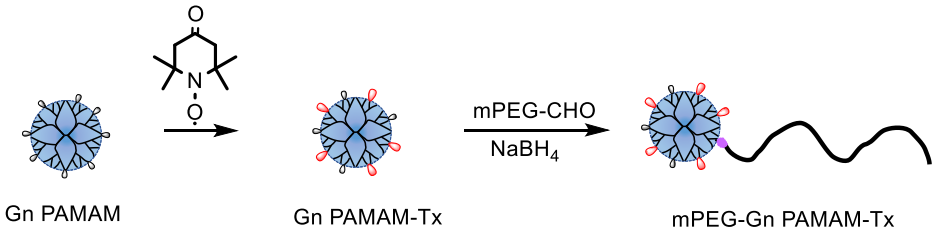

Fig. 5.1 Synthetic route of mPEG-Gn PAMAM-Tx

5.3.2 Characterization of mPEG-Gn PAMAM-Tx

5.3.2.1 FT-IR

The FT-IR spectra of mPEG-CHO, G1.0 PAMAM-T30 and mPEG-G1.0 PAMAM-T30 are shown in Fig. 5.2. In the FT-IR spectrum of mPEG-CHO [8, 25, 26], the C=O band attributed to the aldehyde group in mPEG-CHO was found at 1740 cm^{-1}. This band disappeared in the spectrum of mPEG-G1.0 PAMAM-T30. For the spectrum of G1.0 PAMAM-T30, the C=O stretching vibration band at 1654 cm^{-1}, the N-H deformation vibration band at 1577 cm^{-1} of the amide in PAMAM and the stretching vibration bands of N-O at 1360 cm^{-1} and C-N at 1243 cm^{-1} in TEMPO were observed. These characteristic bands also disappeared in the spectrum of mPEG-G1.0 PAMAM-T30 [8, 15, 16].

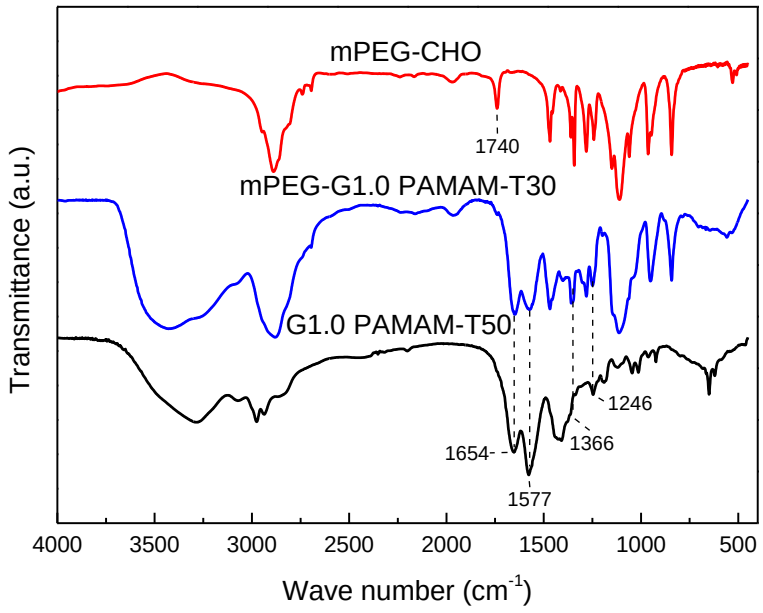

Fig. 5.2 FT-IR spectra of mPEG-G1.0 PAMAM-T30

5.3.2.2 Proton nuclear magnetic resonance spectroscopy (^{1}H NMR)

An unpaired electron within the TEMPO of mPEG-G1.0 PAMAM-T30 makes it paramagnetic [27-29]. Paramagnetic materials can affect the uniformity of the magnetic field, resulting in an abnormally wide NMR spectrum. To address this issue, the TEMPO moiety should be reduced to the hydroxylamine form (TEMPO-OH) before NMR characterization. In order to further prove successful synthesis of mPEG1000-G1.0 PAMAM-T30, its TEMPO moieties were reduced to TEMPO-OH by phenyl hydrazine and characterized by ^{1}H NMR. As shown in Fig. 5.3, the methylene shift peak of PEG appeared at 3.5 ppm and the characteristic shift peak of N-OH ascribed to the reduction of nitroxide radical was observed at 7.2 ppm.

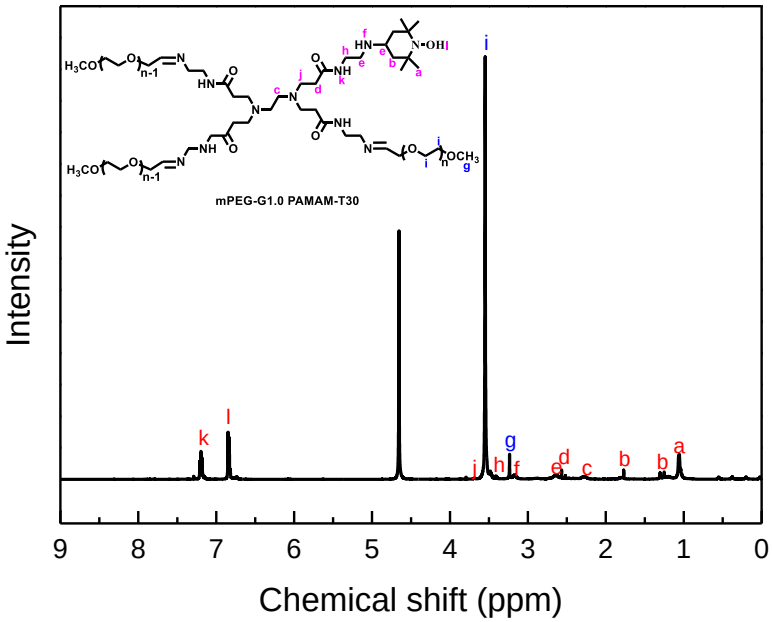

Fig. 5.3 ^{1}H NMR spectra of mPEG-G1.0 PAMAM-T30 in D_2O

5.3.2.3 X-ray photoelectron spectrometer (XPS)

The XPS results of mPEG-G1.0 PAMAM-T30 are shown in Table 5.1. As expected,

mPEG-G1.0 PAMAM-T30 mainly included C (61.7%), N (8.6%) and O (29.7%). Four fitting C peaks corresponding to O-C=O (C1, 286.1 eV), C-O (C2, 285.7 eV), C-N (C3, 285.1 eV) and C=O (C4, 283.95 eV) were observed in Fig. 5.4. The following were also found: four types of N species, i.e C-N (N1, 401.1 eV, -NH- (N2, 399.1 eV), -NH_2 (N3,398.51 eV) and pyridinic-N (N4, 398.1 eV)); three types of O species, i.e. C-O-C (O1, 532.3 eV), N-O (O2, 531.5 eV) and C=O (O3, 531.3 eV)). These results further confirmed the covalent attachment of mPEG and G1.0 PAMAM-T30.

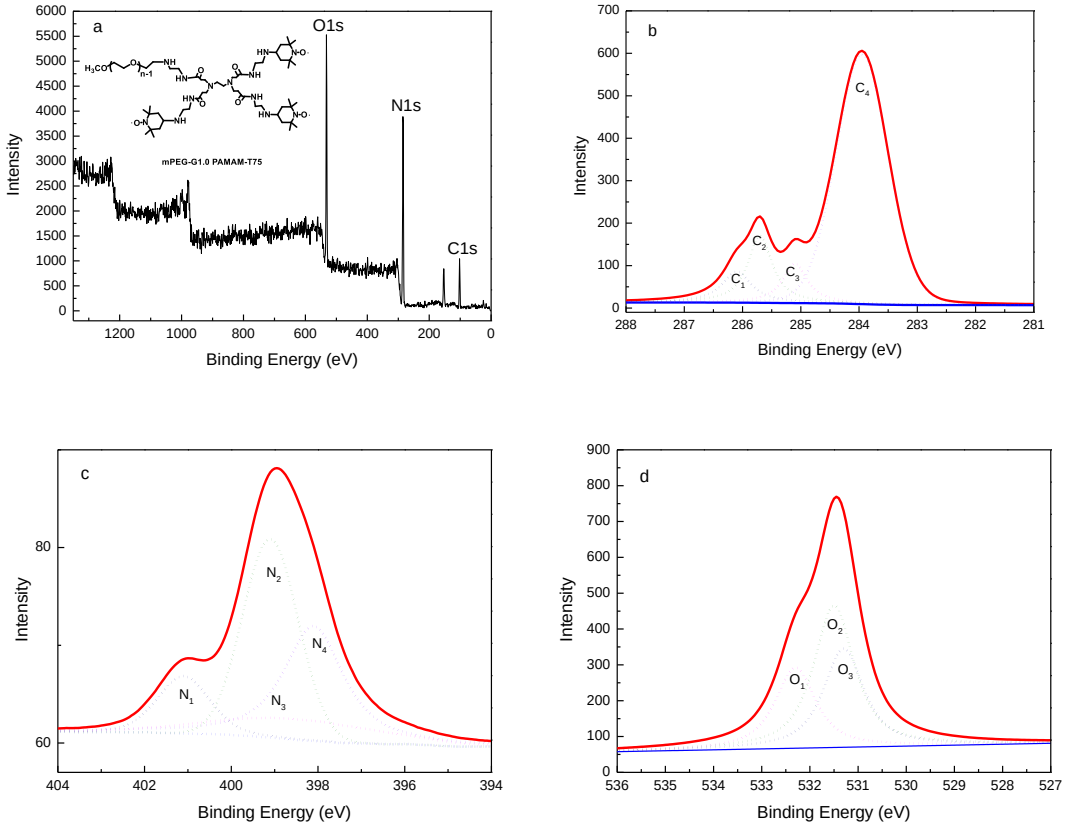

Fig. 5.4 The wide-scan and high-resolution XPS spectra of C1s, N1s and O1s for mPEG-G1.0 PAMAM-T30 in powder form

Table 5.1 Elemental composition of the mPEG-G1.0 PAMAM-T30 determined by XPS

Samples	Theoretical			Measured		
	C (%)	N (%)	O (%)	C (%)	N (%)	O (%)
mPEG	60.0	0	40.00	60.4	0	39.6
mPEG-G1.0 PAMAM-T30	60.9	10.1	29.0	61.7	8.6	29.7

5.3.2.4 GPC

Compared with mPEG, the retention time of mPEG-G1.0 PAMAM-T30 was significantly reduced, but the distribution was unchanged (Fig. 5.5). This suggested that the introduction of G1.0 PAMAM-T30 to the end of the mPEG increased its hydrodynamic volume. As shown in Table 5.2, the measured molecular weight of mPEG-G1.0 PAMAM-T30 was 1682 g/mol, i.e. slightly higher than the theoretical value (1567 g/mol). This was because the GPC measured molecular weight was obtained from the calibration curve of PEG standards, and PAMAM had a different chemical structure to PEG. These results further confirmed successful preparation of mPEG-G1.0 PAMAM-T30.

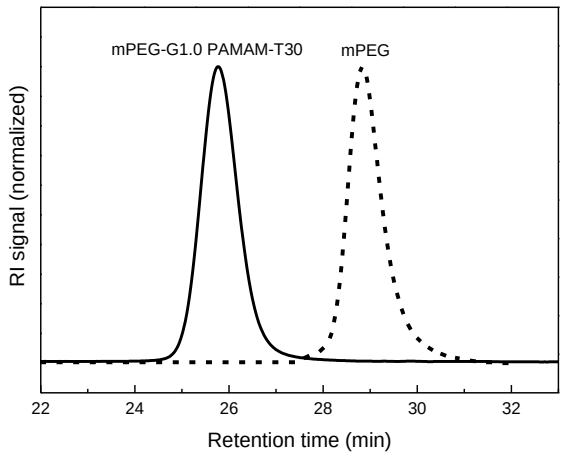

Fig. 5.5 GPC curves of PEG and mPEG-G1.0 PAMAM-T30

5.3.2.5 MS

Fig. 5.6 shows the mass spectra of mPEG-G1.0 PAMAM-T30. The signals at m/z=415.6, 444.6, 545.3, 589.7, 610.8, 619.3 and 655.8 corresponded to the fragment ions of G1.0 PAMAM-T30. The fragment ion of mPEG was detected at m/z=1024.7. These results further confirmed successful preparation of mPEG-G1.0 PAMAM-T30.

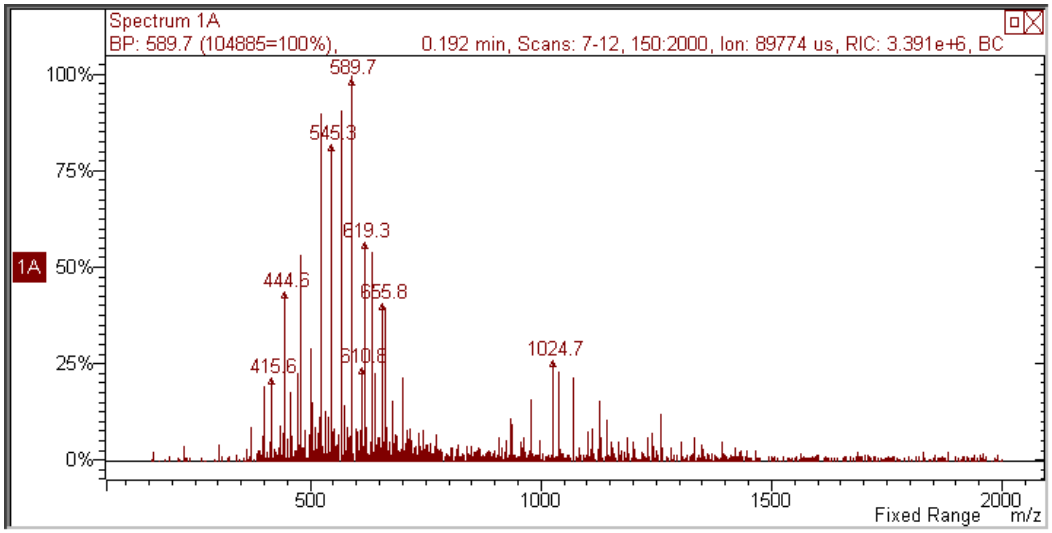

Fig. 5.6 The mass spectrum of mPEG-G1.0 PAMAM-T30

5.3.2 7 Preparation of mPEG-Gn PAMAM-Tx with different PAMAM generations and different TEMPO loading degrees

Table 5.2 Prepared PEG-Gn PAMAM-Tx with different PAMAM generations and different TEMPO loading degrees

mPEG-Gn PAMAM-Tx	TEMPO loading degree (%)	TEMPO loading density (mmol/g)	Theoretical Mn (g/mol)	GPC measured Mn (g/mol)

mPEG-G1.0 PAMAM-T30	30	0.766	1567	1682
mPEG-G1.0 PAMAM-T50	50	1.249	1601	1825
mPEG-G1.0 PAMAM-T70	70	1.712	1635	1840
mPEG-G2.0 PAMAM-T30	30	0.968	2479	2680
mPEG-G3.0 PAMAM-T30	30	1.115	4303	4550

Based on the successful preparation of mPEG-Gn PAMAM-T30, PEG-Gn PAMAM-Tx catalysts with different PAMAM generations (G1.0, G2.0 and G3.0), and different TEMPO loading degrees (30%, 50% and 70%) were designed and prepared (Table 5.2). When the PAMAM generation was fixed (G1.0), the TEMPO loading density and molecular weight of the macromolecular catalyst increased accordingly with an increase in the TEMPO loading degree. When the TEMPO loading degree was fixed (30%), the molecular weight of the macromolecular catalyst increased dramatically with the PAMAM generation. However, the TEMPO loading density changed slightly, because the terminal amino number of PAMAM also multiplied as its generation increased. It should be emphasized that the molecular weights of PEG-Gn PAMAM-Tx were estimated by GPC with a refractive index detector using a calibration curve from PEG standards and this method can only measure the relative molecular weights of these polymers, because the radii of gyration of them must be different from those of PEG. However, it can still be used to characterize the trend of molecular weight change in the preparation of macromolecular catalyst.

5.3.3 mPEG-Gn PAMAM-Tx mediated oxidation of cellulose

The prepared mPEG-Gn PAMAM-Tx catalysts were used for catalytic oxidation of cellulose in water with NaBr as a promoter and NaClO as the oxidant. All reactions were carried out for 4 h at 25 ℃. For comparison purposes, mPEG immobilized TEMPO (mPEG-T) was also prepared by means of the reaction of mPEG-CHO and 4-NH_2-TEMPO.

The FT-IR spectra of mPEG-Gn PAMAM-T30 oxidized cellulose products are shown in Fig. 5.7. It was seen that all mPEG-Gn PAMAM-T30 oxidized cellulose samples had a sharp peak at 1615 cm^{-1} corresponding to -COONa. The peak strength of mPEG-Gn PAMAM-T30 oxidized cellulose at 1615 cm^{-1} was significantly higher than that of raw cellulose, but slightly less than that of TOC, which shows that mPEG-Gn PAMAM-T30 can also give a satisfactory cellulose oxidation performance. The carboxy content of oxidized cellulose seemed to gradually decrease with an increase in PAMAM generation, probably due to the corresponding increase in the size of the macromolecular catalyst.

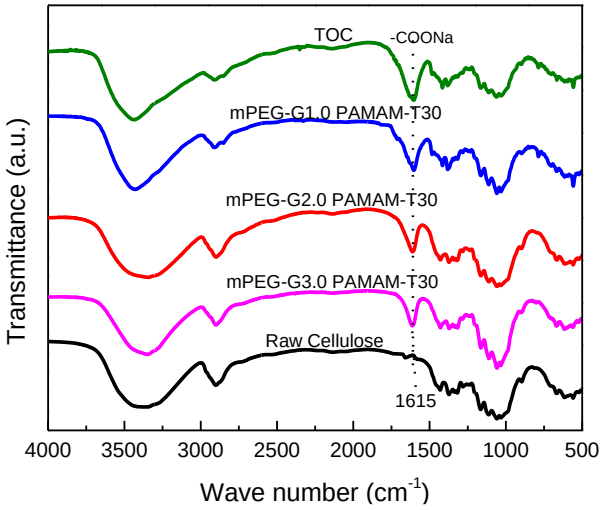

Fig. 5.7 FT-IR spectra of oxidized cellulose obtained with mPEG-Gn PAMAM-T30

5.3.3.1 Cellulose oxidation rate

The cellulose oxidation rate was evaluated by the amount of 0.5 M NaOH consumed. As shown in Fig. 5.8, when the TEMPO loading degree was fixed at 30%, the oxidation rate of mPEG modified PAMAM immobilized TEMPO was decreased with the PAMAM generation increasing, because the molecular size of PAMAM was proportional to its generation. Therefore, mPEG-G1.0 PAMAM was selected as a carrier for further studying the effect of TEMPO loading degree on the catalytic oxidation rate. As the TEMPO loading degree was increased from 30% to 70%, the NaOH consumption amount decreased by half. This may be because increasing the TEMPO loading degree may lead to poor water solubility of the macromolecular catalyst. It should be pointed out that water solubility should be the main factor in determining the catalytic properties of the macromolecular TEMPO catalyst, because G1.0 PAMAM-T30 has excellent water solubility, and has a catalytic oxidation rate similar to that of free TEMPO.

When G1.0 PAMAM-T30 was modified by mPEG (the water solubility of mPEG with Mn=1000 is more hydrophobic than G1.0 PAMAM), the obtained mPEG-G1.0 PAMAM-T30 gave a cellulose oxidation rate lower than G1.0 PAMAM-T30, but higher than mPEG-T. This is because an increase in water solubility can decrease the diffusion hindrance between the macromolecular catalyst and the cellulose surface, and improve the contact of TEMPO moieties on the macromoleclar catalyst with C6 hydroxyl groups on the cellulose surface.

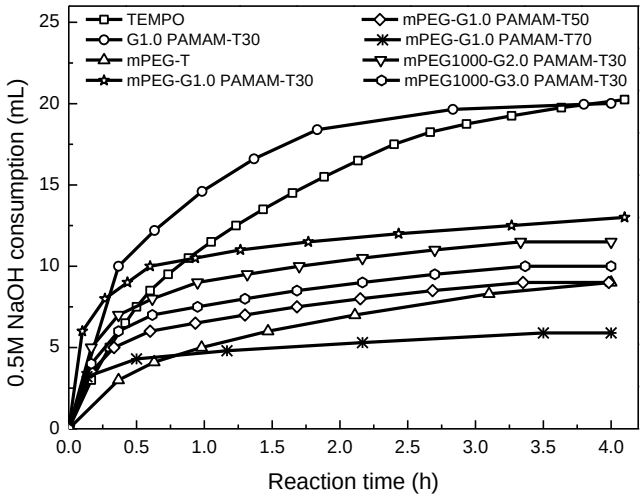

Fig. 5.8 NaOH consumption amounts for mPEG-G1.0 PAMAM-T30, mPEG-G1.0 PAMAM-T50, mPEG-G1.0 PAMAM-T70, mPEG-G2.0 PAMAM-T30, mPEG-G3.0 PAMAM-T30, G1.0 PAMAM-T30, mPEG-T and free TEMPO

5.3.3.2 Cellulose oxidation degree

The carboxyl content of oxidative cellulose can be used to characterize its degree of oxidation. Therefore, when the oxidation time is fixed (4 h), the carboxyl content can be used to evaluate the catalytic activity of the TEMPO-based oxidation catalyst. The

carboxyl content of the samples was measured by conductance titration. The carboxyl content of G1.0 PAMAM-T30 oxidized cellulose was 1.45 mmol/g (Fig. 5.9), i.e. equivalent to the free TEMPO level, because G1.0 PAMAM-T30 has excellent water-solubility and a small molecular size. When G1.0 PAMAM-T30 was modified with mPEG1000 to give mPEG-G1.0 PAMAM-T30, the catalytic performance was decreased and mPEG-G1.0 PAMAM-T30 oxidized cellulose was 1.22 mmol/g, which is equivalent to 84% of the free TEMPO level. However, this was still higher than other reported TEMPO immobilized macromolecular catalysts (0.86 mmol/g when using P(AA-co-TA) as the catalyst [31], and 1.11 mmol/g with PVAm-T as the catalyst [34]). The catalytic oxidation performance of mPEG-G1.0 PAMAM-T30 was significantly higher than that of mPEG-T, which only produced oxidized cellulose with a carboxyl content of 0.80 mmol/g. This further confirmed that water solubility is a key factor in the catalytic oxidation properties of the TEMPO immobilized catalysts.

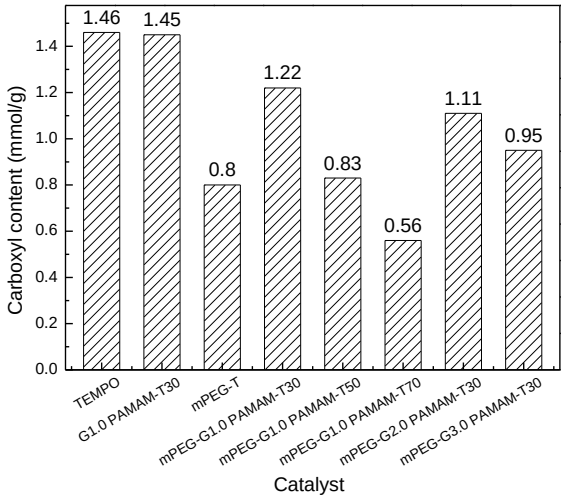

Fig. 5.9 Carboxyl content of oxidized cellulose samples obtained with macromolecular TEMPO catalysts and free TEMPO

5.3.3.3 DP of oxidized cellulose

TEMPO mediated selective catalytic oxidation of cellulose under alkaline conditions shows a high level of oxidative activity, but also causes severe degradation of cellulose. The main reason for cellulose degradation during TEMPO mediated oxidation is a β-elimination reaction. Another reason is a small amount of C6 aldehydes and C2/C3 ketones formed by the non-specific cellulose oxidation of NaClO/NaBr, as these by-products will cause depolymerization of cellulose when it is in a copper ethylenediamine solution for testing DP [30]. After post-reduction treatment of oxidized cellulose with $NaBH_4$, the C6 aldehydes and C2/C3 ketones can be removed. This prevents oxidized cellulose from degrading when testing DP, and the measured DP is generally higher than that of the unreduced sample. This difference can be used to evaluate the selectivity of the cellulose oxidation reaction. It was found that the DP of TOC was only 59, and the corresponding DD was about 63%. After post-reduction treatment, the DP increased to 87, which indicates that TEMPO mediated oxidation of cellulose generated a large amount of C6 aldehydes and C2/C3 ketones.

Compared with TEMPO oxidized cellulose, G1.0 PAMAM-T30 oxidized cellulose gave a similar carboxyl content and increased DP (78). In particular, its DP was significantly increased to 116 after post-reduction, which indicates that PAMAM immobilized TEMPO with a unique molecular structure has the potential to limit cellulose degradation. When the TEMPO loading degree was increased to 70% (G1.0

PAMAM-T70), the macromolecular size increased and the water-solubility decreased, resulting in a decrease in the degree of oxidation and the degree of degradation. mPEG-G1.0 PAMAM-T30 gave the same cellulose oxidation degree with G1.0 PAMAM-T70. However, the cellulose degradation degree of the former was inhibited and the DP of mPEG-G1.0 PAMAM-T30 oxidized cellulose reached 110. Interestingly, the DP was almost unchanged after post-reduction, and similar results were found when the TEMPO loading degree was increased to 50% (mPEG-G1.0 PAMAM-T50). Therefore, modified G1.0 PAMAM immobilized TEMPO can significantly reduce the occurrence of side reactions during the cellulose oxidation process, which indicates that it had high cellulose oxidation selectivity.

Table 5.3 Carboxyl content and DP results of oxidized cellulose samples obtained with mPEG-G1.0 PAMAM-Tx and other mediators

Samples	Carboxyl content	DP	DP after post-reduction
TEMPO oxidized cellulose	1.46	59	87
G1.0 PAMAM-T30 oxidized cellulose	1.45	78	116
G1.0 PAMAM-T70 oxidized cellulose	1.22	95	106
mPEG-G1.0 PAMAM-T30 oxidized cellulose	1.22	110	113
mPEG-G1.0 PAMAM-T50 oxidized cellulose	0.83	95	99

5.3.4 Recyclability

The introduction of mPEG can give mPEG-Gn PAMAM-Tx appropriate oil solubility, thus allowing it to be recycled by extraction. After separating the oxidized cellulose by centrifugation, the macromolecular catalyst was extracted by adding DCM to the

upward supernatant, which was then recovered by precipitation. (See Fig. 5.10.)

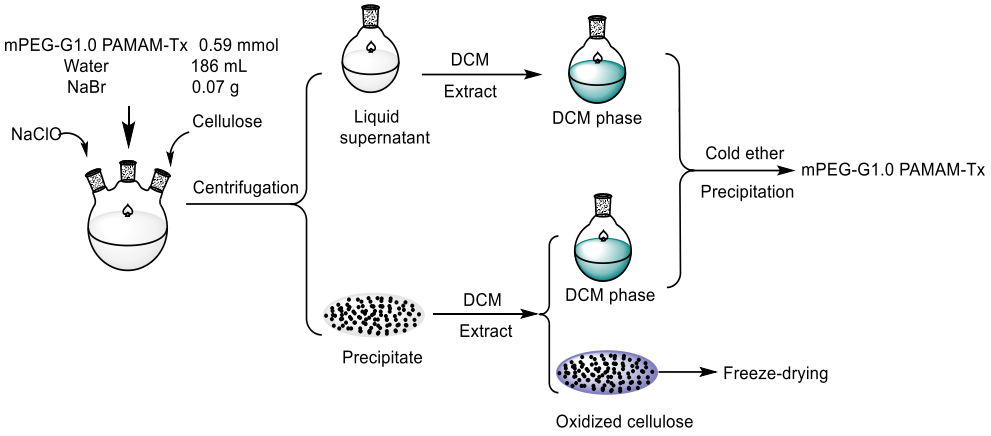

Fig. 5.10 Schematic recycling process of mPEG-G1.0 PAMAM-Tx

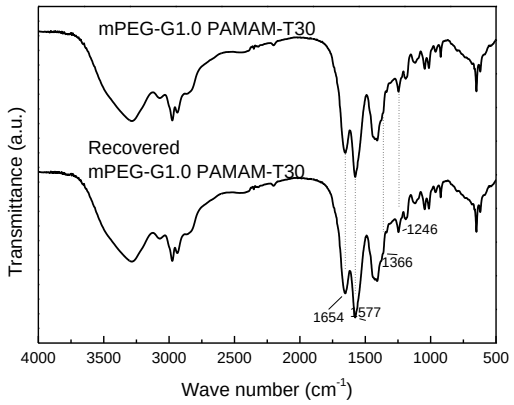

Fig. 5.11 FT-IR spectra of mPEG-G1.0 PAMAM-T30 before and after recovery

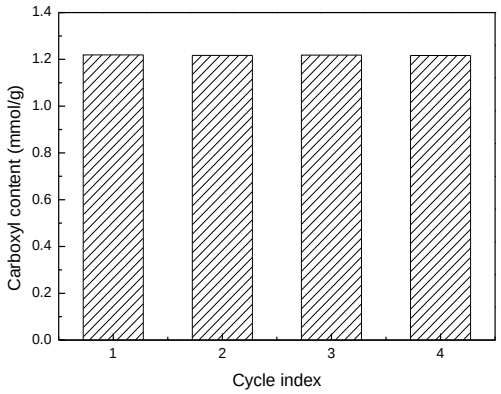

Fig.5.12 Recyclability of mPEG-G1.0 PAMAM-T30 for cellulose oxidation

The recovered mPEG-G1.0 PAMAM-T30 was characterized by means of FT-IR and its structure was seen to have remained unchanged. (See Fig. 5.11.) The recycled catalyst was re-used in the next oxidation. It was found that the catalytic oxidation performance had not decreased after four oxidation cycles (Fig. 5.12).

5.4 Comparison of mPEG-G1.0 PAMAM-Tx and other water-soluble immobilized TEMPO catalysts for cellulose oxidation

mPEG-G1.0 PAMAM-Tx and other reported water-soluble macromolecular catalysts, including P(AA-co-TA) [31], Gn PAMAM-Tx [32,33], PVAm-T [34], mPEG-T [35] and mPEG-G1.0 PAMAM-Tx were compared for selective oxidation of cellulose. The chemical structure of these catalysts is shown in Fig. 5.13.

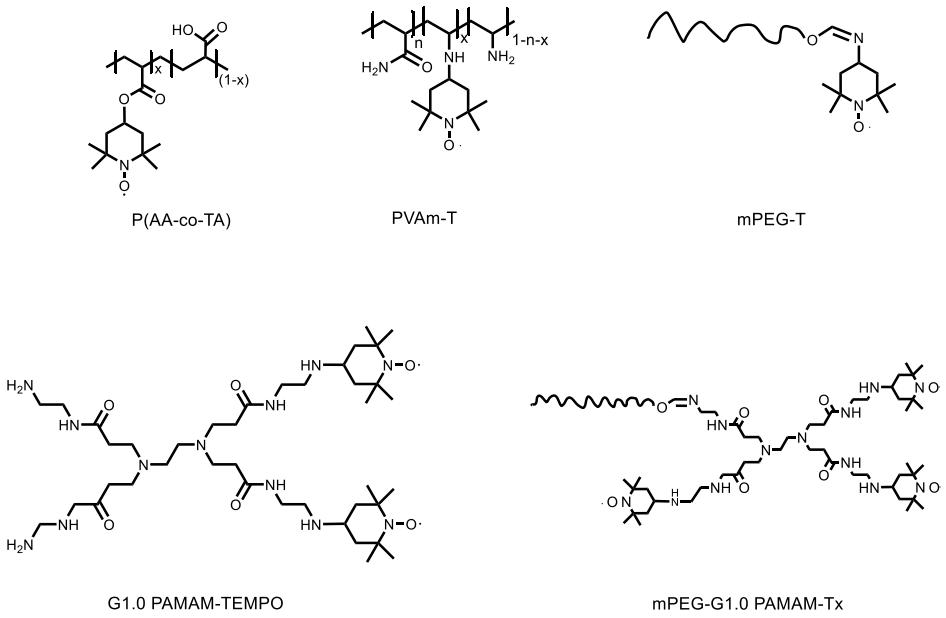

Fig. 5.13 Chemical structure of the macromolecular catalysts

Cellulose oxidation is a diffusion-controlled reaction in the TEMPO/NaBr/NaClO system, in which the TEMPO species can oxidize the cellulose surface and also enter the pores of cellulose to oxidize the interior parts of cellulose. The average pore volume of cellulose is in the range of 2-20 nm [36]. The non-charged hydrophobic TEMPO moieties with no special affinity for cellulose surface can shuttle freely inside the

cellulose (Fig. 5.14). When converted into the positively charged species ($TEMPO^+$) [37], they attract carboxylate cellulose and are prone to oxidation of cellulose. The result is that the oxidation performance of free TEMPO is excellent. The carboxyl content of TEMPO oxidized cellulose was up to 1.46 mmol/g.

The mPEG-T also contains a positive charge due to the presence of free TEMPO. However, the introduction of a PEG chain cannot increase the water solubility and diffusion capacity of TEMPO, and the large molecular size tends to reduce its catalytic activity. The carboxyl content of mPEG-T oxidized cellulose was only 0.80 mmol/g. The P(AA-co-TA) with negatively charged carboxyl repels the oxidized cellulose, resulting in poor performance of oxidized cellulose (equivalent to about 59% of the free TEMPO level).

G1.0 PAMAM-Tx, PVAm-T and mPEG-Gn PAMAM-T with the positive charge of $TEMPO^+$ and $-NH_2$ were more easily adsorbed onto the negatively charged cellulose to induce the oxidation reaction. (See Fig. 5.15.) The carboxyl content of the resultant oxidized cellulose was 1.45 mmol/g for G1.0 PAMAM-T30, 1.114 mmol/g for PVAm-T-55 and 1.22 mmol/g for PEG1000-G1.0 PAMAM-T30, equivalent to 99%, 76% and 84% of the free TEMPO level, respectively. The difference in activity is primarily the result of the different molecular sizes. G1.0 PAMAM-Tx is about 1.4 nm and can freely enter the micropores of cellulose. It had a catalytic oxidation performance similar to that of free TEMPO. PVAm-T has a molecular size of about 15 nm and mPEG-Gn

PAMAM-T with a molecular size of about 17 nm tend to be absorbed on the cellulose surface by electrostatic attraction in order for the oxidation reaction to occur. It is difficult for these two to enter the interior of cellulose, resulting in them having lower catalytic activity than TEMPO.

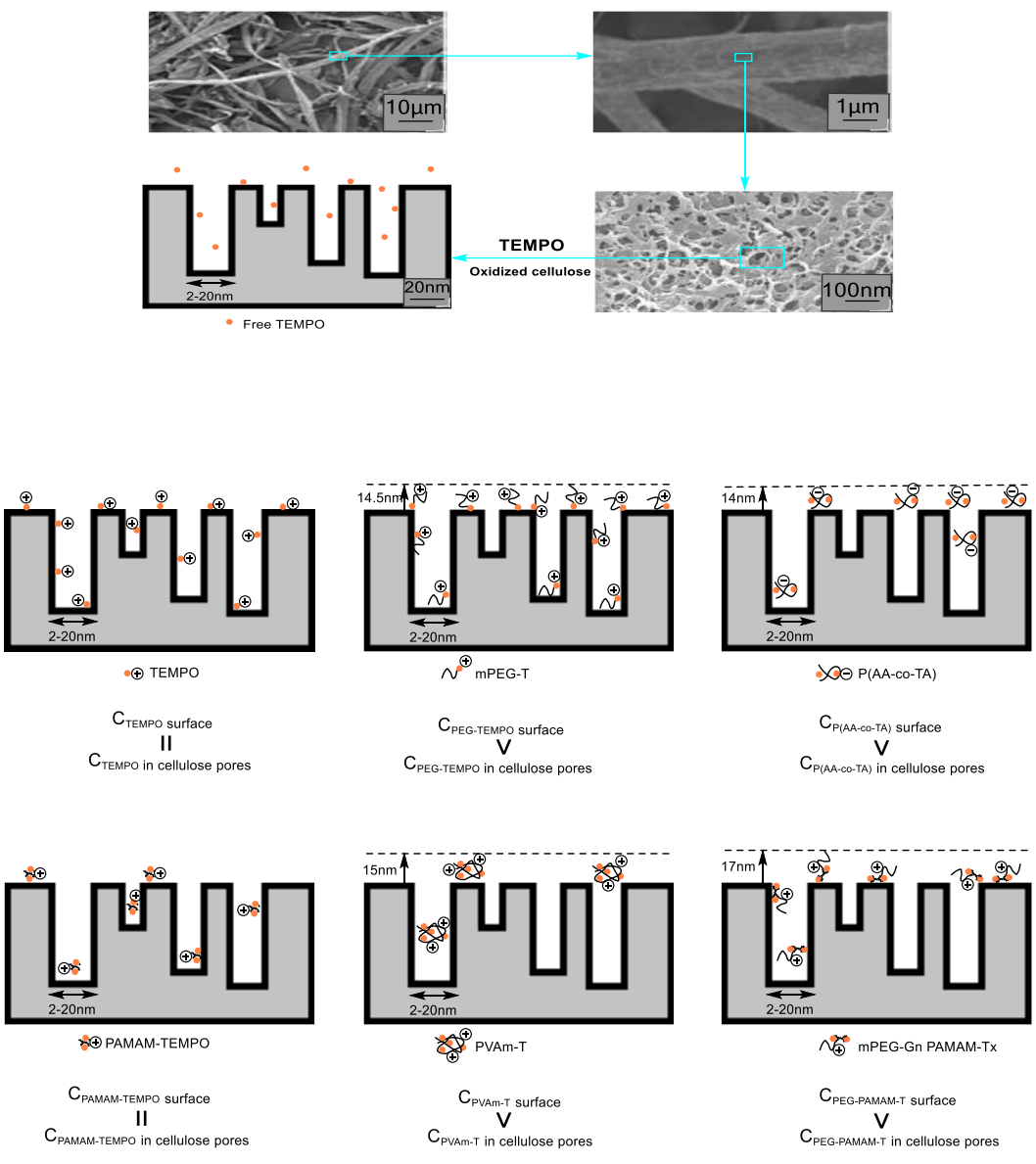

Fig. 5.14 The distribution of TEMPO, mPEG-T, P(AA-co-TA), Gn PAMAM-Tx, PVAm-T and mPEG-Gn PAMAM-Tx on nanopores of cellulose during the oxidation process

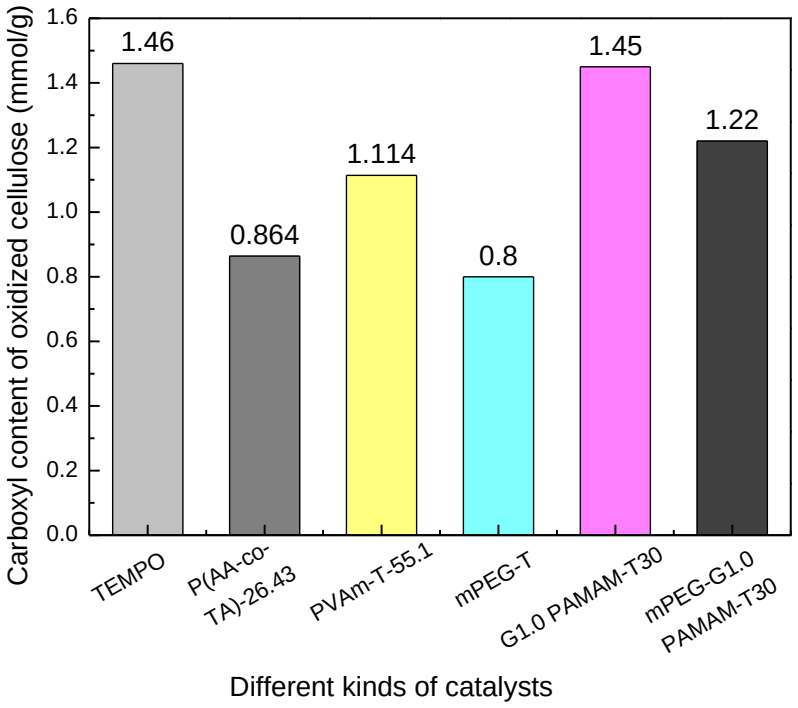

Fig. 5.15 Carboxyl content of oxidized cellulose with macromolecular TEMPO catalysts and free TEMPO

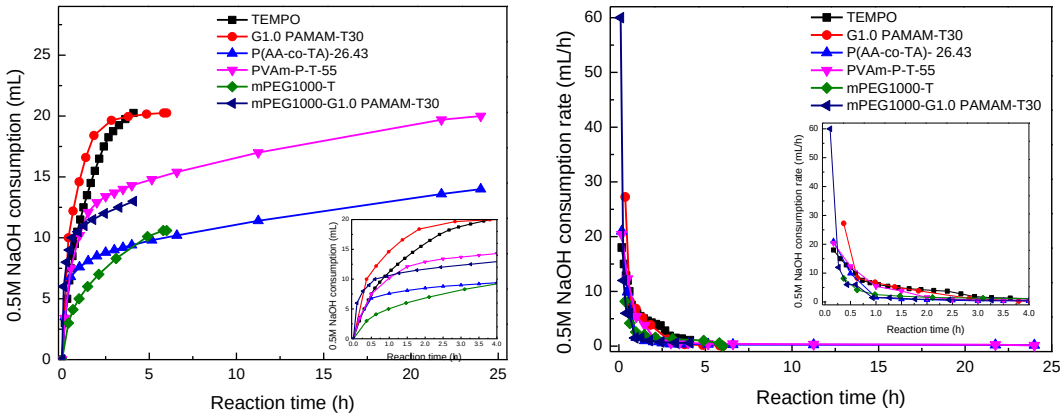

Fig. 5.16 (a) NaOH consumption and (b) the NaOH consumption rate of water-soluble immobilized TEMPO and free TEMPO

The oxidation rates of these water-soluble immobilized TEMPO mediators were also studied and compared with that of TEMPO. For the cellulose oxidation method used in

this work, the oxidation rate can be evaluated by measuring the NaOH consumption during cellulose oxidation. The NaOH was used to maintain the pH of the reaction mixture at 10.5. As seen in Fig. 5.16, at the initial stage of the reaction (within 1 h), G1.0 PAMAM-T30, PVAm-P-T-55 and mPEG-G1.0 PAMAM-T30 had a faster oxidation rate than free TEMPO, while the other immobilized TEMPO catalysts had a slower oxidation rate than TEMPO.

In terms of the reaction mechanism of the TEMPO mediated oxidation of cellulose, the effective contact between TEMPO moieties and cellulose hydroxyl groups is a necessary condition for the oxidation reaction to proceed. Therefore, it can be inferred that the highly positively charged G1.0 PAMAM-T30, PVAm-P-T-55 and mPEG-G1.0 PAMAM-T30 contact the carboxyl groups generated by the oxidation of the hydroxyl groups on the cellulose surface, due to electrostatic attraction. This triggers the oxidation reaction. In the middle and late oxidation stages, the TEMPO reaction rate was faster than that of all the macromolecular catalysts, possibly because the initial oxidation occurred on the surface of cellulose, and the diffusion rates of catalysts with different physical sizes were similar on the surface of the cellulose. The high local TEMPO concentration of the macromolecule catalyst promotes its regeneration. After the reaction proceeded to the middle and later stages, the reaction occurred mainly in the inner pores of the cellulose, which demonstrates the advantage of the small size of free TEMPO. These results are consistent with the carboxyl content results indicated above. Therefore, the catalytic oxidation performance of the catalyst depends on its

charge type, physical size, chain structure and TEMPO loading density.

TEMPO mediated oxidation of cellulose often leads to serious degradation of the cellulose under alkaline conditions. The DP of raw cellulose was about 160, and the value of TEMPO oxidized cellulose was significantly decreased to about 55-72 (Table 5.4 and Fig. 5.17), i.e. equivalent to 55%-66% degradation degree. When the catalysts were applied to catalyze the oxidation of cellulose, the depolymerization of cellulose was inhibited. The DP of P(AA-co-TA), PVAm-T, mPEG-T, Gn PAMAM-Tx and mPEG-Gn PAMAM-Tx oxidized cellulose was higher than that of the TOC and the value recorded was 75-94, 117-126, 95-105, 90-115 and 89-121 respectively, which is equivalent to a degradation degree of 41%-53%, 21%-27%, 34%-41%, 28%-44% and 24%-44%, respectively. This may be because the macromolecular catalyst is confined primarily to the outer surface of porous cellulose, which inhibits cellulose degradation to a certain extent. PVAm-T caused the least cellulose degradation. This suggests that the degradation of cellulose may be closely related to the chain structure of the macromolecular catalyst.

Table 5.4 Comparison of the degree of degradation during cellulose oxidation using a macromolecular TEMPO catalyst compared to TEMPO

TEMPO-containing catalyst	DP	Degradation degree %
TEMPO	55-72	55-66
P(AA-co-TA)	75-94	41-53
Gn PAMAM-Tx	90-115	28-44
mPEG-T	95-105	34-41

PVAm-T	117-126	21-27
mPEG-Gn PAMAM-Tx	89-121	24-44

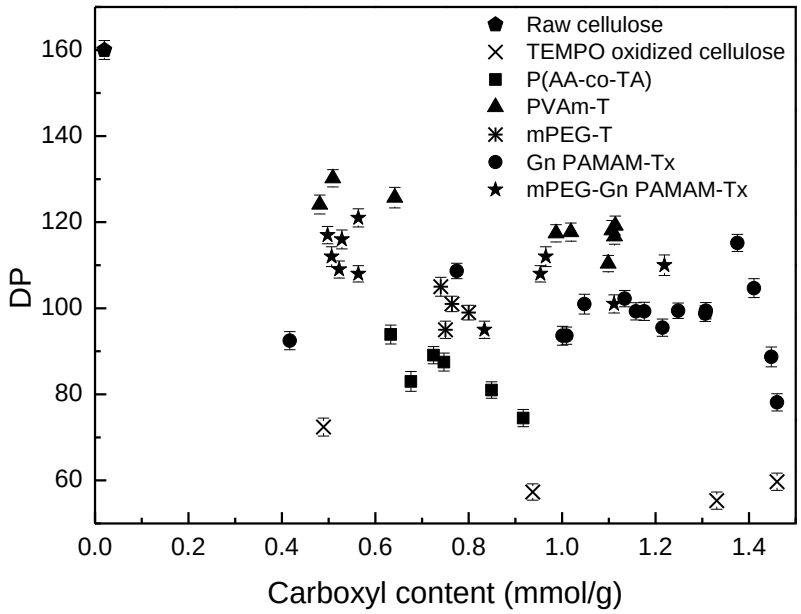

Fig. 5.17 Effect of carboxyl content on the DP of oxidized cellulose when using different catalysts

Table 5.5 Recovery methods used with macromolecular TEMPO catalysts

TEMPO-containing catalysts	Recovery method
TEMPO	---
P(AA-co-TA)	Adjusting the pH
Gn PAMAM-Tx	Salting-out extraction
mPEG-T	DCM extraction
PVAm-T	Dialysis
mPEG-Gn PAMAM-Tx	DCM extraction

TEMPO is a toxic reagent that can pollute water if it is discarded into the environment.

TEMPO can be recovered by loading it onto carries, and the recovery process of the immobilized TEMPO catalyst is mainly determined by the characteristics of the carrier [38]. As shown in Table 5.5, the P(AA-co-TA) catalyst can be recovered as a result of the pH sensitivity of PAA. The Gn PAMAM-Tx catalyst is recovered by salting-out extraction, but the recovery process is complex. The catalyst PVAm-T was recovered from the supernatant by dialysis. The recovery process is simple but time-consuming. mPEG-T and mPEG-Gn PAMAM-Tx can be recovered by DCM extraction, which is a simple and convenient process.

5.5 Conclusion

The water-soluble mPEG-Gn PAMAM-T catalyst was prepared and used as a catalyst, instead of free TEMPO, for selective catalytic oxidation of cellulose. The effects of TEMPO loading degree and PAMAM generation on the reaction rate, the degree of oxidation and the degree of depolymerization were investigated. The results showed that the catalytic oxidation performance of mPEG-G1.0 PAMAM-Tx was up to 83.5% of that of the free TEMPO level. Furthermore, this immobilized polymer catalyst can alleviate the cellulose degradation degree to a certain extent. The catalyst can easily be recycled by means of extraction, and the catalytic performance was not reduced after four oxidation cycles. Furthermore, it was found that the chain structure, charge type and molecular dimensions of the macromolecular catalysts were the main factors affecting the catalytic oxidation properties.

References

[1] Ferreira P, Hayes W, Phillips E, et al. Polymer-supported nitroxyl catalysts for selective oxidation of alcohols [J]. Green Chemistry, 2004, 6(7): 310-312.

[2] Benaglia M, Puglisi A, Holczknecht O, et al. Aerobic oxidation of alcohols to carbonyl compounds mediated by poly (ethylene glycol)-supported TEMPO radicals [J]. Tetrahedron, 2005, 61(51): 12058-12064.

[3] Ferreira P, Phillips E, Rippon D, et al. Poly (ethylene glycol)-supported nitroxyls: Branched catalysts for the selective oxidation of alcohols [J]. The Journal of Organic Chemistry, 2004, 69(20): 6851-6859.

[4] Fey T, Fischer H, Bachmann S, et al. Silica-supported TEMPO catalysts: Synthesis and application in the Anelli oxidation of alcohols [J]. The Journal of Organic Chemistry, 2001, 66(24): 8154-8159.

[5] Lucio Anelli P, Biffi C, Montanari F, et al. Fast and selective oxidation of primary alcohols to aldehydes or to carboxylic acids and of secondary alcohols to ketones mediated by oxoammonium salts under two-phase conditions [J]. The Journal of Organic Chemistry, 1987, 52(12): 2559-2562.

[6] Dickerson T, Reed N, Janda K. Soluble polymers as scaffolds for recoverable catalysts and reagents [J]. Chemical Reviews, 2002, 102(10): 3325-3344.

[7] Chung C, Toy P. Multipolymer reaction system for selective aerobic alcohol oxidation: Simultaneous use of multiple different polymer-supported ligands [J]. Journal of Combinatorial Chemistry, 2007, 9(1): 115-120.

[8] Araki J, Iida M. Surface carboxylation of cellulose nanowhiskers using mPEG-TEMPO: Its recovery and recycling [J]. Polymer Journal, 2016, 48(10): 1029-1033.

[9] Liu S, Xing Y, Han J, et al. Catalytic oxidation of cellulose with a novel amphiphilic nitroxide block copolymer as a recoverable catalyst [J]. Cellulose, 2017, 24(9): 3635-3644.

[10] Wang Y. Dendrimer Functionalized Nanocrystalline Cellulose for Environmental Applications [D]. Schulich School of Engineering, 2020.

[11] Ibrahim S, Hasanin M, Ahmed H, et al. Poly (amidoamine)/cellulose based bio-composites as potential anticancer bio-compatible polymers [J]. Polymer Bulletin, 2021: 1-16.

[12] Esfand R, Tomalia D. Poly (amidoamine) (PAMAM) dendrimers: From biomimicry to drug delivery and biomedical applications [J]. Drug Discovery Today, 2001, 6(8): 427-436.

[13] Camacho C, Urgellés M, Tomás H, et al. New insights into the blue intrinsic fluorescence of oxidized PAMAM dendrimers considering their use as bionanomaterials [J]. Journal of Materials Chemistry B, 2020, 8(45): 10314-10326.

[14] Zhou Y, Luan L, Tang B, et al. Fabrication of Schiff base decorated PAMAM dendrimer/magnetic Fe_3O_4 for selective removal of aqueous Hg (II) [J]. Chemical Engineering Journal, 2020, 398: 125651.

[15] Liang H, Cao M, Yang D, et al. Polyamidoamine immobilized TEMPO mediated oxidation of cellulose: Effect of macromolecular catalyst structure on the reaction rate, oxidation degree and degradation degree [J]. Fibers and Polymers, 2020, 21(6): 1251-

1258.

[16] Liu S, Liang H, Sun T, et al. A recoverable dendritic polyamidoamine immobilized TEMPO for efficient catalytic oxidation of cellulose [J]. Carbohydrate Polymers, 2018, 202: 563-570.

[17] Pal N, Banerjee S, Roy P, et al. Reduced graphene oxide and PEG-grafted TEMPO-oxidized cellulose nanocrystal reinforced poly-lactic acid nanocomposite film for biomedical application [J]. Materials Science and Engineering: C, 2019, 104: 109956.

[18] Anjaly K, Avudaiappan G, Smitha G, et al. Multifunctional polyether grafted dendritic solid supports: Novel class of solvent like high loading hybrid supports for solid phase organic synthesis [J]. Reactive and Functional Polymers, 2021, 166: 104985.

[19] Hao B, Lu G, Zhang S, et al. Gold nanoparticles standing on PEG/PAMAM/thiol-functionalized nanographene oxide as aqueous catalysts [J]. Polymer Chemistry, 2020, 11(25): 4094-4104.

[20] Narmani A, Kamali M, Amini B, et al. Targeting delivery of oxaliplatin with smart PEG-modified PAMAM G4 to colorectal cell line: In vitro studies [J]. Process Biochemistry, 2018, 69: 178-187.

[21] Zou L, Di Wang Y, Fu C, et al. Drug resistance reversal in ovarian cancer cells of paclitaxel and borneol combination therapy mediated by PEG-PAMAM nanoparticles [J]. Oncotarget, 2017, 8(36): 60453.

[22] Diaz C, Benitez C, Vidal F, et al. Cytotoxicity and in vivo plasma kinetic behavior of surface-functionalized PAMAM dendrimers [J]. Nanomedicine: Nanotechnology,

Biology and Medicine, 2018, 14(7): 2227-2234.

[23] Urbiola K, Blanco-Fernández L, Ogris M, et al. Novel PAMAM-PEG-peptide conjugates for siRNA delivery targeted to the transferrin and epidermal growth factor receptors [J]. Journal of Personalized Medicine, 2018, 8(1): 4.

[24] Shah A, Djordjevic I, Steele T. Tertiary blends of PAMAM/PEG/PEG tissue bioadhesives [J]. Journal of the Mechanical Behavior of Biomedical Materials, 2020, 101: 103405.

[25] Papadimitriou S, Achilias D, Bikiaris D. Chitosan-g-PEG nanoparticles ionically crosslinked with poly (glutamic acid) and tripolyphosphate as protein delivery systems [J]. International Journal of Pharmaceutics, 2012, 430(1-2): 318-327.

[26] Yao R, Liu L, Deng S, et al. Synthesis and characterization of PEGylated carboxymethylchitosan nanoparticles [J]. Carbohydrate Polymers, 2011, 85(4): 809-816.

[27] Dane E, Corzilius B, Rizzato E, et al. Rigid orthogonal bis-TEMPO biradicals with improved solubility for dynamic nuclear polarization [J]. The Journal of Organic Chemistry, 2012, 77(4): 1789-1797.

[28] Brasch R, Nitecki D, Brant-Zawadzki M, et al. Brain nuclear magnetic resonance imaging enhanced by a paramagnetic nitroxide contrast agent: Preliminary report [J]. American Journal of Neuroradiology, 1983, 4(5): 1035-1039.

[29] Ma Y, Loyns C, Price P, et al. Thermal decay of TEMPO in acidic media via an N-oxoammonium salt intermediate [J]. Organic & Biomolecular Chemistry, 2011, 9(15): 5573-5578.

[30] Shinoda R, Saito T, Okita Y, et al. Relationship between length and degree of polymerization of TEMPO-oxidized cellulose nanofibrils [J]. Biomacromolecules, 2012, 13(3): 842-849.

[31] Liu S, Sun T, Yang D, et al. Polyacrylic acid supported TEMPO for selective catalytic oxidation of cellulose: Recovered by its pH sensitivity [J]. Cellulose, 2018, 25(10): 5687-5696.

[32] Liu S, Liang H, Sun T, et al. A recoverable dendritic polyamidoamine immobilized TEMPO for efficient catalytic oxidation of cellulose [J]. Carbohydrate Polymers, 2018, 202: 563-570.

[33] Liang H, Cao M, Yang D, et al. Polyamidoamine immobilized TEMPO mediated oxidation of cellulose: Effect of macromolecular catalyst structure on the reaction rate, oxidation degree and degradation degree [J]. Fibers and Polymers, 2020, 21(6): 1251-1258.

[34] Sun T, Wang H, Liu J, et al. Recoverable acrylamide-vinylamine copolymer immobilized TEMPO mediated oxidation of cellulose with good catalytic performance and low cellulose degradation [J]. Cellulose, 2021, 28(7): 4151-4164.

[35] Araki J, Iida M. Surface carboxylation of cellulose nanowhiskers using mPEG-TEMPO: Its recovery and recycling [J]. Polymer Journal, 2016, 48(10): 1029-1033.

[36] Hubbe M, Rojas O, Lucia L, et al. Consequences of the nanoporosity of cellulosic fibers on their streaming potential and their interactions with cationic polyelectrolytes [J]. Cellulose, 2007, 14(6): 655-671.

[37] Pelton R, Ren P, Liu J, et al. Polyvinylamine-graft-TEMPO adsorbs onto, oxidizes,

and covalently bonds to wet cellulose [J]. Biomacromolecules, 2011, 12(4): 942-948.

[38] Isogai A, Hänninen T, Fujisawa S, et al. Catalytic oxidation of cellulose with nitroxyl radicals under aqueous conditions [J]. Progress in Polymer Science, 2018, 86: 122-148.

CHAPTER 6 THE OXIDIZED CELLULOSE/NANO-Fe_3O_4 COMPOSITE FOR EFFICIENT ADSORPTION OF Pb^{2+}

(Note: This work was published in the Journal of Nanoparticle Research. DOI: 10.1007/s11051-020-04904-9)

6.1 Introduction

TEMPO is a toxic reagent that cannot be discarded directly into the environment without complex post-processing. One way to address this issue is to immobilize TEMPO on carriers for recycling [1-8]. Another way is to immobilize TEMPO on oxidized cellulose, so that the oxidation process can be coupled with grafting or crosslinking modification in one step. Pelton et al. prepared polyvinylamine (PVAm)-TEMPO by loading TEMPO onto PVAm chains. PVAm-TEMPO can be spontaneously adsorbed onto cellulose and oxidizes the C6 hydroxyl to aldehyde groups that react with $-NH_2$ on PVAm to form covalent bonds. This can increase adhesion between wet cellulose surfaces [9-13]. Some of the negative environmental impacts of water-soluble TEMPO mediated oxidation of cellulose are minimized, because the cationic polymers fix TEMPO moieties on the cellulose surface.

In recent years, magnetic cellulosic adsorbents that can be recovered easily using an external magnetic field have been developed [14-17]. Compared with common cellulosic materials, TOC has a smaller size and abundant hydrophilic groups, resulting

in it being well dispersed in water and thus difficult to recover. PAMAM is a nanomaterial with a three-dimensional structure that has been used to modify magnetic nanoparticles, in order to endow them abundant terminal amino groups, which can be used as the carrier to support catalysts and other reagents [18]. Recently, PAMAM immobilized TEMPO (Gn PAMAM-Tx) modified magnetic Fe_3O_4 nanoparticle (MNP) called Gn PAMAM-Tx-MNP that was developed for catalyzing oxidation of poly (ethylene glycol) [19]. It showed good catalytic oxidation performance and was easily recovered using an external magnetic field.

In this section of the study, Gn PAMAM-Tx-MNP catalysts with different PAMAM generations and different degrees of TEMPO loading were prepared and used to prepare oxidized cellulose. After oxidation, the NH_2 groups on Gn PAMAM-Tx-MNP can combine with the carboxyl groups on oxidized cellulose through electrostatic action. GLA was then added to react with the -NH_2 groups on Gn PAMAM-Tx-MNP and -OH groups on oxidized cellulose to produce a TOC/nano-Fe_3O_4 composite (TOC-Gn PAMAM-Tx-MNP). TOC-Gn PAMAM-Tx-MNP was used as a recoverable adsorbent for removing Pb^{2+} in water. This strategy has three potential benefits: (1) Compared with free TEMPO mediated oxidation of cellulose, Gn PAMAM-Tx-MNP as the catalyst can inhibit cellulose degradation to a certain extent, to give TOC with a high mechanical performance. (2) Using Gn PAMAM-Tx-MNP as the crosslinker for crosslinking TOC can give the composite magnetic properties, address its separation issue and further improve its mechanical strength. (3) TEMPO is fixed onto the

composite to avoid complex post-processing.

6.2 Experiment

6.2.1 Preparation of Gn PAMAM-Tx-MNP

Gn PAMAM-Tx-MNP catalysts (n represents the generation of PAMAM and x represents the degree of TEMPO loading) were prepared as per our previous work, but with minor modifications [20].

6.2.1.1 Preparation of MNP

At 25 ℃, $FeCl_2 \cdot 4H_2O$ (1.0 g, 5 mmol), $FeCl_3 \cdot 6H_2O$ (2.7 g, 10 mmol) and water (50 mL) were placed in a 500 mL three-necked flask. After stirring for 10 min, 0.4 M ammonium hydroxide solution (190 mL) was added until the pH reached pH=10. The temperature was then raised to 80 ℃. After 30 min, the solid that was obtained was washed with water and lyophilized to give MNP.

6.2.1.2 Preparation of Gn PAMAM-MNP

(1) MNP-APTS

MNP (1.0 g) was dispersed into ethanol (100 mL) using ultrasound. APTS (5 mL, 0.02 mol) was then added. After being reacted at 60 ℃ for 7 h, the product of MNP-APTS was obtained by magnetic separation and vacuum drying.

(2) Gn PAMAM-MNP

MNP-APTS (1.0 g) and MA (10 mL, 0.11 mol) were ultrasonically dispersed into methanol (25 mL) and mechanically stirred for 24 h at 25 ℃. After magnetic separation and vacuum drying, G0.5 PAMAM-MNP was obtained. Ethylenediamine (2 mL, 0.03 mol) and G0.5 PAMAM-MNP was dispersed into methanol (10 mL) and reacted for 24 h to give G1.0 PAMAM-MNP. These steps were repeated to obtain Gn PAMAM-MNP (n=1.0, 2.0, 3.0, 4.0, 5.0).

6.2.1.3 Preparation of Gn PAMAM-Tx-MNP

The synthesis method used for 4-oxo-TEMPO was provided in previous work [20-22]. G1.0 PAMAM-MNP (1.0 g, 0.41 mmol -NH_2) and 4-oxo-TEMPO (the molar ratio of 4-oxo-TEMPO to -NH_2 of G1.0 PAMAM-MNP was from 0.15 to 1.35) were added to methanol (80 mL) at 40 ℃. Then $NaBH_3CN$ with the same molar amount of 4-oxo-TEMPO was added in three equal parts (3 h, 24 h, 48 h after the reaction was started). After 96 h, the product that was obtained was washed with methanol and dried to give G1.0 PAMAM-Tx-MNP. Gn PAMAM-Tx-MNP (n=1.0, 2.0, 3.0, 4.0 and 5.0). The catalysts were prepared using different generations of Gn PAMAM-MNP as carriers.

6.2.2 Preparation of oxidized cellulose/nano-Fe_3O_4 composite

6.2.2.1 Selective oxidation of cellulose using Gn PAMAM-Tx-MNP as the catalyst

Gn PAMAM-Tx-MNP (containing 0.24 mmol TEMPO), NaBr (0.028g, 0.27 mmol), cellulose (1.0 g) and water (70 mL) were placed in a three-necked flask under mechanical agitation. An aqueous NaClO solution (7.44 g, 5 mmol/g cellulose) was

added to start the reaction at 65 ℃. During the reaction, a 0.5 mol/L NaOH solution was added to maintain pH=10.5. When the pH of the reaction mixture stopped changing, 10 mL ethanol was added to quench the reaction. The suspension was centrifuged, and the precipitate was freeze-dried for 24 h to obtain the mixture comprising TOC and Gn PAMAM-Tx-MNP.

6.2.2.2 Cross-linking the mixture of TOC and Gn PAMAM-Tx-MNP

The freeze-dried TOC and the Gn PAMAM-Tx-MNP mixture (1.0 g) was dispersed into methanol (50 mL), and then mechanically stirred at 30 ℃ for 30 min. A 2% GLA solution (2 mL) was added. During the reaction, a 0.01 mol/L NaOH solution was added to adjust to pH=8. After 1 h, a 0.01 M $NaBH_4$ aqueous solution (50 mL) was added and stirred at 25 ℃ for 6 h. The product was centrifuged and immersed in 1 M cold CH_3COOH for 1 h. After being centrifuged and washed with water, the product was freeze-dried to produce the magnetic TOC/nano-Fe_3O_4 composite called TOC-Gn PAMAM-Tx-MNP.

6.2.3 Adsorption of Pb^{2+} by TOC-Gn PAMAM-Tx-MNP

$Pb(NO_3)_2$ (0.025 g, 0.12 mmol) was added to distilled water (100 mL). After the pH was adjusted to 5, TOC-Gn PAMAM-Tx-MNP (0.1 g) was added at 25 ℃ [23, 24]. After stirring for 1 h, TOC-Gn PAMAM-Tx-MNP was recovered using an external magnetic field.

6.2.4 Desorption of Pb^{2+} from TOC-Gn PAMAM-Tx-MNP

The dried TOC-Gn PAMAM-Tx-MNP after Pb^{2+} adsorption (0.1 g) was put into a 0.1 M HCl solution (100 mL). After stirring for 1 h at 25 ℃, TOC-Gn PAMAM-Tx-MNP was recovered using an external magnetic field.

6.3 Results and Discussion

6.3.1 Preparation route of TOC-Gn PAMAM-Tx-MNP

MNP agglomerates easily [25]. PAMAM modified MNP with good dispersion and a unique three-dimensional structure can reduce agglomeration. In addition, the presence of abundant primary amines increases the amount of TEMPO loading. For this reason, Gn PAMAM-MNP is an ideal carrier for the preparation of a recoverable nitroxide catalyst with a high TEMPO loading amount [26-34]. The preparation process of Gn PAMAM-Tx-MNP is shown in Fig. 6.1. First, MNP was prepared using the coprecipitation method; it was then modified by APTS to obtain MNP-APTS. Gn PAMAM-MNP was prepared by means of the continuous Michael addition and ester aminolysis reactions. Finally, the TEMPO was fixed on Gn PAMAM-MNP to obtain Gn PAMAM-Tx-MNP.

These Gn PAMAM-Tx-MNP catalysts were used to catalyze the oxidation of cellulose to prepare oxidized cellulose. After oxidation, a mixture of TOC and Gn PAMAM-Tx-MNP was obtained, which contained a large number of carboxyl and amino groups, and it was crosslinked with GLA. As shown in Fig. 6.2, the one aldehyde group of GLA

can react with the hydroxyl group on TOC to form the acetal linkage, while the other aldehyde group can react with the NH_2 group on PAMAM to form the imine linkage. After the imine bonds were reduced to amino groups by $NaBH_4$, the crosslinked TOC/nano-Fe_3O_4 composite was obtained and designated as TOC-Gn PAMAM-Tx-MNP. The carboxyl groups of TOC and the residual NH_2 groups of Gn PAMAM-Tx-MNP provided heavy metal ion adsorption sites for TOC-Gn PAMAM-Tx-MNP.

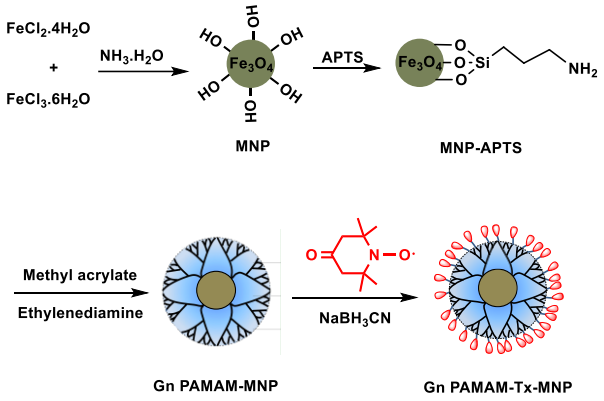

Fig. 6.1 Preparation process of Gn PAMAM-Tx-MNP

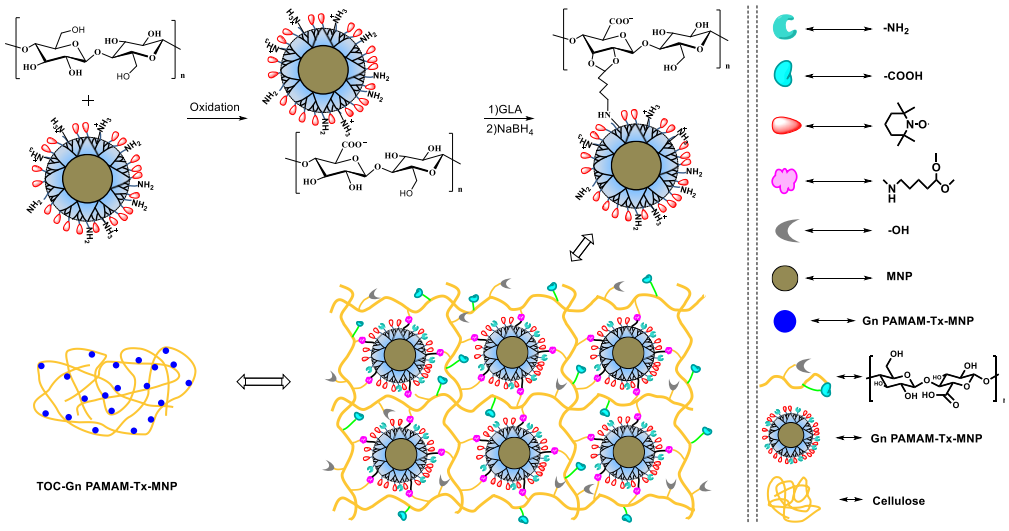

Fig. 6.2 Preparation process of TOC-Gn PAMAM-Tx-MNP

6.3.2 Characterization of Gn PAMAM-Tx-MNP

The structures of MNP and Gn PAMAM-MNP were analyzed by means of TEM and TGA. The structure of Gn PAMAM-Tx-MNP was characterized using FT-IR, and the TEMPO loading amount of Gn PAMAM-Tx-MNP was determined using UV-vis.

6.3.2.1 TEM

Fig. 6.3 shows the TEM images of MNP and PAMAM-modified MNP. PAMAM-modified MNP had better dispersion than MNP, because PAMAM is more soluble in water and has spatial stability due to its unique three-dimensional structure [35, 36]. This reduced the aggregation. However, it was not easy to observe the PAMAM coating layer on the MNP surface directly, because the soluble PAMAM is transparent to TEM.

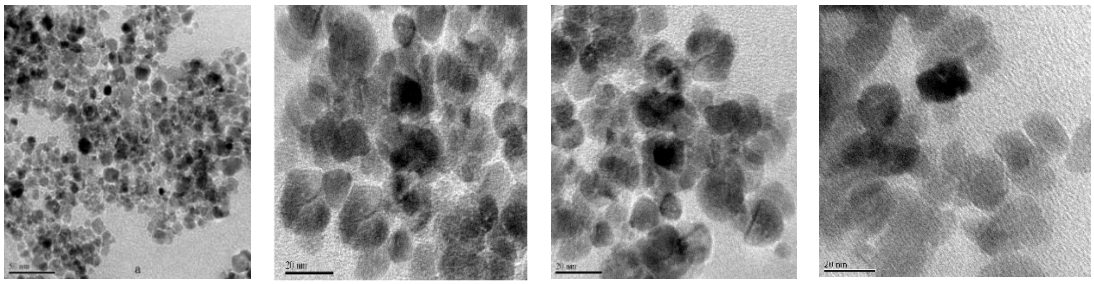

MNP G3.0 PAMAM-MNP G5.0 PAMAM-MNP

Fig. 6.3 TEM images of MNP, G3.0 PAMAM-MNP and G5.0 PAMAM-MNP

6.3.2.2 XRD

The MNP curve showed six characteristic peaks of Fe_3O_4 at 30.1°, 35.7°, 43.1°, 53.4°, 56.9° and 62.5°, corresponding to the crystal faces of (220), (311), (400), (422), (511)

and (440) [39-41]. The MNP crystal structure of modified G5.0 PAMAM-Tx-MNP did not change. On the basis of the Debye-Scherrer equation, using the width of most intense diffraction line, the average crystallite size for MNP was found as 10 nm (Fig. 6.4).

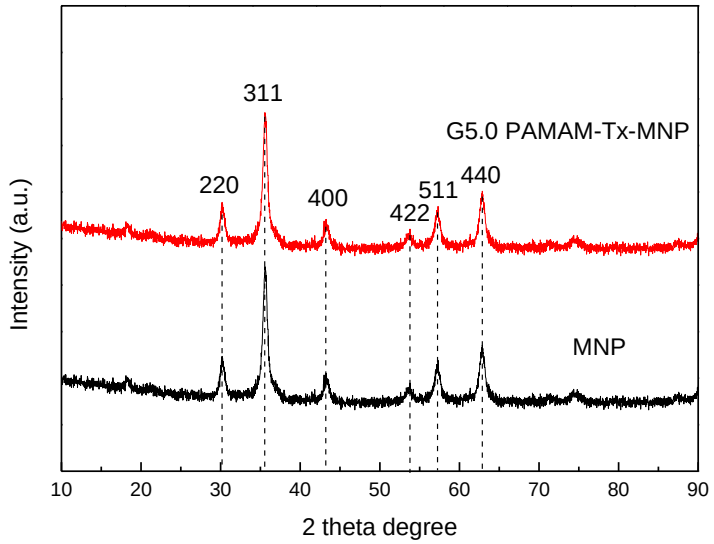

Fig. 6.4 XRD patterns of MNP and G5.0 PAMAM-Tx-MNP

6.3.2.3 TGA

Fig. 6.5 shows the TGA curves of MNP and PAMAM modified MNP. The amount of organic coating on the surface of MNP can be estimated according to the mass loss of the test sample with temperature change. The small mass loss (0.83%) of MNP should be the loss of water during heating. The average crystallite size of the magnetic nanoparticles was about 10 nm, and the thermogravimetric mass loss of MNP-APTS was 2.734%. The loading capacity of APTS in MNP-APTS, calculated using Equation 6-1, was 0.221 mmol/g [37]. The molar amount of -NH_2 on the surface of Gn PAMAM-

MNP was obtained by acid-base titration analysis. These are listed in Table 6.1. The mass loss of PAMAM-modified MNP increased with an increase in dendrimer generation. However, the mass loss of high generation samples was much lower than the theoretical value, which indicates the formation of an imperfect dendritic structure. This may be due to the spherical structure of the high-generation PAMAM, resulting in produce greater spatial interference of dendrimers on the Michael addition reaction and the ester amination reaction.

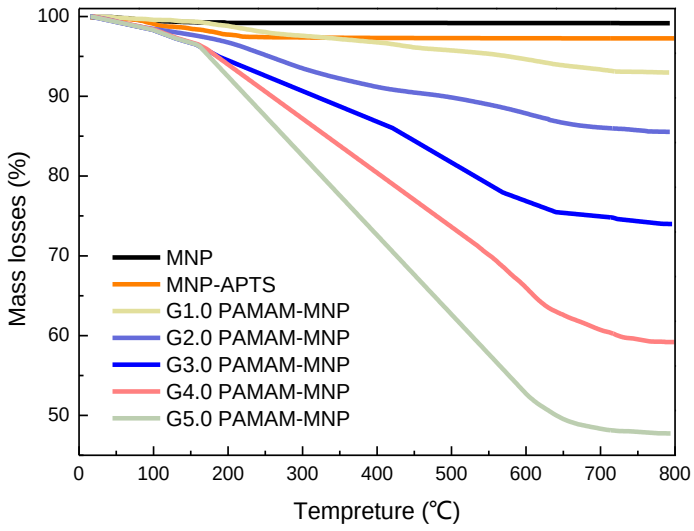

Fig. 6.5 TGA curves of MNP and PAMAM modified MNP

$$N_{APTS} = \frac{wN_a\rho\frac{4}{3}\pi R^3}{(1-w)M_{APTS}} \qquad \text{Equation 6-1}$$

Where:

N_{APTS} is the number of APTS on each MNP particle;

R is the mean radius of MNP;

ρ is the density of magnetite MNP;

N_a is the Avogadro constant;

M_{APTS} is the relative molecular mass of APTS;

w is the mass loss.

Table 6.1 Mass loss and molar amounts of amino groups in PAMAM modified MNP

	Mass loss %	Theoretical mass loss %	Amino groups mmol/g
MNPs	0.83	----	0
MNP-APTS	2.73	----	0.221
G1.0 PAMAM-MNP	7.01	7.30	0.409
G2.0 PAMAM-MNP	15.45	15.54	0.746
G3.0 PAMAM-MNP	26.01	28.35	1.293
G4.0 PAMAM-MNP	40.81	45.18	1.998
G5.0 PAMAM-MNP	53.26	62.99	2.729

6.3.2.4 FT-IR

The FT-IR of MNP, MNP-APTS, G5.0 PAMAM-MNP, G5.0 PAMAM-Tx-MNP and 4-oxo-TEMPO are shown in Fig. 6.6. The characteristic absorption peak at 587 cm^{-1} attributed to the magnetite Fe-O bond was found in all samples. Compared with MNP, MNP-APTS had an absorption band at 986 cm^{-1} due to the stretching vibration of the Si-O bond, which confirmed the aminosilanization reaction. G5.0 PAMAM-MNP had an absorption band at 3264 cm^{-1} due to the bending vibration of the -NH_2 group. The characteristic peaks of the C=O and NH groups in -CO-NH- were also found at 1642 cm^{-1} and 1560 cm^{-1}. These results indicated that PAMAM dendrimers were grafted onto the MNP surface. In the FT-IR spectrum of G5.0 PAMAM-Tx-MNP, the characteristic

absorption peak of N-O was found at 1368 cm^{-1} and the characteristic peak of the C=O of 4-oxo-TEMPO at 1723 cm^{-1} disappeared. These results demonstrated that TEMPO was successfully fixed to PAMAM-modified MNP [20, 21].

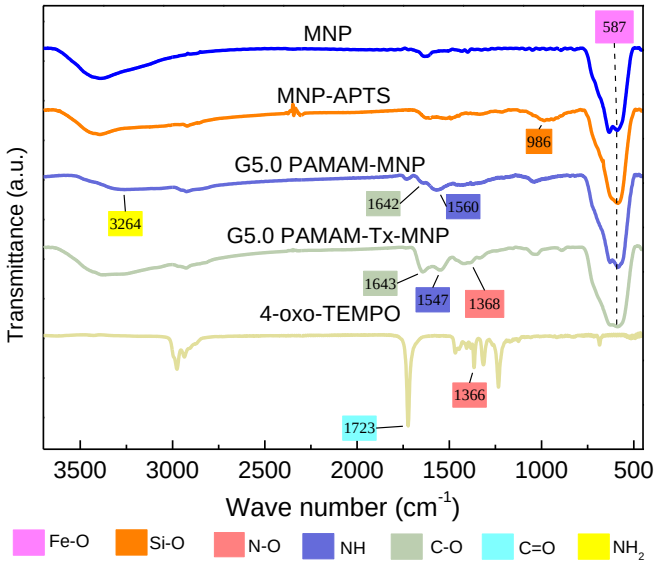

Fig. 6.6 FT-IR spectra of MNP, MNP-APTS, G5.0 PAMAM-MNP, 4-oxo- TEMPO and G5.0 PAMAM-Tx-MNP

6.3.2.5 UV-vis

Table 6.2 Magnetic Gn PAMAM-Tx-MNP catalysts prepared in this work

Gn PAMAM-Tx-MNP	Carrier	TEMPO loading amount (mmol/g)	TEMPO loading ratio (%)	Residual NH_2 content (mmol/g)
G5.0 PAMAM-T90-MNP	G5.0 PAMAM-MNP	1.78	89.4	0.20
G4.0 PAMAM-T90-MNP	G4.0 PAMAM-MNP	1.40	87.3	0.16
G3.0 PAMAM-T90-MNP	G3.0 PAMAM-MNP	0.98	89.7	0.11
G2.0 PAMAM-T90-MNP	G2.0 PAMAM-MNP	0.61	89.0	0.07
G1.0 PAMAM-T90-MNP	G1.0 PAMAM-MNP	0.35	90.5	0.04

Gn PAMAM-Tx-MNP	Carrier	TEMPO loading amount (mmol/g)	TEMPO loading ratio (%)	Residual NH_2 content (mmol/g)
G1.0 PAMAM-T60-MNP	G3.0 PAMAM-MNP	0.24	60.5	0.16
G1.0 PAMAM-T50-MNP		0.20	49.9	0.20
G1.0 PAMAM-T30-MNP		0.12	30.2	0.28
G1.0 PAMAM-T10-MNP		0.04	9.8	0.37
G3.0 PAMAM-T70-MNP		0.79	69.8	0.34
G3.0 PAMAM-T50-MNP		0.58	50.2	0.58
G3.0 PAMAM-T30-MNP		0.36	30.3	0.85
G3.0 PAMAM-T10-MNP		0.13	10.1	1.13

In order to systematically study the influence of the catalyst structure on the catalytic performance of cellulose oxidation, a series of catalysts with different structures were designed and prepared, as listed in Table 6.2. As the prepared magnetic macromolecular polymer of Gn PAMAM-Tx-MNP was water-insoluble, the TEMPO loading amount of Gn PAMAM-Tx-MNP was estimated by UV-vis determination of the unreacted 4-oxo-TEMPO content. By fixing the molar ratio of 4-oxo-TEMPO to -NH_2 at 1.5 and changing the generation of PAMAM from G1.0~G5.0, Gn PAMAM-T90-MNP catalysts were prepared with a similar TEMPO loading ratio (about 90%). Using G1.0 PAMAM-MNP as the carrier, G1.0 PAMAM-Tx-MNP catalysts with TEMPO loading ratios from 10% to 90% were obtained by changing the molar ratio of 4-oxo-TEMPO to -NH_2 of G1.0 PAMAM-MNP from 0.17 to 1.50. When the TEMPO loading ratios were similar, Gn PAMAM-Tx-MNP prepared with a higher PAMAM generation had a higher TEMPO loading amount and a higher residual NH_2 content. This was because the NH_2 content of PAMAM was proportional to its generation. When the generation

of PAMAM was fixed, the TEMPO loading amount increased accordingly and the residual NH_2 amount decreased as the TEMPO loading ratio increased.

6.3.3 Preparation of TOC-Gn PAMAM-Tx-MNP

By changing the structure of Gn PAMAM-Tx-MNP, a series of magnetic oxidized cellulose materials were prepared, as listed in Table 6.3.

Table 6.3 TOC/nano-Fe_3O_4 composites prepared in this work

TOC/nano-Fe_3O_4 composites	Gn PAMAM-Tx-MNP catalysts			
	Type	TEMPO loading amount (mmol/g)	Carboxyl content (mmol/g)	NH_2 content (mmol/g)
TOC-G5.0 PAMAM-T90-MNP	G5.0 PAMAM-T90-MNP	1.78	0.74	0.019
TOC-G4.0 PAMAM-T90-MNP	G4.0 PAMAM-T90-MNP	1.40	0.80	0.018
TOC-G3.0 PAMAM-T90-MNP	G3.0 PAMAM-T90-MNP	0.98	0.88	0.013
TOC-G2.0 PAMAM-T90-MNP	G2.0 PAMAM-T90-MNP	0.61	0.81	0.008
TOC-G1.0 PAMAM-T90-MNP	G1.0 PAMAM-T90-MNP	0.35	0.77	0.005
TOC-G1.0 PAMAM-T60-MNP	G1.0 PAMAM-T60-MNP	0.24	0.73	0.068
TOC-G1.0 PAMAM-T50-MNP	G1.0 PAMAM-T50-MNP	0.20	0.65	0.093
TOC-G1.0 PAMAM-T30-MNP	G1.0 PAMAM-T30-MNP	0.12	0.50	0.173
TOC-G1.0 PAMAM-T10-MNP	G1.0 PAMAM-T10-MNP	0.04	0.22	0.303
TOC-G3.0 PAMAM-T70-MNP	G3.0 PAMAM-T70-MNP	0.79	0.77	0.070
TOC-G3.0 PAMAM-T50-MNP	G3.0 PAMAM-T50-MNP	0.58	0.71	0.151
TOC-G3.0 PAMAM-T30-MNP	G3.0 PAMAM-T30-MNP	0.36	0.61	0.330
TOC-G3.0 PAMAM-T10-MNP	G3.0 PAMAM-T10-MNP	0.13	0.34	0.728

The effect of PAMAM generation on the carboxyl content of the TOC/nano-Fe_3O_4 composite was studied by fixing the TEMPO loading ratio of the magnetic catalyst at 90%. It was found that the carboxyl content increased at first and then decreased with the PAMAM generation increasing from G1.0 to G5.0. G3.0 PAMAM-T90-MNP gave

the highest degree of cellulose oxidation (the carboxyl content of the obtained TOC/nano-Fe_3O_4 composite was 0.88 mmol/g). As PAMAM generation increased, the TEMPO loading amount increased accordingly. With the same molar dosage of TEMPO moieties, the mass of added solid magnetic TEMPO catalyst would be decreased and the diffusion resistance between solid catalyst and cellulose decreased accordingly. However, the size of solid magnetic catalyst increased with the PAMAM generation, which was not conducive to its contact with the reactants. Therefore, the catalyst with G3.0 PAMAM modified nano-Fe_3O_4 as a carrier gave the best catalytic performance.

The effect of TEMPO loading ratio on the carboxyl content of the TOC/nano-Fe_3O_4 composite was then studied by fixing the PAMAM generation of the magnetic catalyst at G1.0 or G3.0. When the TEMPO loading ratio increased, the TEMPO loading amount increased accordingly, and the catalytic oxidation performance also increased. With similar TEMPO loading amounts (G1.0 PAMAM-T90-MNP with 0.35 mmol/g TEMPO loading amount) vs G3.0 PAMAM-T30-MNP with 0.36 mmol/g TEMPO loading amount and G1.0 PAMAM-T30-MNP with 0.12 mmol/g TEMPO loading amount vs G3.0 PAMAM-T10-MNP with 0.13 mmol/g TEMPO loading amount), the catalyst with G1.0 PAMAM as modifier gave better catalytic oxidation performance than that with G3.0 PAMAM as modifier, further confirming that the small catalyst size was conducive to improving the catalytic performance.

6.3.3.1 FT-IR

Fig. 6.7 shows the FT-IR spectra of TOC, G5.0 PAMAM-T90-MNP, a TOC/G5.0 PAMAM-T90-MNP mixture and TOC-G5.0 PAMAM-T90-MNP. The apparent absorption band of -COONa appeared at 1610 cm^{-1} in the spectrum of TOC. For the spectrum of Gn PAMAM-Tx-MNP, the characteristic adsorption band of the Fe-O bond appeared at 583 cm^{-1}, the characteristic adsorption band of the Si-O bond appeared at 986 cm^{-1}, and the bending vibration band of the $-NH_2$ group appeared at 3342 cm^{-1}. The band at 1360 cm^{-1} was attributed to the stretching vibration absorption of N-O in TEMPO. These characteristic bands also existed in the mixture of TOC/Gn PAMAM-Tx-MNP. Compared to the spectrum of the TOC/Gn PAMAM-Tx-MNP mixture, a new -NH- bond absorption band was present at 1540 cm^{-1}. (The aldehyde group of GLA reacted with the NH_2 group of Gn PAMAM-Tx-MNP to form the -C=N- linkage, which was then reduced to -C-NH- by $NaBH_4$). A new -O-C-O- stretching vibration peak was present at 1033 cm^{-1}, which indicates that TOC and Gn PAMAM-Tx-MNP were successfully crosslinked by GLA [20-22]].

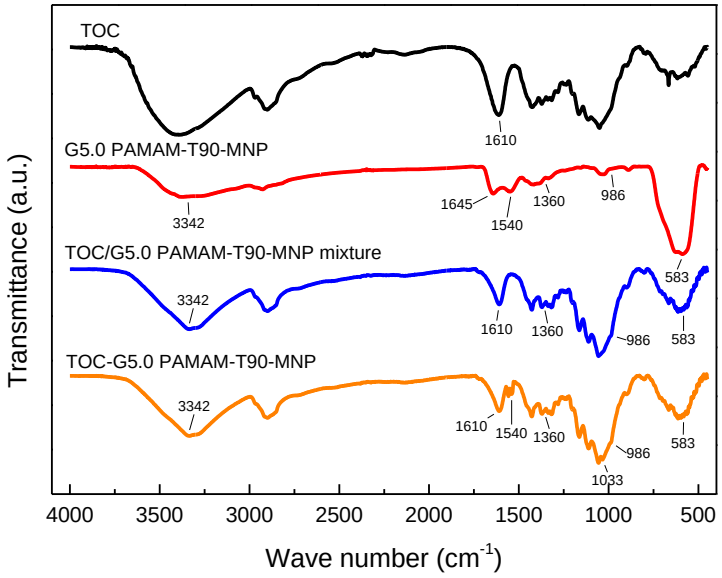

Fig. 6.7 FT-IR spectra of TOC, G5.0 PAMAM-T90-MNP, TOC/G5.0 PAMAM-T90-MNP mixture and TOC-G5.0 PAMAM-T90-MNP

6.3.3.2 XRD

The crystalline structures of RC, TOC, MNP and TOC-G5.0 PAMAM-T90-MNP were characterized by means of XRD (Fig. 6.8). The diffraction peaks at 14.8° and 22.6° assigned to crystalline cellulose I were found in the XRD patterns of RC, TOC and TOC-G5.0 PAMAM-T90-MNP. In addition, the TOC-G5.0 PAMAM-T90-MNP curve showed six characteristic peaks of Fe_3O_4 at 30.1°, 35.7°, 43.1°, 53.4°, 56.9° and 62.5°, corresponding to the crystal faces of (220), (311), (400), (422), (511) and (440) [39-41]. This indicates that the magnetic nanoparticles were successfully introduced into oxidative cellulose materials.

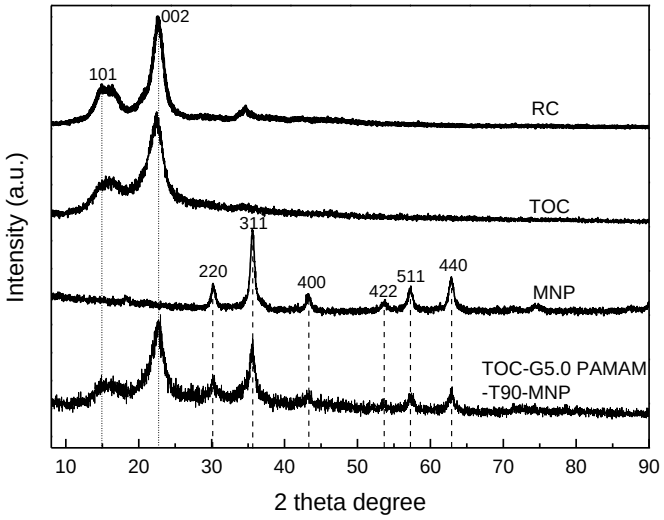

Fig. 6.8 XRD patterns of RC, TOC, MNP and TOC-G5.0 PAMAM-T90-MNP

6.3.3.3 TEM

TEM images of MNP, Gn PAMAM-MNP and TOC-G5.0 PAMAM-T90-MNP are shown in Fig. 6.9. It can be seen that the particle size of MNP is about 20 nm (Fig. 6.8(a)) and G5.0 PAMAM-MNP shows good dispersion (Fig. 6.9(b)). After being crosslinked with TOC, the magnetic particles were linked to the rod-like oxidized cellulose and the particle size did not change (Fig. 6.8(c)).

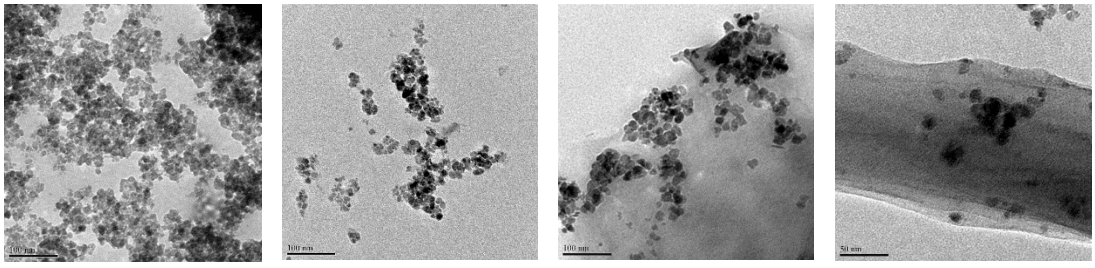

(a) MNP (b) G5.0 PAMAM-MNP (c) TOC-G5.0 PAMAM-T90-MNP

Fig. 6.9 TEM images of: (a) MNP; (b) G5.0 PAMAM-T90-MNP; (c) TOC-G5.0 PAMAM-T90-MNP

6.3.3.4 TGA

Fig. 6.10 shows the TGA curves of TOC, G5.0 PAMAM-T90-MNP and TOC-G5.0 PAMAM-T90-MNP. Compared with TOC, the thermal stability of the magnetic composite had improved. This may be because the metal particles were mixed with some polymer chains in the crystal lattice, which prevented early degradation. 9.40% of residue (carbon and ash) was found after the decomposition of TOC. The magnetic nanoparticles in G5.0 PAMAM-T90-MNP and TOC-G5.0 PAMAM-T90-MNP are inorganic Fe_3O_4, which cannot be decomposed within 800 ℃. The residues (carbon, ash and Fe_3O_4) of G5.0 PAMAM-T90-MNP and TOC-G5.0 PAMAM-T90-MNP were 18.67% and 10.50%, respectively. Thus, it was estimated that the mass ratio of TOC and G5.0 PAMAM-T90-MNP in TOC-G5.0 PAMAM-T90-MNP was about 7.39:1, which was close to the feeding ratio of cellulose and G5.0 PAMAM-T90-MNP (7.42:1).

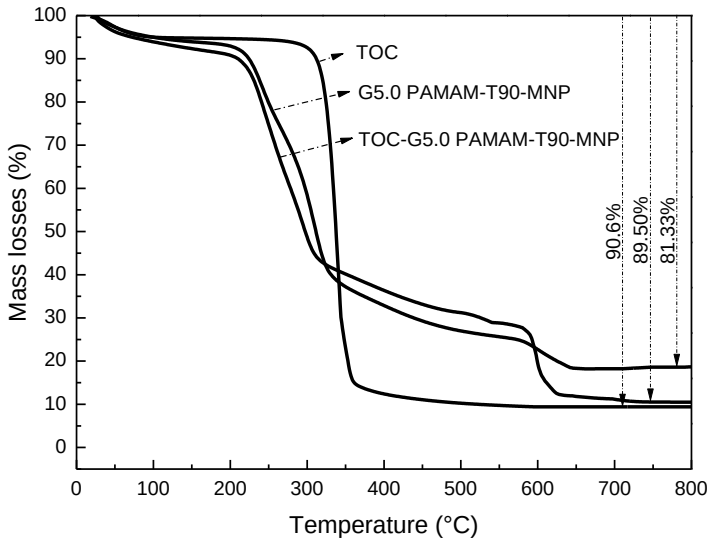

Fig. 6.10 TGA curves of TOC, G5.0 PAMAM-T90-MNP and TOC-G5.0 PAMAM-T90-MNP

6.3.4 Pb^{2+} adsorption performances of TOC-Gn PAMAM-Tx-MNP

Abundant carboxyl groups (derived from TOC) and a small amount of NH_2 groups (derived from PAMAM) in TOC-Gn PAMAM-Tx-MNP provided potential adsorption sites for heavy metal ions. In order to understand the Pb^{2+} adsorption capacity of the carboxyl group and the amino group, the Pb^{2+} adsorption performances of TOC with different carboxyl contents and PAMAM of different generations were evaluated. As indicated in Table 6.4, the Pb^{2+} adsorption capacity was proportional to the carboxyl content of TOC. The NH_2 content of PAMAM was approximately one order of magnitude higher than the carboxyl content of TOC. However, the Pb^{2+} adsorption capacity of the former was only about twice as high as the latter.

These results indicated that the carboxyl group in TOC had a high binding affinity for Pb^{2+}. TOC-Gn PAMAM-Tx-MNP with large amounts of carboxyl groups should have excellent Pb^{2+} adsorption performance and can be effectively recovered by magnetic separation. Based on this assumption, the Pb^{2+} adsorption properties of this magnetic recoverable adsorbent were systematically investigated.

Table 6.4 Pb^{2+} adsorption capacities of TOC and PAMAM

Adsorption materials	Carboxyl content (mmol/g)	NH_2 content (mmol/g)	Pb^{2+} adsorption capacity (mg Pb^{2+}/g)
TOC	0.69	0	94.1
	0.98	0	119.1
	1.10	0	127.8
	1.49	0	157.9

G1.0 PAMAM	0	19.38	237.8
G2.0 PAMAM	0	18.21	231.7
G3.0 PAMAM	0	17.84	206.2
G4.0 PAMAM	0	17.68	199.2
G5.0 PAMAM	0	17.61	194.4

6.3.4.1 Effect of initial Pb^{2+} concentration on Pb^{2+} adsorption

The initial Pb^{2+} concentration provides the necessary driving force to overcome the mass transfer resistance of Pb^{2+} between the aqueous and solid phases. Using TOC-G5.0 PAMAM-T90-MNP as the adsorbent, the effect of initial Pb^{2+} concentration in the range 100 to 500 mg/L on Pb^{2+} adsorption capacity was investigated at pH=5. With an increase in the initial Pb^{2+} concentration, the Pb^{2+} adsorption capacity increased (Fig. 6.11). When the initial concentration was over 250 mg/L, the growth of the adsorption capacity slowed down. Therefore, 250 mg/L was set as the initial Pb^{2+} concentration in the following adsorption study.

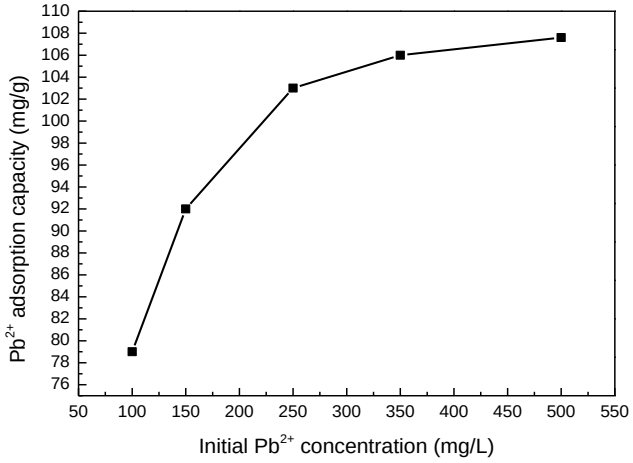

Fig. 6.11 Effect of initial Pb^{2+} concentration on Pb^{2+} adsorption of TOC-G5.0 PAMAM-T90-MNP

6.3.4.2 Effect of adsorption time on Pb^{2+} adsorption

Under the condition of pH=5 and an initial Pb^{2+} concentration of 250 mg/L, the effect of adsorption time on Pb^{2+} adsorption of TOC-G5.0 PAMAM-T90-MNP was investigated. Fig. 6.12 illustrates that the Pb^{2+} concentration decreased sharply in the first 5 minutes, which indicates that the adsorbent had a high adsorption rate for Pb^{2+}. When the adsorption time was further extended, the Pb^{2+} concentration slowly decreased and the adsorption equilibrium was reached at about 30 min, because most of the active adsorption sites had been occupied by Pb^{2+}.

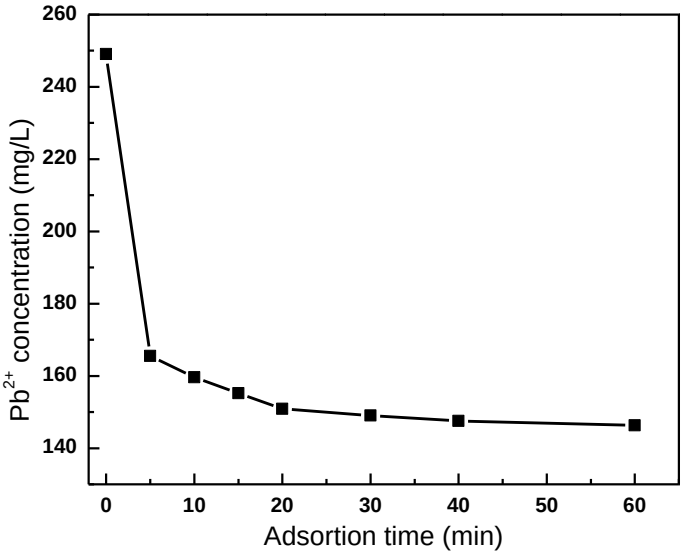

Fig. 6.12 Effect of adsorption time on Pb^{2+} adsorption of TOC-G5.0 PAMAM-T90-MNP

6.3.4.3 Adsorption kinetics and capacities

The kinetic curves and Pseudo-second order sorption kinetics of Pb^{2+} adsorption with RC, TOC, TOC-G5.0 PAMAM, G5.0 PAMAM-T90-MNP and TOC-G5.0 PAMAM-

T90-MNP were analyzed and compared. It was found that the adsorption processes of TOC, TOC-G5.0 PAMAM and TOC-G5.0 PAMAM-T90-MNP all conform to the pseudo-second-order model (Fig. 6.13). Fig. 6.14 and Table 6.5 indicated that the adsorption rate constants of TOC-G5.0 PAMAM-T90-MNP were very close at five tested initial Pb^{2+} concentrations. This further confirmed that Pb^{2+} adsorption on TOC-G5.0 PAMAM-T90-MNP is a typical pseudo-second order process. Furthermore, the increase in Pb^{2+} concentration from 103 mg/L to 801 mg/L resulted in the initial adsorption rate growing from 61.35 mg/(g min) to 106.4 mg/(g min). These results indicated that the adsorption of Pb^{2+} by TOC-G5.0 PAMAM-T90-MNP was a chemisorption process.

Table 6.5 Parameters of the pseudo-second order model for Pb^{2+} adsorption on TOC-G5.0 PAMAM-T90-MNP

Initial Pb^{2+} concentration mg/L	Experimental q_e mg/g	Calculated q_e mg/g	Initial adsorption rate mg/(g min)	R^2
103	74	74.07±0.7	61.35	0.999
149	83	84.03±0.9	77.52	0.999
250	96	96.2±0.6	79.37	0.999
362	103	102.0±0.4	85.47	0.999
427	106	104.2±0.4	94.34	0.999
801	110	111.1±0.4	106.4	0.999

Various low cost sorbents such as TiO_2, activated carbon, zeolite, lignin, chitin, and raw cellulose, have been widely used in the adsorption of lead ions. The adsorption capacities of a series of adsorption materials reported in the literature were listed in

Table 6.6. It was found that the adsorption capacity of material prepared in this work was higher than those most other adsorption materials reported in the literature.

Table 6.6 The adsorption capacities of a series of adsorption materials reported in the literature

Adsorbent	pH	q_e (adsorption capacity) mg/g	Reference
Nano-TiO_2	6	7.41	[42]
Commercial granular activated carbon	---	2.337	[43]
Peanut shell activated carbon	---	35.5	
Zeolite	4	66.96	[44]
Magnetically modified zeolite	4	84	
Alkaline lignin	5, T=30℃	12.8	[45]
Lignin xanthate resin	5, T=30℃	62.6	
Chitin	5	22.79	[46]
Cellulose/chitin blend materials	5	58.02	
Cellulose powder	---	55.9	[47]
Mercerized cellulose (Cell 2, Cell 4)	6	147, 192.3	[48]
Guanyl modified cellulose	6	52	[49]
Thiol-functionalized cellulose nanofiber membrane	4	22	[50]
Titanium oxide-bacterial cellulose bioadsorbent	7	160	[51]
Carboxylated cellulose fabric filters	5	81.3	[52]
Acrylic acid functionalized cellulose	4.5	55.9	[53]
Imidazole functionalized cellulose	---	72	[54]
Fe-Cu@CNC	---	81.94	[55]
Magnetic CNC@Zn-benzene-1, 3, 5-tricarboxylic acid	---	558.66	[56]
Fe_3O_4/ATP@BCNs/Chitosan	---	67.8	[57]

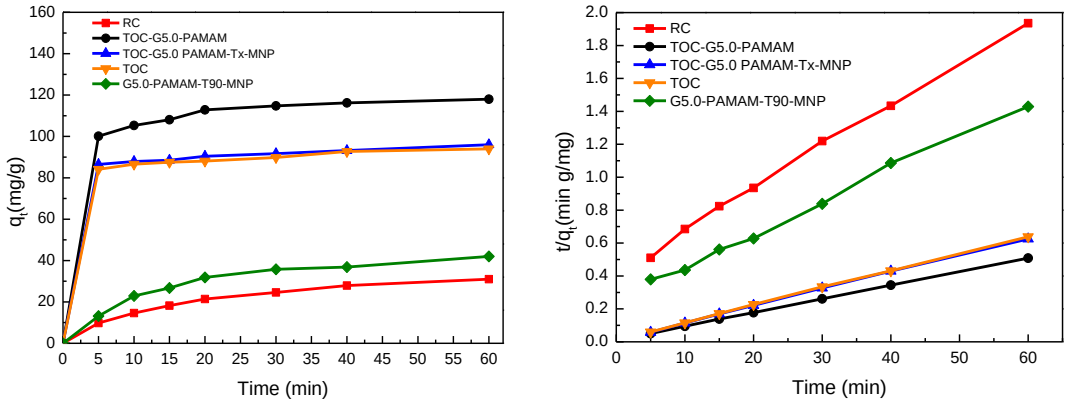

(a) Kinetic curves of Pb^{2+} adsorption (b) Pseudo-second order sorption kinetics

Fig. 6.13 (a) Kinetic curves and (b) Pseudo-second order sorption kinetics of Pb^{2+} adsorption by RC, TOC, G5.0 PAMAM-T90-MNP, TOC-G5.0 PAMAM, TOC-G5.0 PAMAM-T90-MNP at 250 mg/L Pb^{2+} concentration

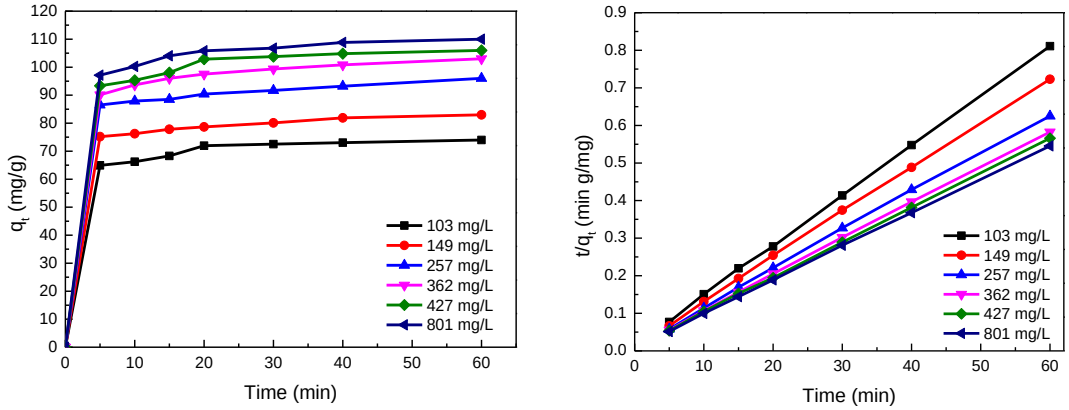

(a) Kinetic curves of Pb^{2+} adsorption (b) Pseudo-second order sorption kinetics

Fig. 6.14 (a) Kinetic curves and (b) Pseudo-second order sorption kinetics of Pb^{2+} adsorption by TOC-G5.0 PAMAM-T90-MNP at various initial Pb^{2+} concentrations

6.3.4.4 Adsorption isotherms

The Langmuir and Freundlich models for TOC-G5.0 PAMAM-T90-MNP are shown in Fig. 6.15, and the adsorption isotherm parameters are listed in Table 6.7. The Langmuir model proved to be a good fit for the adsorption process of TOC-G5.0 PAMAM-T90-MNP, and the fitting coefficient was over 0.999, i.e. greater than that of Freundlich

model (0.988). It was proved that the Pb^{2+} adsorption of this composite material conformed to the Langmuir adsorption model, which indicates that the adsorption of Pb^{2+} by TOC-G5.0 PAMAM-T90-MNP was primarily due to single molecular layer adsorption. According to the Langmuir model, the maximum saturation adsorption capacity of TOC-G5.0 PAMAM-T90-MNP was 120 mg/g.

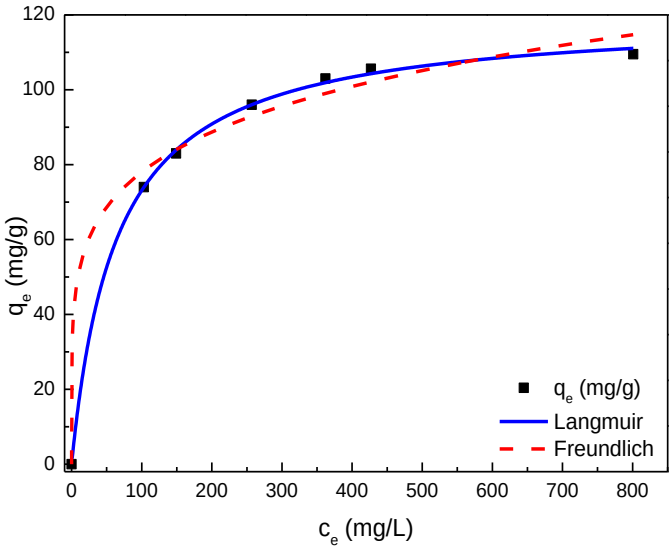

Fig. 6.15 Pb^{2+} adsorption isotherms and fitting result using TOC-G5.0 PAMAM-T90-MNP

Table 6.7 Adsorption isotherm parameters of TOC-G5.0 PAMAM-T90-MNP for Pb^{2+} adsorption

Equations	Parameters		
Langmuir	q_m=120 mg/g	b=0.0156 L/mg	R^2=0.99915
Freundlich	k_F=33.243	n=5.3975	R^2=0.98825

6.3.4.5 Comparison of the Pb^{2+} adsorption properties of TOC-Gn-PAMAM-Tx-MNP and TOC

The adsorption capacity of RC, TOC, G5.0 PAMAM-T90-MNP, TOC-G5.0 PAMAM and TOC-G5.0 PAMAM-T90-MNP were compared under the same adsorption conditions. As shown in Fig. 6.16, the Pb^{2+} adsorption capacity of RC containing 0.02 mmol/g carboxyl group and 6.09 mmol/g hydroxyl group was only 31 mg/g, which indicates that the hydroxyl group of the cellulose had a low binding affinity for Pb^{2+}. The Pb^{2+} adsorption capacity of G5.0 PAMAM-T90-MNP with 0.20 mmol/g amino group was 42 mg/g, which indicates that the amino group had a higher Pb^{2+} adsorption capacity than the hydroxyl group. The Pb^{2+} adsorption capacity of TOC-G5.0 PAMAM (G5.0 PAMAM modified TOC with GLA as the crosslinker) containing 0.86 mmol/g carboxyl groups and 0.53 mmol/g amino groups was up to 118 mg/g, i.e. slightly higher than that of TOC with the same carboxyl content. This suggests that modifying TOC with PAMAM can improve its adsorption properties. Introduction of the water-soluble PAMAM could further improve the water dispersion of the TOC, thus making it more difficult to separate from the water. The Pb^{2+} adsorption capacity of TOC-G5.0 PAMAM-T90-MNP containing 0.74 mmol/g carboxyl groups and 0.019 mmol/g NH_2 was close to that of TOC with the same carboxyl content, indicating that the introduction of magnetic nanoparticles did not have much of a negative impact on the adsorption capacity of the TOC.

The above results showed that the carboxyl group played a major role in the Pb^{2+} adsorption performance of the magnetic composite, because the residual NH_2 content in PAMAM was very low after GLA crosslinking. As shown in Table 6.4, the carboxyl

content of TOC prepared using Gn PAMAM-Tx-MNP as a catalyst was affected mainly by the structure of this dendrimer conjugated magnetic catalyst. For this reason, the Pb^{2+} adsorption performances of magnetic composites with various carboxyl contents prepared by Gn PAMAM-Tx-MNP catalysts with different PAMAM generations and TEMPO loading ratios were evaluated.

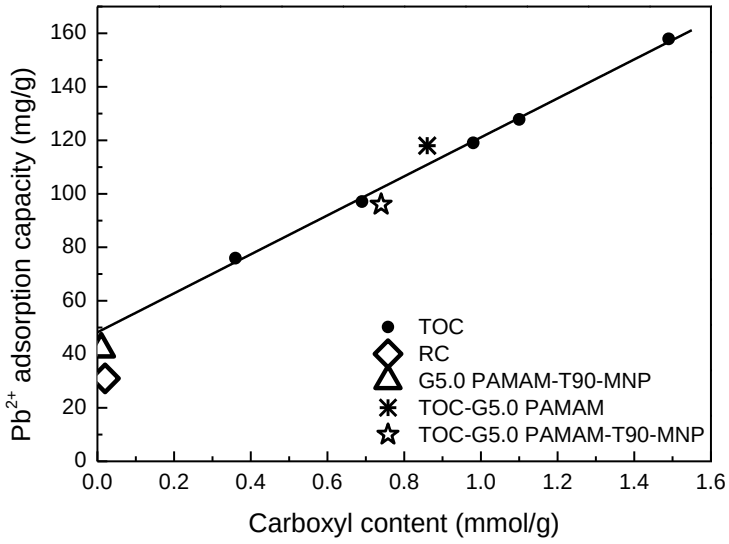

Fig. 6.16 Comparison of Pb^{2+} adsorption properties of RC, TOC, G5.0 PAMAM-T90-MNP, TOC-G5.0 PAMAM and TOC-G5.0 PAMAM-T90-MNP

6.3.4.6 Effect of the dendrimer conjugated magnetic catalyst structure on Pb^{2+} adsorption

By fixing the TEMPO loading ratio (about 90%), the effects of PAMAM generation on the carboxyl contents and Pb^{2+} adsorption properties of TOC-Gn PAMAM-T90-MNP were studied. As shown in Fig. 6.17, the Pb^{2+} adsorption capacity of the magnetic TOC adsorbent was proportional to the carboxyl content. The magnetic adsorbent prepared with G3.0 PAMAM modified MNP supported TEMPO as the catalyst gave the highest

carboxyl content (0.88 mmol/g) and Pb^{2+} adsorption capacity (109 mg/g).

By fixing the PAMAM generation (G3.0 PAMAM), the effects of the TEMPO loading ratio on carboxyl content and the Pb^{2+} adsorption capacity of magnetic composites prepared by G3.0 PAMAM-Tx-MNP were studied. As shown in Fig. 6.18, with an increase in the TEMPO loading ratio, the carboxyl content of the magnetic composite obtained increased. All magnetic adsorbents had an adsorption capacity similar to TOC with the same carboxyl content, further confirming that the carboxyl group played a major role in the adsorption of Pb^{2+}.

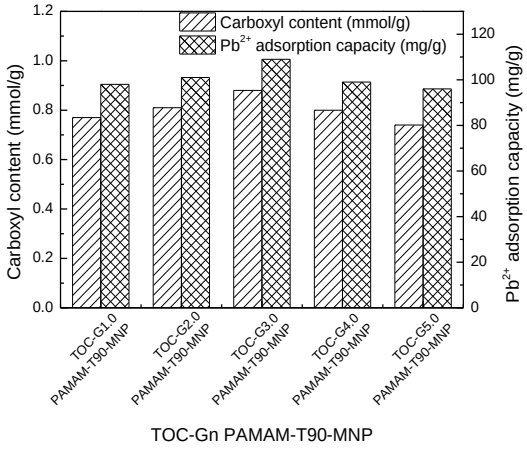

Fig. 6.17 Effects of PAMAM generation on carboxyl contents and Pb^{2+} adsorption properties of TOC-Gn PAMAM-T90-MNP

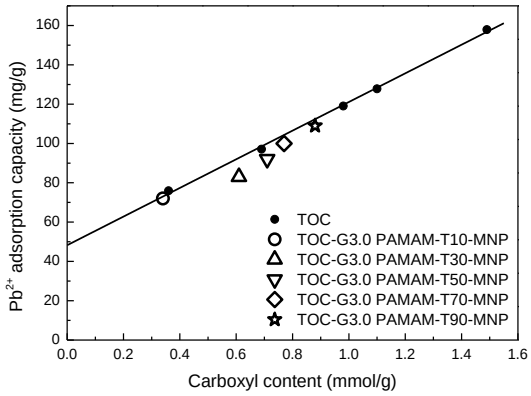

Fig. 6.18 Effects of TEMPO loading ratio on carboxyl contents and Pb^{2+} adsorption properties of TOC-Gn PAMAM-Tx-MNP

6.3.5 Cyclic adsorption and desorption

The magnetic TOC adsorbent prepared in this work can be easily recovered using an external magnetic field. The adsorption-desorption experiments of TOC-G3.0

PAMAM-T90-MNP were conducted to determine its re-usability. 0.1 M HCl was used to desorb Pb^{2+} from this magnetic adsorbent in order to evaluate its regeneration ability. As shown in Fig. 6.19 the adsorption/desorption capacity of TOC-G3.0 PAMAM-T90-MNP did not decrease significantly in the three cycles, proving that this magnetic adsorbent has good recycling performance.

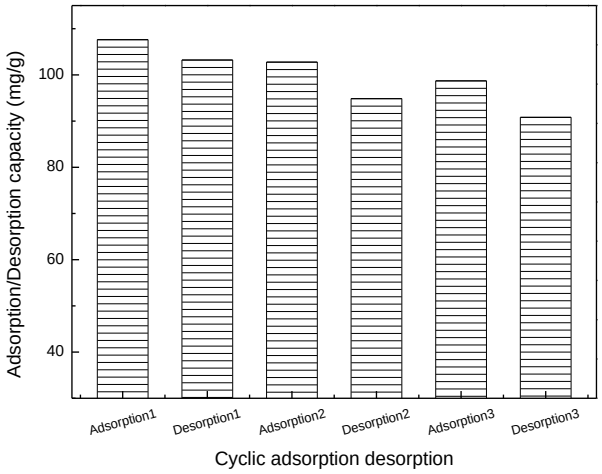

Fig. 6.19 Recycling performance of TOC-G3.0 PAMAM-T90-MNP for the adsorption of Pb^{2+}

6.4 Conclusion

The magnetic oxidized cellulose composite called TOC-Gn PAMAM-Tx-MNP was prepared using PAMAM modified nano-Fe_3O_4 supported TEMPO as the oxidation catalyst and cellulose cross-linker for efficient adsorption of Pb^{2+}. The carboxyl content of TOC-Gn PAMAM-Tx-MNP was mainly affected by the structure of this dendrimer conjugated magnetic TEMPO catalyst. Pb^{2+} adsorption conformed to the Langmuir adsorption model. The Pb^{2+} adsorption capacity of the magnetic TOC adsorbent was

proportional to its carboxyl content. The maximum saturation adsorption capacity of this magnetic composite was up to 120 mg/g, which is comparable with that of TOC with the same carboxyl content. After three cycles of adsorption and desorption, the adsorption and desorption capacity of the composites were maintained at a high level, which indicates that the magnetic oxidized cellulose composite had good regeneration ability.

References

[1] Bolm C, Fey T. TEMPO oxidations with a silica-supported catalyst [J]. Chemical Communications, 1999 (18): 1795-1796.

[2] Tanyeli C, Gümüş A. Synthesis of polymer-supported TEMPO catalysts and their application in the oxidation of various alcohols [J]. Tetrahedron Letters, 2003, 44(8): 1639-1642.

[3] Patankar S, Renneckar S. Greener synthesis of nanofibrillated cellulose using magnetically separable TEMPO nanocatalyst [J]. Green Chemistry, 2017, 19(20): 4792-4797.

[4] Araki J, Iida M. Surface carboxylation of cellulose nanowhiskers using mPEG-TEMPO: Its recovery and recycling [J]. Polymer Journal, 2016, 48(10): 1029-1033.

[5] Liu S, Xing Y, Han J, et al. Catalytic oxidation of cellulose with a novel amphiphilic nitroxide block copolymer as a recoverable catalyst [J]. Cellulose, 2017, 24(9): 3635-3644.

[6] Liu S, Sun T, Yang D, et al. Polyacrylic acid supported TEMPO for selective catalytic oxidation of cellulose: Recovered by its pH sensitivity [J]. Cellulose, 2018, 25(10): 5687-5696.

[7] Liu S, Liang H, Sun T, et al. A recoverable dendritic polyamidoamine immobilized TEMPO for efficient catalytic oxidation of cellulose [J]. Carbohydrate Polymers, 2018, 202: 563-570.

[8] Karim Z, Hakalahti M, Tammelin T, et al. In situ TEMPO surface functionalization

of nanocellulose membranes for enhanced adsorption of metal ions from aqueous medium [J]. RSC Advances, 2017, 7(9): 5232-5241.

[9] Shi S, Pelton R, Fu Q, et al. Comparing polymer-supported TEMPO mediators for cellulose oxidation and subsequent polyvinylamine grafting [J]. Industrial & Engineering Chemistry Research, 2014, 53(12): 4748-4754.

[10] Pelton R, Ren P, Liu J, et al. Polyvinylamine-graft-TEMPO adsorbs onto, oxidizes, and covalently bonds to wet cellulose [J]. Biomacromolecules, 2011, 12(4): 942-948.

[11] Pelton R. Polyvinylamine: A tool for engineering interfaces [J]. Langmuir, 2014, 30(51): 15373-15382.

[12] Yang D, Stimpson T, Soucy J, et al. Increasing wet adhesion between cellulose surfaces with polyvinylamine [J]. Cellulose, 2019, 26(1): 341-353.

[13] Pelton R, Yang D, Gustafsson E. Polymers that strengthen never-dried joints between wet cellulose surfaces-A review [J]. BioResources, 2019, 14(1): 2389-2419.

[14] Feng Y, Gong J, Zeng G, et al. Adsorption of Cd (II) and Zn (II) from aqueous solutions using magnetic hydroxyapatite nanoparticles as adsorbents [J]. Chemical Engineering Journal, 2010, 162(2): 487-494.

[15] Li B, Zhang Q, Pan Y, et al. Functionalized porous magnetic cellulose/Fe_3O_4 beads prepared from ionic liquid for removal of dyes from aqueous solution [J]. International Journal of Biological Macromolecules, 2020, 163: 309-316.

[16] Wang X, Jiang S, Cui S, et al. Magnetic-controlled aerogels from carboxylated cellulose and $MnFe_2O_4$ as a novel adsorbent for removal of Cu(II) [J]. Cellulose, 2019, 26(8): 5051-5063.

[17] Abou-Zeid R, Kamal K, Abd El-Aziz M, et al. Grafted TEMPO-oxidized cellulose nanofiber embedded with modified magnetite for effective adsorption of lead ions [J]. International Journal of Biological Macromolecules, 2021, 167: 1091-1101.

[18] Bosman A, Janssen H, Meijer E. About dendrimers: structure, physical properties, and applications [J]. Chemical Reviews, 1999, 99(7): 1665-1688.

[19] Liang H. Preparation and Catalytic Oxidation Performance of Polyamidoamine Immobilized TEMPO [D]. Hebei University of Science and Technology. 2020.

[20] Sun T, Liang H, Liu S, et al. Magnetic nanoparticles modified by polyamidoamine-immobilized TEMPO for catalytic oxidation of monomethoxy poly (ethylene glycol) [J]. Journal of Nanoparticle Research, 2020, 22(6): 1-11.

[21] Liu S, Liang H, Sun T, et al. A recoverable dendritic polyamidoamine immobilized TEMPO for efficient catalytic oxidation of cellulose [J]. Carbohydrate Polymers, 2018, 202: 563-570.

[22] Liu S, Sun T, Yang D, et al. Polyacrylic acid supported TEMPO for selective catalytic oxidation of cellulose: recovered by its pH sensitivity [J]. Cellulose, 2018, 25(10): 5687-5696.

[23] Li Y, Peng L, Li W. Adsorption behaviors on trace Pb^{2+} from water of biochar adsorbents from konjac starch [J]. Adsorption Science & Technology, 2020, 38(9-10): 344-356.

[24] Tan Y, Chen M, Hao Y. High efficient removal of Pb(II) by amino-functionalized Fe_3O_4 magnetic nano-particles [J]. Chemical Engineering Journal, 2012, 191: 104-111.

[25] Lewis L N. Chemical catalysis by colloids and clusters [J]. Chemical Reviews,

1993, 93(8): 2693-2730.

[26] Beejapur H, Zhang Q, Hu K, et al. TEMPO in chemical transformations: From homogeneous to heterogeneous [J]. ACS Catalysis, 2019, 9(4): 2777-2830.

[27] Tang J, Zhang Q, Hu K, et al. Novel high TEMPO loading magneto-polymeric nanohybrids: An efficient and recyclable Pickering interfacial catalyst [J]. Journal of Catalysis, 2017, 353: 192-198.

[28] Zheng Z, Wang J, Zhang M, et al. Magnetic polystyrene nanosphere immobilized TEMPO: A readily prepared, highly reactive and recyclable polymer catalyst in the selective oxidation of alcohols [J]. ChemCatChem, 2013, 5(1): 307-312.

[29] Karimi B, Farhangi E. One-pot oxidative Passerini reaction of alcohols using a magnetically recyclable TEMPO under metal-and halogen-free conditions [J]. Advanced Synthesis & Catalysis, 2013, 355(2-3): 508-516.

[30] Zhu J, Wang P, Lu M. Synthesis of novel magnetic silica supported hybrid ionic liquid combining TEMPO and polyoxometalate and its application for selective oxidation of alcohols [J]. RSC Advances, 2012, 2(22): 8265-8268.

[31] Shylesh S, Schünemann V, Thiel W R. Magnetically separable nanocatalysts: Bridges between homogeneous and heterogeneous catalysis [J]. Angewandte Chemie International Edition, 2010, 49(20): 3428-3459.

[32] Tucker-Schwartz A, Garrell R. Simple preparation and application of TEMPO-coated Fe_3O_4 superparamagnetic nanoparticles for selective oxidation of alcohols [J]. Chemistry-A European Journal, 2010, 16(42): 12718-12726.

[33] Schätz A, Grass R, Stark W, et al. TEMPO supported on magnetic C/Co-

nanoparticles: A highly active and recyclable organocatalyst [J]. Chemistry-A European Journal, 2008, 14(27): 8262-8266.

[34] Patankar S, Renneckar S. Greener synthesis of nanofibrillated cellulose using magnetically separable TEMPO nanocatalyst [J]. Green Chemistry, 2017, 19(20): 4792-4797.

[35] Guo X, Zhang J, Cui Y, et al. Highly biocompatible jujube polysaccharide-stabilized palladium nanoparticles with excellent catalytic performance [J]. New Journal of Chemistry, 2019, 43(20): 7646-7652.

[36] Cui Y, Zhang J, Yu Q, et al. Highly biocompatible zwitterionic dendrimer-encapsulated platinum nanoparticles for sensitive detection of glucose in complex medium [J]. New Journal of Chemistry, 2019, 43(23): 9076-9083.

[37] Huang J, Chen S, Zeng T, et al. Acid-Base titration applied in characterization of poly (amidoamine) [J]. Polymer Materials Science and Engineering, 2007, 23(4): 185.

[38] Sun T, Liang H, Liu S, et al. Magnetic nanoparticles modified by polyamidoamine-immobilized TEMPO for catalytic oxidation of monomethoxy poly (ethylene glycol) [J]. Journal of Nanoparticle Research, 2020, 22(6): 1-11.

[39] Ur Rahman O, Mohapatra S, Ahmad S. Fe_3O_4 inverse spinal super paramagnetic nanoparticles [J]. Materials Chemistry and Physics, 2012, 132(1): 196-202.

[40] Chen X, Cui J, Xu X, et al. Bacterial cellulose/attapulgite magnetic composites as an efficient adsorbent for heavy metal ions and dye treatment [J]. Carbohydrate Polymers, 2020, 229: 115512.

[41] Mahdavi M, Ahmad M, Haron M, et al. Synthesis, surface modification and

characterisation of biocompatible magnetic iron oxide nanoparticles for biomedical applications [J]. Molecules, 2013, 18(7): 7533-7548.

[42] Poursani A, Nilchi A, Hassani A, et al. The synthesis of nano TiO_2 and its use for removal of lead ions from aqueous solution [J]. Journal of Water Resource and Protection, 2016, 8(04): 438.

[43] Tao X, Xiaoqin L. Peanut shell activated carbon: characterization, surface modification and adsorption of Pb^{2+} from aqueous solution [J]. Chinese Journal of Chemical Engineering, 2008, 16(3): 401-406.

[44] Yuan M, Xie T, Yan G, et al. Effective removal of Pb^{2+} from aqueous solutions by magnetically modified zeolite [J]. Powder Technology, 2018, 332: 234-241.

[45] Li Z, Kong Y, Ge Y. Synthesis of porous lignin xanthate resin for Pb^{2+} removal from aqueous solution [J]. Chemical Engineering Journal, 2015, 270: 229-234.

[46] Zhou D, Wang H, Guo S. Preparation of Cellulose/Chitin Blend Materials and Influence of Their Properties on Sorption of Heavy Metals [J]. Sustainability, 2021, 13(11): 6460.

[47] Güçlü G, Gürdağ G, Özgümüş S. Competitive removal of heavy metal ions by cellulose graft copolymers [J]. Journal of Applied Polymer Science, 2003, 90(8): 2034-2039.

[48] Gurgel L, Gil L. Adsorption of Cu(II), Cd(II), and Pb(II) from aqueous single metal solutions by succinylated mercerized cellulose modified with triethylenetetramine [J]. Carbohydrate polymers, 2009, 77(1): 142-149.

[49] Kenawy I, Hafez M, Ismail M, et al. Adsorption of Cu(II), Cd(II), Hg(II), Pb(II) and Zn(II) from aqueous single metal solutions by guanyl-modified cellulose [J]. International journal of biological macromolecules, 2018, 107: 1538-1549.

[50] Choi H, Bae J, Hasegawa Y, et al. Thiol-functionalized cellulose nanofiber membranes for the effective adsorption of heavy metal ions in water [J]. Carbohydrate Polymers, 2020, 234: 115881.

[51] Shoukat A, Wahid F, Khan T, et al. Titanium oxide-bacterial cellulose bioadsorbent for the removal of lead ions from aqueous solution [J]. International

journal of biological macromolecules, 2019, 129: 965-971.

[52] Li C, Ma H, Venkateswaran S, et al. Highly efficient and sustainable carboxylated cellulose filters for removal of cationic dyes/heavy metals ions [J]. Chemical Engineering Journal, 2020, 389: 123458.

[53] Güçlü G, Gürdağ G, Özgümüş S. Competitive removal of heavy metal ions by cellulose graft copolymers [J]. Journal of Applied Polymer Science, 2003, 90(8): 2034-2039.

[54] O'Connell D, Birkinshaw C, O'Dwyer T. Removal of lead(II) ions from aqueous solutions using a modified cellulose adsorbent [J]. Adsorption Science & Technology, 2006, 24(4): 337-348.

[55] Chen L, Yu H, Deutschman C, et al. Novel design of Fe-Cu alloy coated cellulose nanocrystals with strong antibacterial ability and efficient Pb^{2+} removal [J]. Carbohydrate Polymers, 2020, 234: 115889.

[56] Wang N, Ouyang X, Yang L, et al. Fabrication of a magnetic cellulose nanocrystal/metal–organic framework composite for removal of Pb(II) from water [J]. ACS Sustainable Chemistry & Engineering, 2017, 5(11): 10447-10458.

[57] Chen X, Cui J, Xu X, et al. Bacterial cellulose/attapulgite magnetic composites as an efficient adsorbent for heavy metal ions and dye treatment [J]. Carbohydrate polymers, 2020, 229: 115512.

CHAPTER 7 PAMAM DENDRIMER-SILVER MODIFIED OXIDIZED CELLULOSE FOR EFFICIENT REDUCTION OF 4-NITROPHENOL

7.1 Introduction

4-nitrophenol (4-NP) is a typical pollutant in agriculture and industrial wastewater [1-11]. However, its reductive form, 4-aminophenol (4-AP), is an important intermediate in the production of analgesic and antipyretic drugs. 4-AP is also widely used as a developer, corrosion inhibitor, preservative lubricant and hair colorant. Catalytic reduction of 4-NP to 4-AP is generally carried out in the presence of nanoparticle catalysts, such as gold (Au), silver (Ag), platinum (Pt), rhodium (Rh), bismuth (Bi) or palladium (Pd) [12-16]. Among them, Ag has always been widely used for its high catalytic reduction performance and low price. However, the high surface energy of Ag nanoparticles can lead to their instability in solution, resulting in aggregation and reduction or even loss of catalytic activity. Therefore, it is particularly important to select an appropriate stabilizer to address the aggregation issue. PAMAM is a dendrite macromolecule with good biocompatibility that can stably wrap Ag nanoparticles in cavities and so achieve uniform dispersion of Ag nanoparticles. It has been proven that the PAMAM-Ag composite has high catalytic activity for reducing 4-NP to 4-AP, but the catalyst is difficult to recycle and re-use due to its high water-solubility [17, 18].

Recently, some studies combined polysaccharides with PAMAM-Ag. Dai et al. prepared a nanocomposite hydrogel linked between oxidized water-soluble polysaccharides (oxidized with sodium periodate) and cationic G5.0 PAMAM-Ag to research its antibacterial performance. Due to the instability of the imine bonds and the water-solubility of polysaccharides, it is not suitable for applications in the field of catalysis [19].

A Pd nanoparticle catalyst was supported on a natural polymer-based hydrogel by cationic nanocellulose cross-linked with anionic alginate in $CaCl_2$ solution. It was used as a recoverable catalyst for the Suzuki reaction and had good catalytic performance, but it was physically crosslinked and had poor stability [20]. Ag nanoparticles stabilized by an -NH_2 terminated fourth generation poly(amido amine) dendrimer (DENAgNPs) were covalently immobilized on TEMPO oxidized cellulose by using a condensing agent to achieve amide bond formation between cellulose and DENAgNPs. It was used in the catalytic reaction of Rhodamine B. However, the preparation method was cumbersome and the amide bond was easily hydrolyzed [21].

Since the catalytic reduction reaction of 4-NP to 4-AP takes place in a water system, TEMPO oxidation of cellulose is necessary to introduce carboxyl groups for purposes of improving the hydrophilicity [22, 23]. In this part of the study, TEMPO was first used to oxidize cellulose to prepare TOC with a large number of carboxyl groups. Then

sodium periodate was used to introduce aldehyde groups to prepare oxidized cellulose-containing carboxyl groups and aldehyde groups (TOC-CHO). PAMAM was used as a template to coat Ag nanoparticles that were used to prepare PAMAM-Ag. Finally, the composite of TOC-PAMAM-Ag was prepared by means of an aldehyde-amine reaction between the aldehyde group of TOC-CHO and the amino groups of PAMAM-Ag. This was used for catalytic reduction of 4-NP in order to produce 4-AP efficiently. It was found that the imine bonds contained in TOC-PAMAM-Ag were transformed into stable amine bonds in the catalytic reduction process, thus making the TOC-PAMAM-Ag stable. The influence of the catalyst loading amount and carboxyl content was investigated, and the cyclic catalytic performance was also evaluated.

7.2 Experiment

7.2.1 Preparation of Ag nanoparticle-immobilized oxidized cellulose composite of TOC-PAMAM-Ag

7.2.1.1 Oxidation of cellulose with TEMPO

The experimental method used was the same as that indicated in 4.2.2. By changing the amount of the NaClO added (1 mmol, 3 mmol, 5 mmol and 10 mmol), TOC samples with different types of carboxy content were obtained and named TOC1, TOC3, TOC5 and TOC10, respectively.

7.2.1.2 Oxidation of TOC with sodium periodate

Oxidation of TOC with sodium periodate was processed according to the reported

method with minor modifications [24, 25]. TOC (1.0 g) was dispersed into water (50 mL), and the pH was adjusted to 3 with 0.1 M HCl. Then a measured amount of sodium periodate (the molar ratio of cellulose unit to sodium periodate was 1:3) was added at 35 ℃. After 3 h, 1 mL of glycol was added to quench the reaction. Thorough centrifugation, washing and freeze-drying was done and the TOC-CHO product was obtained.

7.2.1.3 Preparation of PAMAM-Ag

Ag nanoparticles were prepared with G4.0 PAMAM as a template. 0.1 M $AgNO_3$ (1.6 mL) was added to 1 mM G4.0 PAMAM (5 mL) (in a N_2 environment) using a constant pressure drip funnel at 30 ℃. After dripping, the reaction was continued for 30 min and 0.2 M $NaBH_4$ (9.6 mL) was added. After 3 h, the G4.0 PAMAM-Ag aqueous solution was obtained.

7.2.1.4 Preparation of TOC-PAMAM-Ag

G4.0 PAMAM-Ag (4 mL) was added to TOC-CHO (0.4 g) and oscillated for 6 h. After centrifugation, washing and freeze-drying, TOC-PAMAM-Ag was obtained. The Ag loading of the composite was changed by changing the dosage of G4.0 PAMAM-Ag.

7.2.2 Catalytic reaction of 4-NP by TOC-PAMAM-Ag

The reduction of 4- nitrophenol texts was carried out based on the reported method and conditions [26, 27]. 12.75 mM of a 4-NP solution (30 μL), 0.2 M $NaBH_4$ solution (350

μL), deionized water (2.5 mL) and a measured amount of TOC-PAMAM-Ag were added to a colorimetric dish at room temperature. The change in absorbance with time was monitored using a UV-vis spectrophotometer at λ=400 nm in a scanning range of 250-500 nm.

7.3 Results and Discussion

7.3.1 Synthetic route of TOC-PAMAM-Ag

As shown in Fig. 7.1, TOC-CHO was prepared by introducing an aldehyde group to TOC through sodium periodate oxidation. G4.0 PAMAM-Ag was prepared by coating G4.0 PAMAM with Ag nanoparticles. The aldehyde group of TOC-CHO and the amino group of PAMAM-Ag were then subjected to the aldol-amine reaction in order to obtain TOC-PAMAM-Ag. The dosage of G4.0 PAMAM-Ag was changed to obtain composites with different Ag loading densities.

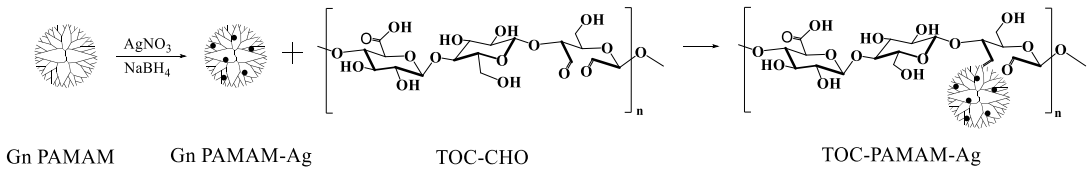

Fig. 7.1 Synthetic route of TOC-PAMAM-Ag

The TOC was characterized using FT-IR, as shown in Fig. 7.2. It was seen that the absorption peak due to -COONa at 1608 cm^{-1} increased significantly with an increase in NaClO dosage. The carboxyl content determined by conductometric titration (Table 7.2) was consistent with the FT-IR results. The absorption peak of the aldehyde group

that was introduced was seen at 1614 cm^{-1}. The aldehyde group content of TOC-CHO was determined by acid-base titration. After reacting TOC-CHO with G4.0 PAMAM-Ag, it was clearly seen that the brown G4.0 PAMAM-Ag solution became clear and transparent, while the oxidized cellulose turned brown. This indicated that the TOC-PAMAM-Ag composite was successfully prepared.

The amount of Ag loading was determined by XPS. The content of each element in TOC-PAMAM-Ag is provided in Table 7.1. The peaks relating to C1s, N1s and Ag3d are shown in Fig. 7.4. The five peaks relating to the C1s corresponded with: C-C (284.15 eV); C-O (285.0 eV); C-N (285.9 eV); C=N (286.8 eV); C=O (288.0 eV). The three peaks relating to N1s were C=N (397.7 eV), -NH- (399.1 eV) and C-N (401.1 eV), respectively. The differences between the $3d_{5/2}$ (367.9 eV) and $3d_{3/2}$ (373.9 eV) peaks for Ag were exactly the same as the values of zero valent silver [28]. The content of each element in TOC-PAMAM-Ag is provided in Table 7.1. The Ag loading obtained by XPS content is consistent with that obtained by TGA (Fig. 7.5).

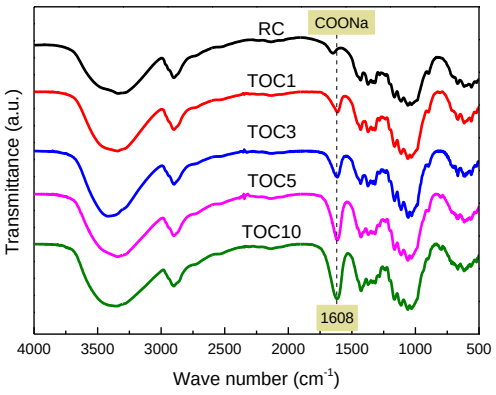

Fig. 7.2 FT-IR spectra of TOC

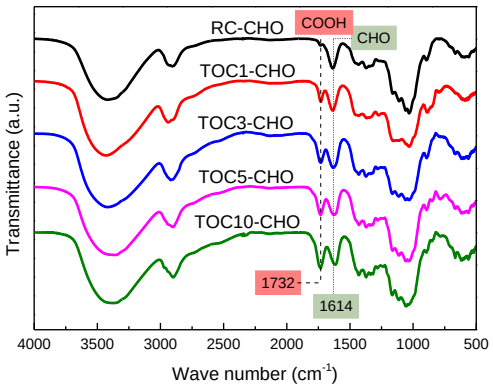

Fig. 7.3 FT-IR spectra of TOC-CHO

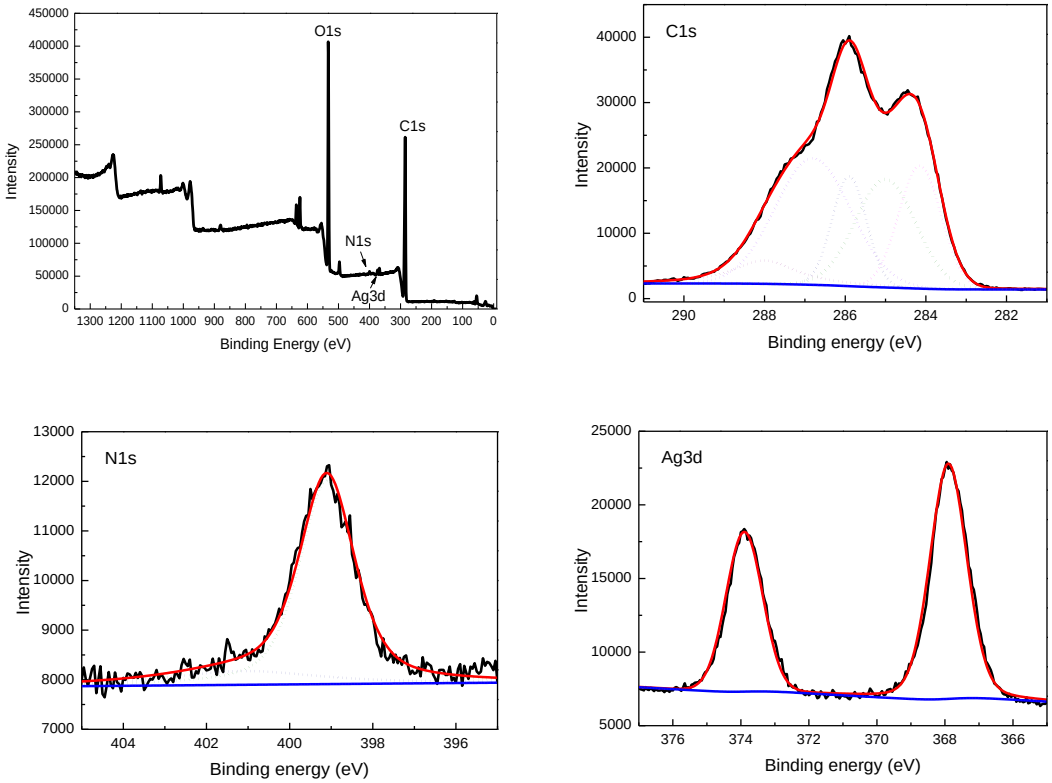

Fig. 7.4 The XPS spectra of C1s, N1s and Ag3d in TOC5-PAMAM-Ag

Table 7.1 XPS elemental compositions for the TOC5-PAMAM-Ag

Catalyst	n_{Ag} mmol	Measured				Ag loading mmol/g
		C %	N %	O %	Ag %	
TOC5-CHO	---	61.24	---	38.76	---	---
TOC5-PAMAM-Ag	0.01235	78.37	0.81	20.71	0.11	0.0407
	0.02469	68.78	1.26	29.77	0.20	0.0741
	0.04938	78.05	1.23	20.33	0.39	0.1444
	0.09877	65.65	2.88	30.54	0.92	0.3407

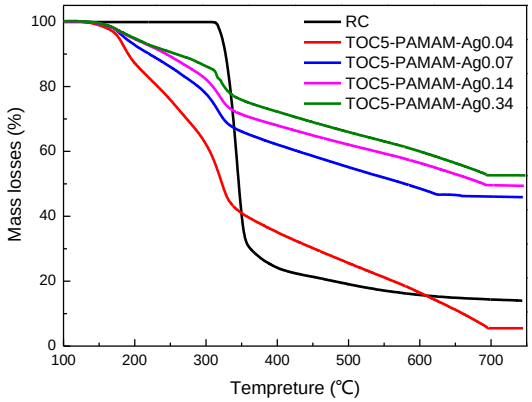

Fig. 7.5 TGA curves of TOC-PAMAM-Ag

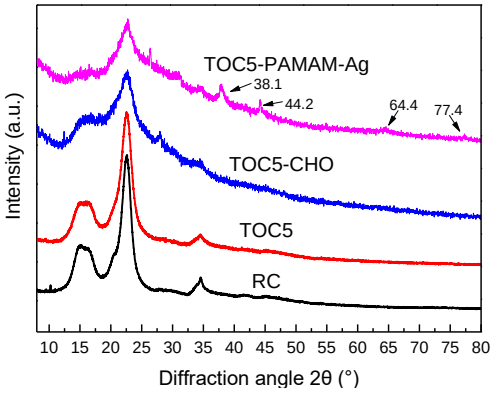

Fig. 7.6 XRD patterns of RC, TOC5, TOC5-CHO and TOC5-PAMAM-Ag

A comparison of the XRD patterns of RC, TOC5, TOC5-CHO and TOC5-PAMAM-Ag in the 2θ range 10-80° is shown in Fig. 7.6. Compared with RC, the crystalline structure of TOC5-CHO had a slight change, which indicates that a part of the cellulose in the amorphous area was oxidized to soluble oxidized cellulose. The XRD pattern of TOC5-PAMAM-Ag showed peaks at 2θ=38.1, 44.2, 64.4 and 77.4, which were attributed to Ag [29]. It can be proved that TOC-PAMAM-Ag was successfully prepared by the reaction of G4.0 PAMAM-Ag and cellulose. The morphologies and dispersion of the composite were investigated by means of TEM. Fig. 7.7 shows that the composite showed good dispersion of Ag, and the diameter of the silver nanoparticle size was about 7 nm.

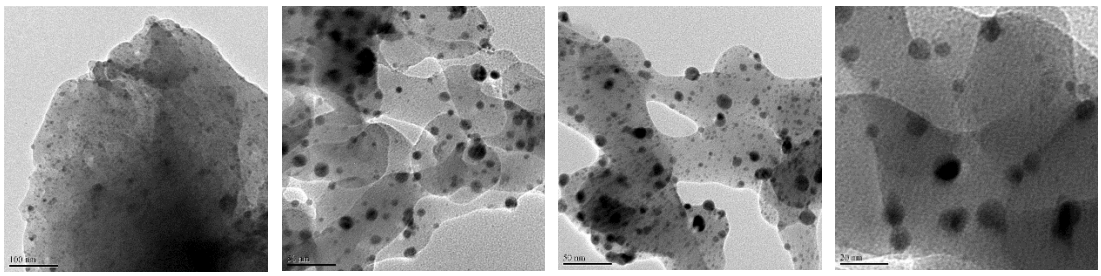

Fig. 7.7 TEM images of TOC-PAMAM-Ag

In order to systematically study the effect of TOC-PAMAM-Ag on the catalytic reduction of 4-NP, TOC-PAMAM-Ag with different Ag loading amounts and different carboxyl contents were designed and prepared (Table 7.2).

Table 7.2 Prepared composites of TOC-PAMAM-Ag

Composite	Carboxyl content mmol/g	Ag content mmol/g
RC-PAMAM-Ag0.07	0.02	0.0741
TOC1-PAMAM-Ag0.07	0.329	0.0738
TOC3-PAMAM-Ag0.07	0.973	0.0736
TOC5-PAMAM-Ag0.04	1.46	0.0407
TOC5-PAMAM-Ag0.07	1.46	0.0741
TOC5-PAMAM-Ag0.14	1.46	0.1444
TOC5-PAMAM-Ag0.34	1.46	0.3407
TOC10-PAMAM-Ag0.07	2.25	0.0738

7.3.2 Catalytic reduction of 4-NP to 4-AP by TOC-PAMAM-Ag

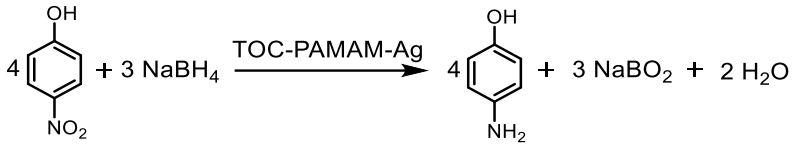

Fig. 7.8 Schematic diagram of catalytic reduction of 4-NP to 4-AP

As shown in Fig. 7.9 (a), 4-NP has an absorption peak at approximately 317 nm, and it is remarkably redshifted to 400 nm in presence of $NaBH_4$. This redshift is accompanied by the change from colorless to light yellow owing to the formation of the 4-nitrophenolate ion [30]. Due to the kinetic restriction of the reduction reaction, $NaBH_4$

alone cannot catalyze the reduction of 4-NP, and the use of a catalyst is required. The prepared composites were used for catalytic reduction of 4-NP to 4-AP in water (Fig. 7.8). It was observed that the system was light yellow when there was no catalyst. After adding the catalyst, the reaction system was light yellow at first and then became transparent (Fig. 7.9 (c)). This is due to the change of 4-NP (light yellow) to 4-AP (transparent). It was noted that the maximum UV-vis absorption peaks of 4-NP and 4-AP were at 400 nm and 296 nm, respectively. The catalytic performance of G4.0 PAMAM-Ag was evaluated first. After adding G4.0 PAMAM-Ag, the peak at 296 nm gradually increased, and the peak at 400 nm became smaller. At 9 min, the peak at 400 nm basically disappeared. The conversion rate was 98%, which proved that the homogeneous G4.0 PAMAM-Ag demonstrated good catalytic activity (Fig. 7.10).

(a) UV-vis spectra of 4-NP and in presence or absence of NaBH4

(b) No catalyst

(c) Initial stage of reaction

(d) End of reaction

Fig. 7.9 State of the reaction mixture in the cuvette

After G4.0 PAMAM-Ag was immobilized on TOC5, the composite of TOC5-PAMAM-Ag obtained gave a satisfactory conversion rate (95%), although the reaction was extended to 70 min (Fig. 7.11). The reduced reaction rate of TOC5-PAMAM-Ag

was due to the heterogeneous reaction of TOC-PAMAM-Ag.

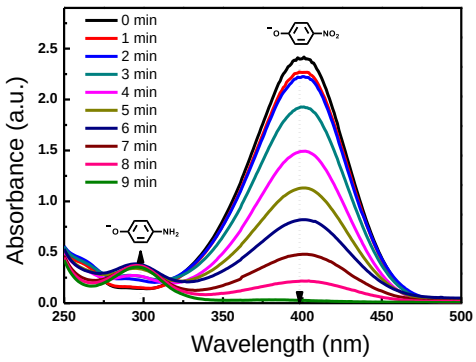

Fig. 7.10 UV-vis spectra of the catalytic reduction of 4-NP using G4.0 PAMAM-Ag as the catalyst

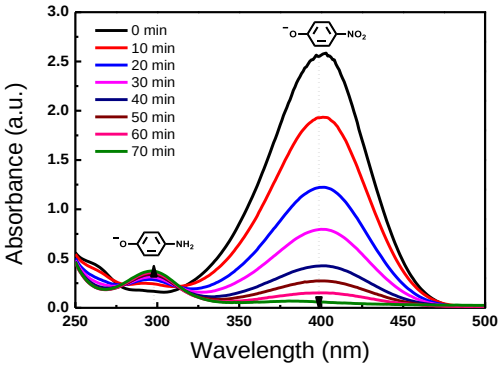

Fig. 7.11 UV-vis spectra of the catalytic reduction of 4-NP using TOC5-PAMAM-Ag0.07 as the catalyst

The effect of the Ag loading amount on the catalytic performance of TOC-PAMAM-Ag was investigated. The same dosage of Ag was added to each reaction system using TOC5-PAMAM-Ag0.04, TOC5-PAMAM-Ag0.07, TOC5-PAMAM-Ag0.14 and TOC5-PAMAM-Ag0.34. Fig. 7.12 shows that the catalytic performance first increased and then decreased with the increase in Ag loading. By increasing the silver loading, while maintaining a constant amount of silver added to the reaction system, it was possible to reduce the total catalyst mass added, thus reducing the diffusion resistance of the heterogeneous catalytic reaction and improving the reaction rate. However, PAMAM-Ag also acts as a crosslinker for oxidized cellulose, and excessive loading makes the crosslinking network of the composite too dense, thus reducing the reaction rate.

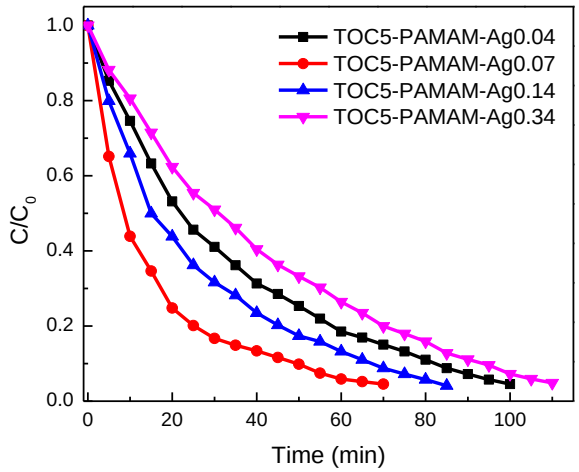

Fig. 7.12 C/C_0 vs reaction time plots of TOC5-PAMAM-Ag with different levels of Ag loading

The effect of TOC-PAMAM-Ag dosage on catalytic performance was explored. It was found that the reaction occurred rapidly in the initial stage of the reaction and gradually slowed down (Fig. 7.13). This was because the composite is rapidly dispersed in the reaction system and the reactants interact on a large scale immediately after the TOC5-PAMAM-Ag is added. As the reaction progressed, the concentration of 4-NP decreased, and the reaction rate slowed down. The more catalyst that was added, the shorter the time that was required to complete the reaction (from 100 min to 70 min). However, when the catalyst dosage was over 4 mg, the Ag interfered with the measurement of UV-vis. Therefore, the optimal dosage of TOC5-PAMAM-Ag0.07 was 4 mg.

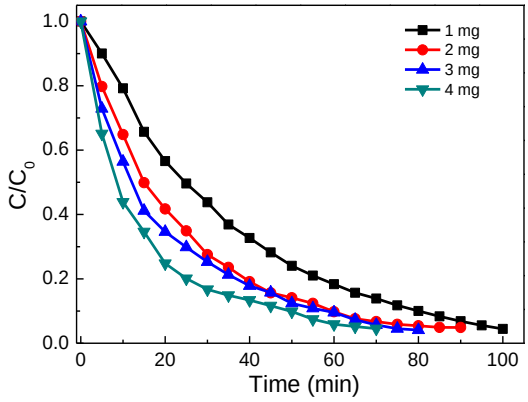

Fig. 7.13 C/C_0 vs reaction time plots of TOC5-PAMAM-Ag0.07 with different dosages

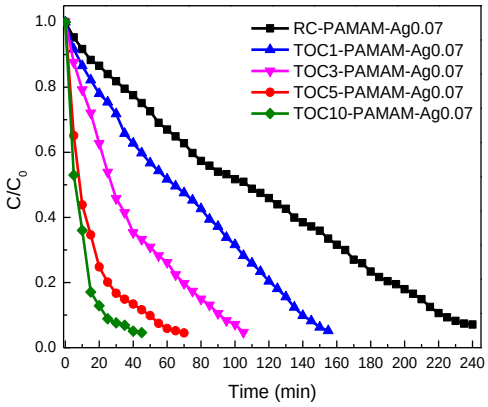

Fig. 7.14 C/C_0 vs reaction time plots of composite catalysts with different carboxyl content

To explore the effect of the carboxyl content on the composite catalyst, RC-PAMAM-Ag0.07, TOC1-PAMAM-Ag0.07, TOC3-PAMAM-Ag0.07, TOC5-PAMAM-Ag0.07 and TOC10-PAMAM-Ag0.07 was added to the reaction system in separate tests. Fig. 7.14 indicates that the reaction time decreased with an increase in the carboxyl content of oxidized cellulose. The reaction time of TOC10-PAMAM-Ag with a carboxyl content of 2.25 mmol/g was only 45 min. The carboxyl group in cellulose can increase its hydrophilicity, thus facilitating the contact between the reactant and the catalyst and accelerating the reaction rate.

Table 7.3 Comparison of various catalysts in the reduction of 4-NP.

Sample	Catalyst	Reaction rate ($*10^{-3}s^{-1}$)	References
1	Ag/PS	3.49	[30]
2	Fe_3O_4@PS/PDA-Ag	6.55	[31]
3	PSMAA-Ag	8.17	[32]
4	Ag-PANI	0.93	[33]

5	Ag/Cellulose	13	[34]
6	CNC@PDA-Ag	4.26	[35]
7	Ag-chitosan	1.33	[36]
8	G4.0 PAMAM-Ag	5.36	[18]
9	TOC-PAMAM-Ag	1.42	This work

To evaluate the catalytic performance of TOC-PAMAM-Ag, we compared the NP conversion rate of TOC-PAMAM-Ag with previously reported catalysts. As shown in Table 7.3, TOC-PAMAM-Ag have a comparable catalytic performance with other reported catalysts for reduction of 4-NP.

7.3.3 Cyclic catalytic property of TOC-PAMAM-Ag

After reaction, TOC5-PAMAM-Ag was recovered by centrifugation to explore its cycling performance. The recovered TOC5-PAMAM-Ag was characterized using XPS and XRD. Fig. 7.15 a and a' showed that the C=N of TOC5-PAMAM-Ag0.07 was reduced to stable C-N. Fig. 7.15 b and b' showed that the Ag loading remained unchanged after recovery. Fig. 7.15 c showed that the XPS spectra unchanged after recovery. Fig. 7.16 showed that the crystal structure did not change significantly after reduction. The recovered TOC-PAMAM-Ag was re-used for five cycles. When the reaction was carried out for 70 min, the conversion rate was almost constant (Fig. 7.17), which indicates that TOC-PAMAM-Ag had good recyclability.

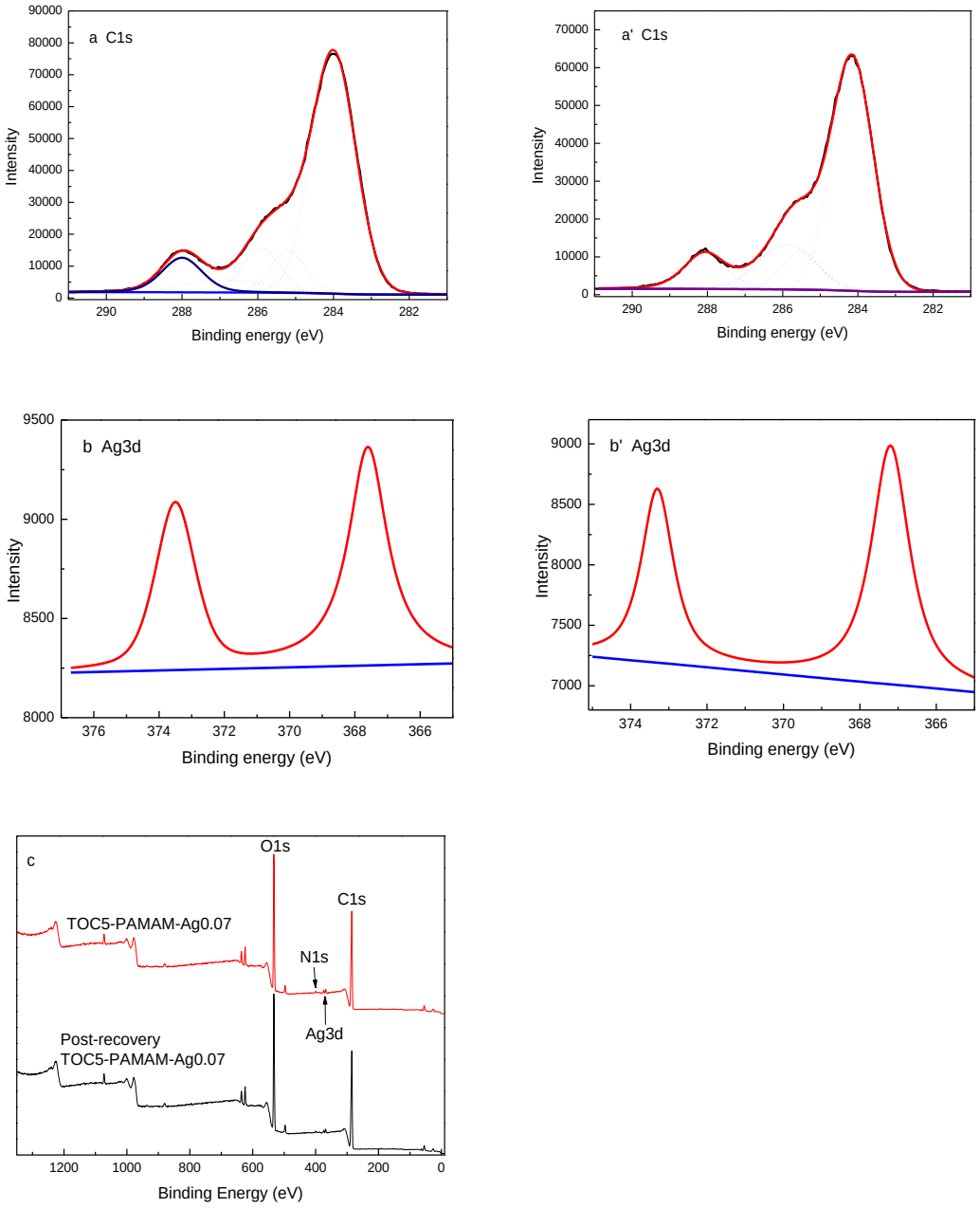

Fig. 7.15 The XPS spectra of C1s and Ag3d in TOC5-PAMAM-Ag0.07. (a and b were spectra for the fresh catalyst; a' and b' were spectra for the recycled catalyst)

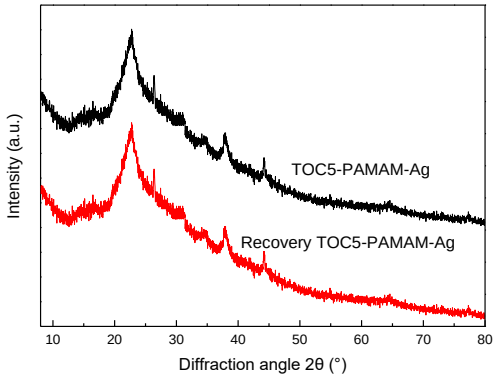

Fig. 7.16 XRD patterns of TOC-PAMAM-Ag before and after recovery

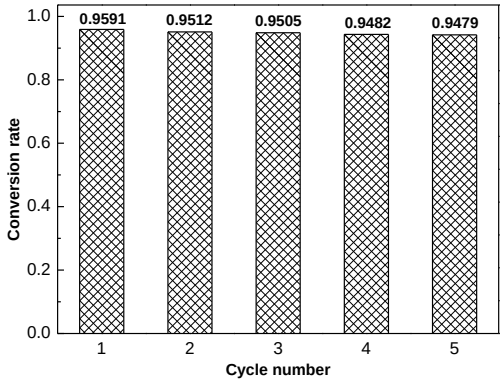

Fig. 7.17 The recyclability of TOC5-PAMAM-Ag for catalytic reduction of 4-NP

7.4 Conclusion

A series of TOC-PAMAM-Ag samples with different carboxyl groups and different Ag loadings were prepared in order to study the catalytic reduction of 4-NP to 4-AP. It was found that the catalytic performance was best when the Ag loading of TOC-PAMAM-Ag was 0.07 mmol/g. The effect of carboxyl content in TOC-PAMAM-Ag on the reaction was explored and it was found that increased carboxyl content was favorable for the catalytic reaction. In the catalytic reduction process, the unstable imine bond contained in TOC-PAMAM-Ag can be transformed into a stable amine bond, which made it more stable. The experimental results showed that it had good catalytic performance and stable recycling performance.

References

[1] Rode C, Vaidya M, Chaudhari R. Synthesis of p-aminophenol by catalytic hydrogenation of nitrobenzene [J]. Organic Process Research & Development, 1999, 3(6): 465-470.

[2] Corbett J. An historical review of the use of dye precursors in the formulation of commercial oxidation hair dyes [J]. Dyes and Pigments, 1999, 41(1-2): 127-136.

[3] Zhang Y, Liu S, Lu W, et al. In situ green synthesis of Au nanostructures on graphene oxide and their application for catalytic reduction of 4-nitrophenol [J]. Catalysis Science & Technology, 2011, 1(7): 1142-1144.

[4] Du Y, Chen H, Chen R, et al. Synthesis of p-aminophenol from p-nitrophenol over nano-sized nickel catalysts [J]. Applied Catalysis A: General, 2004, 277(1-2): 259-264.

[5] Zhang Z, Shao C, Zou P, et al. In situ assembly of well-dispersed gold nanoparticles on electrospun silica nanotubes for catalytic reduction of 4-nitrophenol [J]. Chemical Communications, 2011, 47(13): 3906-3908.

[6] Ivančev-Tumbas I, Hobby R, Küchle B, et al. p-Nitrophenol removal by combination of powdered activated carbon adsorption and ultrafiltration–comparison of different operational modes [J]. Water Research, 2008, 42(15): 4117-4124.

[7] Mehrizad A, Zare K, Aghaie H, et al. Removal of 4-chloro-2-nitrophenol occurring in drug and pesticide waste by adsorption onto nano-titanium dioxide [J]. International Journal of Environmental Science and Technology, 2012, 9(2): 355-360.

[8] Das S, Khan M, Guha A, et al. Bio-inspired fabrication of silver nanoparticles on

nanostructured silica: Characterization and application as a highly efficient hydrogenation catalyst [J]. Green Chemistry, 2013, 15(9): 2548-2557.

[9] Holden M S, Nick K E, Hall M, et al. Synthesis and catalytic activity of pluronic stabilized silver-gold bimetallic nanoparticles [J]. RSC Advances, 2014, 4(94): 52279-52288.

[10] Yao Y, Li H, Liu J, et al. Removal and adsorption of p-nitrophenol from aqueous solutions using carbon nanotubes and their composites [J]. Journal of Nanomaterials, 2014, 2014.

[11] Magdy Y, Altaher H, ElQada E. Removal of three nitrophenols from aqueous solutions by adsorption onto char ash: Equilibrium and kinetic modeling [J]. Applied Water Science, 2018, 8(1): 1-15.

[12] Veisi H, Kazemi S, Mohammadi P, et al. Catalytic reduction of 4-nitrophenol over Ag nanoparticles immobilized on Stachys lavandulifolia extract-modified multi walled carbon nanotubes [J]. Polyhedron, 2019, 157: 232-240.

[13] Kuroda K, Ishida T, Haruta M. Reduction of 4-nitrophenol to 4-aminophenol over Au nanoparticles deposited on PMMA [J]. Journal of Molecular Catalysis A: Chemical, 2009, 298(1-2): 7-11.

[14] Krajczewski J, Kołątaj K, Kudelski A. Enhanced catalytic activity of solid and hollow platinum-cobalt nanoparticles towards reduction of 4-nitrophenol [J]. Applied Surface Science, 2016, 388: 624-630.

[15] Yan Q, Wang X, Feng J, et al. Simple fabrication of bimetallic platinum-rhodium alloyed nano-multipods: A highly effective and recyclable catalyst for reduction of 4-

nitrophenol and rhodamine B [J]. Journal of Colloid and Interface Science, 2021, 582: 701-710.

[16] Liang Y, Manioudakis J, Macairan J, et al. Facile aqueous-phase synthesis of an ultrasmall bismuth nanocatalyst for the reduction of 4-nitrophenol [J]. ACS Omega, 2019, 4(12): 14955-14961.

[17] Gürbüz M, Ertürk A. Synthesis and characterization of jeffamine core PAMAM dendrimer-silver nanocomposites (Ag JCPDNCs) and their evaluation in the reduction of 4-Nitrophenol [J]. Journal of the Turkish Chemical Society Section A: Chemistry, 2018, 5(2): 885-894.

[18] Yang D, Zhang R, Zhao T, et al. Efficient reduction of 4-nitrophenol catalyzed by 4-carbo-methoxypyrrolidone modified PAMAM dendrimer-silver nanocomposites [J]. Catalysis Science & Technology, 2019, 9(21): 6145-6151.

[19] Dai T, Wang C, Wang Y, et al. A nanocomposite hydrogel with potent and broad-spectrum antibacterial activity [J]. ACS Applied Materials & Interfaces, 2018, 10(17): 15163-15173.

[20] Wang B, Ran M, Fang G, et al. Palladium nano-catalyst supported on cationic nanocellulose-alginate hydrogel for effective catalytic reactions [J]. Cellulose, 2020, 27: 6995-7008.

[21] Ramaraju B, Imae T, Destaye A. Ag nanoparticle-immobilized cellulose nanofibril films for environmental conservation [J]. Applied Catalysis A: General, 2015, 492: 184-189.

[22] Mendoza D, Browne C, Raghuwanshi V, et al. One-shot TEMPO-periodate

oxidation of native cellulose [J]. Carbohydrate Polymers, 2019, 226: 115292.

[23] Tahiri C, Vignon M. TEMPO-oxidation of cellulose: Synthesis and characterisation of polyglucuronans [J]. Cellulose, 2000, 7(2): 177-188.

[24] Xing X, Han Y, Jiang Q, et al. Immobilization of laccases onto cellulose nanocrystals derived from waste newspaper: Relationship between immobilized laccase activity and dialdehyde content [J]. Cellulose, 2021, 28(8): 4793-4805.

[25] Sun B, Hou Q, Liu Z, et al. Sodium periodate oxidation of cellulose nanocrystal and its application as a paper wet strength additive [J]. Cellulose, 2015, 22(2): 1135-1146.

[26] Kurnaz Yetim N, Koç M, Nartop D. Magnetic dendrimer-encapsulated metal nanoparticles (Au, Ag): Effect of dendrimerization on catalytic reduction of 4-nitrophenol [J]. Journal of the Iranian Chemical Society, 2022: 1-12.

[27] Narayanan K, Sakthivel N. Heterogeneous catalytic reduction of anthropogenic pollutant, 4-nitrophenol by silver-bionanocomposite using cylindrocladium floridanum [J]. Bioresource Technology, 2011, 102(22): 10737-10740.

[28] Moulder J. Handbook of X-ray photoelectron spectroscopy [J]. Physical Electronics, 1995: 230-232.

[29] Maleki A, Movahed H, Paydar R. Design and development of a novel cellulose/γ-Fe_2O_3/Ag nanocomposite: A potential green catalyst and antibacterial agent [J]. RSC Advances, 2016, 6(17): 13657-13665.

[30] Li Y, Wu Y, Gao Y, et al. A facile method to fabricate polystyrene/silver composite particles and their catalytic properties [J]. RSC Advances, 2013, 3(48): 26361-26366.

[31] Peng F, Wang Q, Shi R, et al. Fabrication of sesame sticks-like silver nanoparticles/polystyrene hybridnanotubes and their catalytic effects [J]. Scientific reports, 2016, 6(1): 1-9.

[32] Liao G, Chen J, Zeng W, et al. Facile preparation of uniform nanocomposite spheres with loading silver nanoparticles on polystyrene-methyl acrylic acid spheres for catalytic reduction of 4-nitrophenol [J]. The Journal of Physical Chemistry C, 2016, 120(45): 25935-25944.

[33] Yuan C, Xu Y, Zhong L, et al. Heterogeneous silver-polyaniline nanocomposites with tunable morphology and controllable catalytic properties [J]. Nanotechnology, 2013, 24(18): 185602.

[34] Wu J, Zhao N, Zhang X, et al. Cellulose/silver nanoparticles composite microspheres: eco-friendly synthesis and catalytic application [J]. Cellulose, 2012, 19(4): 1239-1249.

[35] Tang J, Shi Z, Berry R M, et al. Mussel-inspired green metallization of silver nanoparticles on cellulose nanocrystals and their enhanced catalytic reduction of 4-nitrophenol in the presence of β-cyclodextrin [J]. Industrial & Engineering Chemistry Research, 2015, 54(13): 3299-3308.

[36] Murugadoss A, Chattopadhyay A. A ‘green’chitosan-silver nanoparticle composite as a heterogeneous as well as micro-heterogeneous catalyst [J]. Nanotechnology, 2007, 19(1): 015603.

CHAPTER 8 OVERALL CONCLUSIONS

The TEMPO/NaBr/NaClO system is generally used to selectively catalyze the oxidation of the cellulose C6 primary hydroxyl group to a carboxyl group to obtain TOC. In this work, TEMPO was loaded onto the water-soluble polymer to achieve TEMPO recycling and to reduce the degradation of the cellulose because of the specific structure of the polymer carrier.

8.1 Selective catalytic oxidation of cellulose with acrylamide-vinylamine copolymer immobilized TEMPO

An acrylamide-vinylamine copolymer (PVAm) supported TEMPO, called (PVAm-T), was designed and developed for using in the selective catalytic oxidation of cellulose. The amine groups in PVAm react with the carbonyl groups in 4-oxo-TEMPO to give PVAm-T. This was used as a catalyst (instead of free TEMPO) for selective catalytic oxidation of the C6 primary hydroxyl groups of cellulose in water. It was found that the catalyst has good catalytic performance, and the carboxyl content of oxidized cellulose was equivalent to 76% of that of the free TEMPO. Furthermore, PVAm-T was recycled by dialysis and the recycling performance was excellent. Interestingly, it was found that PVAm-T could effectively reduce degradation of the oxidized cellulose. The degree of degradation of PVAm-T oxidized cellulose was 21%-27%, which was much lower than that of free TEMPO (61%-66%). PVAm-T with a positive charge and suitable size can effectively avoid the formation of C6 aldehydes and C2/C3 ketones by side reactions,

and restrict oxidation, mainly to the exterior surface of porous cellulose, which results in significant reduction in the degradation of cellulose.

8.2 mPEG-modified polyamidoamine (PAMAM) supported TEMPO mediated oxidation of cellulose

Water-soluble mPEG-modified PAMAM supported TEMPO catalysts (mPEG-Gn PAMAM-T) with different PAMAM generations and different TEMPO loading degrees were prepared and used as catalysts in place of free TEMPO for purposes of selective catalytic oxidation of cellulose. The effects of the TEMPO loading degree, PAMAM generation and molecular weights of PEG on the reaction rate, the oxidation degree and the depolymerization of cellulose were investigated. The results showed that the catalytic performance of mPEG-Gn PAMAM-Tx was up to 84% the level of that of free TEMPO. Furthermore, this immobilized TEMPO catalyst can alleviate the degree of degradation of cellulose to a large degree. The catalyst was extracted using methylene chloride after the supernatant was concentrated, and the catalytic performance of the cellulose was not reduced after cyclic oxidation. It was found that the structure, charge and molecular size of the polymer carrier affected the degree of oxidation, the degree of degradation and the selectivity for cellulose oxidation.

TEMPO-mediated cellulose oxidation still has some deficiencies, which need to be solved to further promote the application of TOC in industry. Chlorinated oxidants such as NaClO should be avoided for environmental reasons. If sufficient quantities of the

C6-sodium carboxylate group can be efficiently introduced into oxidized cellulose, O_2, H_2O_2, O_3 or other chlorine-free compounds are preferred oxidants. For the establishment of environmentally friendly cellulose modification process, the treatment or recovery of related pollutants in wastewater formed during industrial production of TOC should be considered.

8.3 Use the composite of oxidized cellulose/nano-Fe_3O_4 for efficient adsorption of Pb^{2+}

The magnetic oxidized cellulose composite, called TOC-Gn PAMAM-Tx-MNP, was prepared using PAMAM modified nano-Fe_3O_4 supported TEMPO as an oxidation catalyst and cellulose cross-linker for the efficient adsorption of Pb^{2+}. The carboxyl content of TOC-Gn PAMAM-Tx-MNP was mainly affected by the structure of this dendrimer conjugated magnetic TEMPO catalyst. Pb^{2+} adsorption was confirmed as behaving in terms of the Langmuir adsorption model. The Pb^{2+} adsorption capacity of the magnetic TOC adsorbent was proportional to its carboxyl content. The maximum saturation adsorption capacity of this magnetic composite was up to 120 mg/g, which is comparable with that of TOC with the same carboxyl content. After three cycles of adsorption and desorption, the adsorption and desorption capacity of the composite were both maintained at a high level, which indicates that the magnetic oxidized cellulose composite had good regeneration ability.

TEMPO-oxidized cellulose has been found to be a potential candidate material for

wastewater treatment. However, continuous experiments must be carried out in the future to further explore the opportunities of TOC in wastewater treatment, especially in the form of aerogel or hydrogel.

8.4 Reduction of 4-nitrophenol to 4-aminophenol by oxidized cellulose immobilized nano-silver

TEMPO oxidized cellulose (TOC) was partly oxidized by sodium periodate to give TOC-CHO with aldehyde groups. PAMAM-Ag was prepared by coating Ag on the carrier. TOC immobilized nano-silver (TOC-PAMAM-Ag) was prepared by means of an aldehyde-amine reaction between the aldehyde groups of TOC-CHO and the amino groups of PAMAM-Ag. TOC-PAMAM-Ag was used in the catalytic reduction of 4-nitrophenol (4-NP) to 4-aminophenol (4-AP). In this catalytic reduction process, the unstable imine bond contained in TOC-PAMAM-Ag can be transformed into a stable amine bond, which makes TOC-PAMAM-Ag more stable. The experimental results show that it has good catalytic performance and stable recycling performance.

Ag nanoparticles are considered to be the most promising catalyst toward $NaBH_4$-assisted 4-NP reduction because of the unique advantages such as adjustable shape and size, simple preparation and environmental friendliness. However, the catalytic performance of Ag nanoparticles should be further improved.

8.5 Outlook

TOC and its related composite materials have been developed as novel bio-based materials. Further industrial applications of these new materials need to accumulate more basic information and data on the basis of experimental and theoretical studies. On the basis of the vast amount of science and technology that has been accumulated, it is necessary to improve it so that these materials can be produced and used under conditions of high reproducibility, operability and reliability.